

THESIS FOR THE DEGREE OF DOCTOR OF PHILOSOPHY

Charge transport through superconducting nanodevices

Daniel PERSSON



Applied Quantum Physics Laboratory
Department of Microtechnology and Nanoscience
CHALMERS UNIVERSITY OF TECHNOLOGY
Göteborg, Sweden, 2016

Charge transport through superconducting nanodevices
Daniel PERSSON

© DANIEL PERSSON

ISBN 978-91-7597-406-4
Doktorsavhandlingar vid Chalmers tekniska högskola
Ny serie nr 4087
ISSN 0346-718X

ISSN 1652-0769 Technical Report MC2-338
Applied Quantum Physics Laboratory
Department of Microtechnology and Nanoscience
Chalmers University of Technology
SE-412 96 Göteborg
Sweden
Telephone +46 (0)31-772 1000

Chalmers reproservice
Göteborg, Sweden, 2016

Charge transport through superconducting nanodevices

Daniel PERSSON

Applied Quantum Physics Laboratory
Department of Microtechnology and Nanoscience
CHALMERS UNIVERSITY OF TECHNOLOGY

Abstract

This thesis concerns the interplay of superconductivity and other materials in nanodevices, or more specifically how transport properties are affected.

In the first part of the thesis we consider superconducting junctions with nanowires serving as weak links. A combined experimental and theoretical study has been made, spanning junctions from the short, ballistic, point-contact limit, all the way to the long diffusive limit. Good agreement was found between theory and experiment, even though the longer junctions showed a reduction in the Josephson critical current not explained by the theory.

In the second part of the thesis, we consider a superconductor doped with magnetic impurities. We consider two different limits for the magnetic impurities, random and aligned impurity spins, and calculate how thermodynamic properties are influenced by the introduction of the impurities. The aligned impurity spins induce a background Zeeman field, which has the consequence that the superconducting phase transition changes from being 2nd order to 1st.

The magnetic impurities induce subgap states, so called Yu-Shiba-Rusinov states. By studying the noise and consequently the differential Fano factor, we show that, in the tunneling limit, single particle transfer dominates the transport in the impurity band. For the aligned impurity case, we also find that this transport is completely spin-polarized.

KEYWORDS: Quasiclassical theory of superconductivity, nanowires, Yu-Shiba-Rusinov states, Riccati parametrization, shot noise, differential Fano factor, spin polarized currents

List of Publications

This lists the publications which the thesis is built upon. In the text they are referred to by their Roman numeral.

I Quantized Conductance and Its Correlation to the Supercurrent in a Nanowire Connected to Superconductors

Simon Abay, Daniel Persson, Henrik Nilsson, H. Q. Xu, Mikael Fogelström, Vitaly Shumeiko, and Per Delsing

Nano Letters **13**, 3614 (2013)

DOI: 10.1021/nl4014265

II Charge transport in InAs nanowire Josephson junctions

Simon Abay, Daniel Persson, Henrik Nilsson, Fan Wu, H. Q. Xu, Mikael Fogelström, Vitaly Shumeiko, and Per Delsing

Physical Review B **89**, 214508 (2014)

DOI: 10.1103/PhysRevB.89.214508

III Spectral properties of superconductors with ferromagnetically ordered magnetic impurities

Daniel Persson, Oleksii Shevtsov, Tomas Löfwander, Mikael Fogelström

Physical Review B **92**, 245430 (2015)

DOI: 10.1103/PhysRevB.92.245430

IV Spin-polarized currents and noise in NS junctions with Yu-Shiba-Rusinov impurities

Daniel Persson, Oleksii Shevtsov, Tomas Löfwander, Mikael Fogelström

arXiv:1605.02657 (2016)

Submitted to Physical Review B.

Specification of my contribution to the included papers:

- I-II Papers I-II is a combined theoretical and experimental study of the proximity effect in superconductor-nanowire junctions. I did the theoretical work, and computed and estimated the Josephson effect in the nanowires. In Paper II, a large ensemble of devices were studied with a large range of nanowire lengths. I estimated the number of conducting modes and could by this also draw conclusions on the distribution of the conducting modes in the nanowire. I did the numerical work that made a comparison between theory and experiments possible. I also actively contributed to the writing of the manuscripts.
- III Paper III studies a model of a superconductor doped with magnetic impurities. I derived the self-consistency equations for the impurity self-energies for both the case of aligned and random impurity spins. I also derived the self-consistency equations for the order parameter, and the equation for the critical temperature. I did all the numerical work, and wrote a first draft of the paper. Oleksii Shevtsov later refined the study and we finished the draft together.
- IV Paper IV is an extension of Paper III, where we also study transport properties. I did all the calculations, including deriving the spin-dependent current and noise formulas, and performed all the numerical work. I wrote the paper, including making all the figures, with comments and input from the co-authors.

Acknowledgments

First of all thanks to Mikael Fogelström for accepting me as a student. I knew nothing about superconductivity and Green's functions before I started. Now I like to think that I at least know something.

I want to believe that the best work not is done in a vacuum, and I am indebted to all of my collaborators for not accepting my mediocrity, but always pushing me to better results.

The joyful atmosphere at the Applied Quantum Physics Laboratory is a huge part of why I will always remember this period of my life fondly. Our endless coffee breaks with terrible coffee and discussions about everything from the housing market to the different stages of the stomach flu are highlights!

I also had the pleasure of sharing many lunches and coffees with the experimentalists of the Quantum Device Physics Laboratory, I always enjoyed the company!

There are too many friends over the years that deserve thanks, but you all know who you are. In the immortal words of Queen: Friends will be friends, when you're in need of love they give you care and attention.

Thanks to Mamma and Pappa for always rewarding curiosity and encouraging education, without your help I wouldn't be here. And thanks to Håkan, Anneli, Hans, Annika and Annett for being my family and always being there when needed!

Always, thanks to Sara for believing in me, and for your enduring love.

Contents

Abstract	iii
List of Publications	v
Acknowledgments	vii
Contents	ix
List of Figures	xi
1 Introduction	1
1.1 Nanowires	2
1.2 Superconductors	3
1.3 Noise	4
1.4 Outline of the thesis	6
2 Quasiclassics	7
2.1 Eilenberger equation	7
2.2 Riccati parametrization	9
2.2.1 Bulk solutions	11
2.3 Boundary conditions	11
2.4 Impurities	14
2.4.1 t -matrix equation	14
2.5 Diffusive limit - the Usadel equation	15
2.6 Charge transport	16
2.6.1 Supercurrent in an s-wave point contact	16
2.6.2 Voltage bias	18
2.7 Spin transport	26
2.7.1 SN junction in a Zeeman field	26
2.8 Current fluctuations	29
2.8.1 Noise from an SN junction	32

3	Superconductor-nanowire junctions	35
3.1	Experiment	35
3.1.1	Normal state characteristics	35
3.2	Theoretical model	36
3.2.1	Results	38
3.3	Comparison with experiments	41
4	Magnetic impurities	43
4.1	Impurity self-energy	43
4.2	Gap equation	47
4.3	Density of states	49
4.4	Transport	50
5	Conclusions & Outlook	55
5.1	Outlook	56
	Appendices	59
A	Technical Details	61
A.1	Convolution Product	61
A.2	Properties of the Riccati Equations	61
A.3	Numerics	62
B	Gibbs free energy	65
	Bibliography	67
	Appended papers	77

List of Figures

2.1	Scattering region.	12
2.2	The t -matrix expansion.	15
2.3	(a) Andreev bound states, (b) zero temperature supercurrent	18
2.4	Scattering probabilities at a clean SN interface	20
2.5	Zero temperature conductance of an SN-junction	23
2.6	Multiple Andreev Reflection	24
2.7	Current-voltage characteristics of a superconducting point contact.	25
2.8	Electron and hole contributions to spin and charge currents.	27
2.9	Conductance in a Zeeman split SN-junction	28
2.10	Zero temperature noise of an SN-junction	33
3.1	The experimental and theoretical view of the junctions.	36
3.2	Local density of states across the nanowire	37
3.3	Supercurrent across the nanowire as a function of phase difference.	38
3.4	Current over the nanowire as a function of applied voltage.	39
3.5	Comparison experimental and theoretical values.	40
3.6	The temperature fit of the critical current.	41
4.1	Position of YSR bound state.	46
4.2	Effect of magnetic impurities on critical temperature and order parameter.	48
4.3	Density of states.	50
4.4	Scattering probabilities with magnetic impurities.	51
4.5	Conductance and fluctuations tunneling into YSR bands.	53

1 Introduction

The field of nanophysics is concerned with physics in systems with a size on the order of nanometers. On this length-scale, quantum effects become increasingly important. These are effects that work against traditional electronics, with for example an increased gate-leakage in metal-oxide-semiconductor field-effect transistors (MOSFETs) due to quantum tunneling, at the same time they could be utilized in designing nanostructured electronics. By harnessing these quantum effects one could possibly give an extension to Moore's law [1, 2], which is the observation that the number of transistors on integrated circuits approximately doubles every other year. Moore's law has held true since it was first stated by Gordon Moore in 1965, but is expected to soon run into fundamental limits of traditional manufacturing designs. Using these quantum effects as an advantage instead of a hindrance, new directions have shown promise as a way to extend Moore's law even further. An example of such a direction is spintronics, where the electron's spin instead of charge is utilized for logic operations[3]. Another problem with current manufacturing design is that they are limited size-wise to what is achievable by lithography, but an alternative method allowing for smaller sizes is nanowires[4]. Nanowires can be designed and grown directly in the laboratory.

In any device, the combination of different materials or the inclusion of barriers is a necessity. This makes it important to study and understand how different materials affect each other and whether any new characteristics appear in the interface region of the materials.

It is interesting to consider superconductors both as a source of long-range spin-polarized supercurrents in a spintronics setup, and as part of a nanowire junction to study fundamental quantum phenomena. Through the superconductor, non-locality and quantum coherence enters in a natural way, with for example the possibility to

produce pairs of electrons which are entangled[5].

This thesis concerns the interplay of superconductivity and other materials in nanodevices, or more specifically how transport properties are affected. In the first part of the thesis we study experimentally and theoretically how transport in superconductor-nanowire junctions can be modeled. The second part concerns a superconductor with a concentration of magnetic impurities. We investigate how thermodynamic properties change by the introduction of the impurities and calculate how transport characteristics, such as charge transport and fluctuations, are affected.

1.1 Nanowires

The electronics industry has so far limited themselves to using a, so called, top-down approach, where bulk materials are carved into a desired shape. This approach is dimension-wise limited to what is achievable using lithographic techniques. Another promising route is the bottom-up approach, where tiny, hair-like wires are designed and grown in a laboratory. The diameters of these wires can be less than even 10 *nm*[6], awarding them the name nanowires, while the length on the other hand can be on the order of microns. The use of semiconducting nanowires is prompted by their relative ease to manufacture, where the control of dimension, location, and composition, amongst other properties, is extremely precise. This makes nanowires promising as a way of having self-assembling electronics in the future[7, 8].

The nanowires are effectively one-dimensional objects, where the movement of the conduction electrons are highly restricted to propagation in the length direction of the wires. This strong confinement of the nanowire also affects the electronic properties of the nanowires. If the diameter of the nanowire is comparable to the Fermi wavelength of the conduction electrons, the energy spacing of the conducting modes will be significant, allowing the controlled access to individual channels, and the chance to observe conductance quantization, see Ref. [9] and Paper I.

The extreme control of the growth stage enables one to create nanowire heterostructures, by varying the nanowire material in the growth direction. The difference in the band structure of the different materials then creates tunnelbarriers and allows for defining, for example, quantum dots[10].

Nanowires can also serve as a connecting weak link between superconductors, allowing a supercurrent to flow between them. Semiconducting nanowires in proximity with a superconductor, with an externally applied magnetic field, have been predicted to hold the sought-after Majorana quasi-particles[11, 12]. The Majorana quasi-particle is a topologically protected excitation that has been proposed as a building block in a quantum computation setup[13].

1.2 Superconductors

At the beginning of the last century much of the physics at temperatures close to the absolute zero was shrouded in mystery, since there existed no way to reach these temperatures. Kamerlingh Onnes was one of the physicists that devoted much time to developing schemes by which he could reach ever lower temperatures, and eventually in 1908 succeeding in liquefying hydrogen. He worked on improving this apparatus and had by 1911 developed a helium cryostat, able to maintain the liquid helium at a constant low temperature, and was ready to start investigating other substances at these temperatures.

At this time, many competing theories existed on what behavior the electrical resistance would show at absolute zero. Kelvin thought that the electrons would be frozen in place at absolute zero, making the resistance infinite, Dewar thought that the resistance would smoothly approach zero for lower temperatures, while Matthiessen thought that the resistance would reach a finite value since the resistance due to impurities would dominate. With his new helium cryostat, Kamerlingh Onnes turned to this problem. He measured the resistance of mercury¹ as the temperature decreased and found to his astonishment that at a temperature close to 4.2 K the resistance suddenly vanished[14]. Kamerlingh Onnes had discovered a new phase of matter, which he dubbed superconductivity. His work on low-temperature physics, which among other things led to the liquefying of helium, awarded him the Nobel prize in physics two years later and was the starting point of the research field of superconductivity.

In 1933 it was followed by the discovery[15] by Meißner and Ochsenfeld that superconductors are perfect diamagnets, and will expel (almost) any externally applied magnetic field. It would take until 1957 before a complete microscopic theory of superconductivity was put forward by Bardeen, Cooper, and Schrieffer[16], the so called BCS theory. In the BCS theory superconductivity is possible through the creation of pairs of electrons, so called Cooper pairs[17], in the material. The pairing of the electrons is possible by an effectively attractive interaction between the electrons, mediated by an electron-phonon coupling. By pairing up, the Cooper pairs take on some bosonic traits and condense in a common ground state. The condensation of the Cooper pairs opens an energy gap around the Fermi energy in the density of states of the superconductors. In this energy gap single particle excitations are forbidden, which means that scattering with energies below this gap is impossible. This is a simple way of thinking about why the resistance in superconductors vanish.

Shortly after, it was predicted by Josephson that a junction made of two superconductors connected by an insulating layer would support tunneling of Cooper pairs, producing a current without any applied voltage[18]. This is true even if we replace the insulating layer with an extended piece of normal metal. The intuitive feeling is perhaps that the superconducting gap would completely prohibit transport at energies

¹He used mercury since he could produce a very clean sample, thereby excluding impurity effects.

below it. But what actually happens is that an electron incident from the normal metal, when it hits the superconducting gap, will form a Cooper pair inside the superconductor by producing a hole that propagates back into the normal metal. By doing so, the forbidden single-particle excitation is circumvented and a charge of $2e$ is transferred to the superconductor, since a new Cooper pair is formed. This process, where an incident electron is retro-reflected as a hole, is called Andreev reflection[19]. At the same time a phenomenon dubbed the proximity effect[20, 21] was discussed. The proximity effect describes how Cooper pairs leak into the normal metal, thereby giving it characteristics normally only found in superconductors. In the end, it turned out that Andreev reflection and the proximity effect just are two different viewpoints of the same kind of effect.

In conventional superconductors, such as Hg or Al, the Cooper pairs have a spin-singlet pairing, meaning that the pairs are made of electrons with opposite spins. This makes them susceptible to detrimental effects of spin-dependent scattering, which also was shown already in the 1960s[22], with a linear decrease in both the transition temperature and the order parameter for even small impurity concentrations. But spin-effects are not always detrimental. In hybrid structures made of ferromagnets and superconductors it has been shown that long-range spin-triplet correlations may be induced. For a review on the subject, see Ref. [23]. Spin-triplet correlations are pairing between electrons of the same spin, which due to their long-range supercurrents and their use as a possible controllable source of spin states, among other things, make them promising for use in spintronics applications[24, 25, 26]. Spintronics is an emerging field that uses the electron's spin instead of charge for electronic devices.

In the late 1960s it was also shown that magnetic impurities with classical spins will induce subgap states[27, 28, 29] in conventional superconductors. This topic has seen a resurgence in popularity in the last half-decade. This newfound interest has two explanations; the last decade has brought a huge technological advancement in the ability to manufacture and control these type of systems, even down to the single impurity level[30, 31] and it has also been shown that special arrangements of the impurities will give rise to topologically protected states[32, 33, 34, 35, 36].

1.3 Noise

In the last decade it has become more and more evident that it is important to not only consider the charge current, but to also consider its fluctuations. Some information that vanishes in the average current, such as statistics and charge of the current carriers, can still be seen in the fluctuations.

In an electrical conductor there are many sources of noise. Perhaps the first noise that comes to mind is noise caused by thermal excitations. For non-zero temperatures, the occupation numbers of the states of a system are not fixed, rather they will fluctuate. This gives rise to a non-zero current, which of course is zero on average,

but that fluctuates in time. This thermal noise is commonly called Johnson-Nyquist noise[37, 38], and it relates the fluctuations in the conductor to its conductance and temperature. The Johnson-Nyquist noise is nothing else but a manifestation of the fluctuation-dissipation theorem, which, simply put, states that fluctuations and dissipation are related in equilibrium[39, 40]. Since we have this relationship between the equilibrium current fluctuations and the conductance we will gain nothing new from studying the thermal noise.

Another form of noise in a conductor comes from the discreteness of the electrical charge of the current carriers. This noise is called the shot noise[41], a name that can be understood by the thought of “shooting” individual, uncorrelated, charges at a conductor. Shot noise can also be called Poisson noise, since it can be modeled by a Poisson process. A simple way to understand shot noise, is to think about coin tosses. After many tosses, the difference between the number of heads and tails will be tiny but if we instead repeatedly perform an experiment with only a few tosses, the outcome will fluctuate a lot. In the same way as the fluctuations in the coin toss outcome will vanish for larger number of coin tosses, the shot noise tends to not be the dominating noise source for large currents.

In tunnel junctions there is a simple relation between the fluctuations and the time-averaged current

$$S = 2qj. \quad (1.1)$$

where q is the effective charge of the current carriers. This relation between the shot noise, average current and the charge of the current carriers was used to definitely show that the charges in the fractional quantum Hall effect had the value $q = e/3$ [42, 43].

Away from the tunneling case it can be shown that the noise is proportional to the product of the reflection and transmission probability of the conductor, $\propto \mathcal{D}\mathcal{R}$. [44, 45] The consequence of this is that the shot noise actually will identically vanish for a completely open and a completely closed channel, and take its maximum value for $\mathcal{D} = 1/2$. That the fluctuations vanish for the open and closed cases can be understood by thinking of the noise as the fluctuations between different transport channels. When the conductor is completely transparent or completely reflecting, there exist only one possibility. There is no other transport channel to fluctuate with.

The problem of shot noise in a superconducting setup has been studied quite a bit. Khlus[46] looked at a superconductor connected by a tunnel junction with arbitrary transparency to a normal metal, and found that the noise spectrum is highly non-linear at sub-gap voltages. For a transparency $\mathcal{D} = 1$, he found that the high voltage fluctuations do not vanish, as in the normal case, but rather the noise tends to a fixed value of $S = 8\Delta_0/15R_N$, where Δ_0 is the superconducting gap and R_N the normal state resistance of the interface. The reason for this “excess” noise is the existence of the Andreev reflection process at the interface, which introduces a separate process to fluctuate with. Following him a number of people[47, 48, 49, 50] could show by using different techniques that the Andreev reflection process play an important role in the noise. The

double charge of the Cooper pair is visible in the doubling of the low voltage noise to current ratio compared to the normal state case.

With multiple superconductors the complexity of the problem grows, with the possibility of multiple Andreev reflections (MAR). For decreasing voltages the MAR roughly transfers a charge $q \propto 1/V$, from which one would expect a similar enhancement of the fluctuations. This was also shown theoretically by several different groups[51, 52, 53]. Experimentally, this was qualitatively seen by Dieleman *et al.*[54] and later quantitatively confirmed by Cron *et al.*[55].

A comprehensive review on the subject of shot noise, both in the normal and the superconducting state, has been written by Blanter and Büttiker [45].

1.4 Outline of the thesis

This thesis consists of two distinctly different, yet related, parts. One concerned with transport through superconductor-nanowire junctions, and the other with thermodynamics and transport properties of a superconductor with a concentration of magnetic impurities.

Even though these may look like separate topics there are many things connecting them. First of all is the fact that they both concern superconductivity. The nanowires are connected to superconductors, and we study how the magnetic impurities affect superconductors. Secondly, is the fact that we for both of our systems calculate transport characteristics. And finally, all through the thesis we use the same theoretical framework to solve the problem, the quasiclassical theory of superconductivity.

The outline of the thesis is as follows: In Chapter 2 we will review the quasiclassical theory of superconductivity, which is the general theoretical framework that is used in the thesis, and we will also give some simple examples of its usage. In Chapter 3 we will present the theoretical model that we used to explain the measurements that were made in Papers I and II. In Chapter 4, a model of a superconductor with a concentration of magnetic impurities is presented. General results on thermodynamics, on one hand, and transport measurements, on the other, is then shown. These results were the basis of Papers III and IV. Finally in Chapter 5 we will present our conclusions, and discuss possible future directions of the work.

2

Quasiclassics

The idea behind the quasiclassical formulation of superconductivity is that all processes relevant to the physics of superconductivity happen on a scale that is much smaller than the Fermi energy [56, 57]. The Green's functions can then be decomposed into a fast oscillating component and a slowly varying envelope that varies on scale with the superconducting coherence length. These fast oscillating components can then be integrated out and we are left with a more manageable theory that still can calculate all relevant physical observables, as long as all energy scales in the system are small compared to the Fermi energy. A problem arises when dealing with interfaces, since in the interface region the electronic potential may change very rapidly on a microscopic length scale. This problem is dealt with by deriving boundary conditions for the quasiclassical Green's function in terms of the microscopic ones.

In this Chapter we will briefly try to show the general idea behind the derivation of the quasiclassical equations, for a detailed derivation we refer the reader to Refs. [58, 59]. Next we will present a parametrization, which is useful for numerical studies, and finally at the end of the chapter we will, as a demonstration, solve some simpler problems using the formalism presented in the Chapter.

2.1 Eilenberger equation

The object of interest in quasiclassical theory is the quasiclassical Green's function, which is the full Gor'kov Green's function with the fast oscillating components integrated out [58],

$$\check{g}(\hat{p}, R, \varepsilon, t) = \frac{1}{a} \int_{-\varepsilon_c}^{\varepsilon_c} d\xi_p \hat{\tau}_3 \check{G}(p, R, \varepsilon, t),$$

where the factor $1/a$ is a normalization factor, ε_c is a cut-off in energy and $\check{\zeta}_p = v_F(p - p_F)$. The Green's function \check{g} is in general a 8×8 matrix, in the combined Keldysh \times Nambu \times spin-space. The “ $\check{\cdot}$ ” denote a 2×2 matrix structure in Keldysh [60] space

$$\check{g} = \begin{pmatrix} \hat{g}^R & \hat{g}^K \\ 0 & \hat{g}^A \end{pmatrix},$$

where the Retarded (R) and Advanced (A) components contain information about the quasiclassical spectra while the Keldysh (K) about the dynamics of the system. The “ $\hat{\cdot}$ ” denote a 2×2 matrix structure in Nambu, or particle-hole, space. Each component of the Nambu matrix is then a 2×2 matrix in Pauli spin-space. We will let $\hat{\tau}_i$ denote Pauli matrices in Nambu space, and σ_i in spin-space.

In deriving the quasiclassical equations we start from the Dyson equation for the full Gor'kov Green's function

$$\left(\check{G}_0^{-1} - \check{\Sigma}[\check{G}] \right) \circ \check{G} = \check{1}, \quad (2.1)$$

where the “ \circ ” is a convolution product, a matrix product in Nambu-space followed by an integral over common energy or time variables, see Appendix A.1. \check{G}_0 is the free Green's function and $\check{\Sigma}$ the self-energy. The self-energy $\check{\Sigma}$ is a functional of the full Green's function \check{G} . By expanding the self-energy in orders of $k_B T_c / E_F, \hbar / p_F \xi_0, \dots \ll 1$ it can be shown to be weakly momentum dependent[58], while the Green's function it appears together with is sharply peaked around the Fermi surface. This allows us to approximate the self-energy with its Fermi surface value, $\check{\Sigma}(\mathbf{p}, \dots) \rightarrow \check{\Sigma}(\mathbf{p}_F, \dots)$, and replace $\check{\Sigma}(\mathbf{p}_F, \dots)$ with its quasiclassical equivalent $\check{\sigma}$.

The unperturbed Green's function is in Nambu space given by $\check{G}_0^{-1} = \varepsilon \hat{\tau}_3 \check{1} - \check{\zeta}_p$. So we have the Dyson equation

$$(\varepsilon \hat{\tau}_3 \check{1} - \check{\zeta}_p - \check{\sigma}) \circ \check{G} = \check{1}.$$

Now we would like to take the integral over $\check{\zeta}_p$, and replace all the full \check{G} 's with the quasiclassical \check{g} , but there is a problem with the term $\check{\zeta}_p \circ \check{G}$, since it is not bounded. Subtracting the equivalent right-hand Dyson equation

$$\check{G} \circ (\varepsilon \hat{\tau}_3 \check{1} - \check{\zeta}_p - \check{\sigma}) = \check{1},$$

we can expand $[\check{\zeta}_p, \check{G}]_\circ$ to lowest order, canceling all of the inconvenient terms. We are then left with something that can be integrated. The resulting transport equation is the so called Eilenberger [56] equation¹,

$$[\varepsilon \hat{\tau}_3 \check{1} - \check{\sigma}[\check{g}], \check{g}]_\circ + i \hbar \mathbf{v}_F \cdot \nabla \check{g} = 0, \quad (2.2)$$

where $\check{\sigma}$ contains all self-energies like the superconducting order parameter, impurity potentials and external fields. The Eilenberger equation describes quasi-particles

¹Except to be extra clear at certain points, such as here, we will work in units so that $\hbar = 1$.

moving with the Fermi velocity, \mathbf{v}_F , along classical trajectories in space. For the Retarded/Advanced components we have $\varepsilon \rightarrow \varepsilon \pm i\delta$, where δ is an infinitesimal, while the Matsubara[58] propagator is obtained from the Retarded (Advanced) one for positive (negative) energies through $\varepsilon \rightarrow i\varepsilon_n$, with $\varepsilon_n = 2\pi k_B T(n + 1/2)$.²

In making the “left-right” trick, we lose some information, so that the Eilenberger equation, eq. (2.2), does not determine the Green’s function uniquely. Since the Eilenberger equation is homogeneous and the convolution product associative, it can even be shown that if \check{g} is a solution to eq. (2.2), then so is any multiple of it, $\check{g} \circ \dots \circ \check{g}$. To restore this information Eilenberger[56, 61] found that a normalization condition is needed,

$$\check{g} \circ \check{g} = -\pi^2 \check{1}.$$

Since this is a mean-field theory we will also need selfconsistency equations for the self-energies, like the gap and impurity scattering.

The bulk solution to the Eilenberger equation looks like

$$\hat{g}^{R,A} = \begin{pmatrix} g & fi\sigma_y \\ i\sigma_y \tilde{f} & \sigma_y \tilde{g}\sigma_y \end{pmatrix}^{R,A} = -\pi \frac{\epsilon^{R,A} \hat{\tau}_3 - \Delta_0 i\sigma_y \hat{\tau}_1}{\sqrt{\Delta_0^2 - (\epsilon^{R,A})^2}} \quad (2.3)$$

$$\hat{g}^K = (\hat{g}^R - \hat{g}^A) \tanh \frac{\varepsilon}{2T},$$

where Δ_0 is the order parameter, and $\tanh \varepsilon/2T = 1 - 2f_F(\varepsilon)$ is directly related to the Fermi function.

2.2 Riccati parametrization

In numerical studies the problem of solving the transport equations is simplified considerably if a certain parametrization is used [62, 63, 64]. If we write \hat{g} in terms of two coherence functions $\gamma^{R,A}$, $\tilde{\gamma}^{R,A}$ and two distribution functions x, \tilde{x} the boundary value problem for \hat{g} is transformed into an initial value problem along trajectories in phase space, meaning that if the value of the coherence functions is known at the start of the trajectory the value of it along the entire trajectory can be calculated. The coherence functions can be thought of as the local probability amplitude of Andreev conversion[65, 64], from a hole-like to a electron-like (γ) quasi-particle and from electron-like to hole-like ($\tilde{\gamma}$). This also means that the coherence functions have to vanish in the normal state.

With this parametrization, the Eilenberger equations are turned into uncoupled stable differential equations of Riccati type. Another neat fact is that with this parametrization the normalization condition is automatically taken care of.

²For equilibrium properties we can choose to either use Keldysh or Matsubara propagators. The Matsubara route is usually to prefer because of numerical stability. The recipe is then $\hat{g}^K \rightarrow \hat{g}^M$ and $\int d\varepsilon/4\pi i \rightarrow k_B T \sum_{\varepsilon_n}$

The Green's functions are in terms of the coherence functions and the distribution functions given as

$$\hat{g}^{R,A} = \mp \pi i \hat{N}^{R,A} \circ \begin{pmatrix} 1 + \gamma \circ \tilde{\gamma} & 2\gamma \\ -2\tilde{\gamma} & -(1 + \tilde{\gamma} \circ \gamma) \end{pmatrix}^{R,A} \quad (2.4)$$

and

$$\hat{g}^K = -2\pi i \hat{N}^R \circ \begin{pmatrix} 1 & \gamma \\ -\tilde{\gamma} & -1 \end{pmatrix}^R \circ \begin{pmatrix} x & 0 \\ 0 & \tilde{x} \end{pmatrix} \circ \begin{pmatrix} 1 & \gamma \\ -\tilde{\gamma} & -1 \end{pmatrix}^A \circ \hat{N}^A, \quad (2.5)$$

where the plus (minus) refers to the Retarded (Advanced) component and

$$\hat{N}^{R,A} = \begin{pmatrix} (1 - \gamma \circ \tilde{\gamma})^{-1} & 0 \\ 0 & (1 - \tilde{\gamma} \circ \gamma)^{-1} \end{pmatrix}^{R,A}.$$

In general $\gamma^{R,A}$, $\tilde{\gamma}^{R,A}$, x , and \tilde{x} are 2×2 spin matrices. The “ \sim ” describe a particle-hole conjugation defined as $\tilde{a}(\varepsilon, \mathbf{p}_F, R) = a(-\varepsilon^*, -\mathbf{p}_F, R)^*$.

The transport equations for the coherence functions are

$$\begin{aligned} (i\hbar \mathbf{v}_F \cdot \nabla + 2\varepsilon) \gamma^{R,A} &= [\gamma \circ \tilde{\Delta} \circ \gamma + \Sigma \circ \gamma - \gamma \circ \tilde{\Sigma} - \Delta]^{R,A} \\ (i\hbar \mathbf{v}_F \cdot \nabla - 2\varepsilon) \tilde{\gamma}^{R,A} &= [\tilde{\gamma} \circ \Delta \circ \tilde{\gamma} + \tilde{\Sigma} \circ \tilde{\gamma} - \tilde{\gamma} \circ \Sigma - \tilde{\Delta}]^{R,A} \end{aligned} \quad (2.6)$$

and for the distribution functions

$$\begin{aligned} i\hbar (\mathbf{v}_F \cdot \nabla + \partial_t) x - [\gamma \circ \tilde{\Delta} + \Sigma]^R \circ x - x \circ [\Delta \circ \tilde{\gamma} - \Sigma]^A &= \\ -\gamma^R \circ \tilde{\Sigma}^K \circ \tilde{\gamma}^A + \Delta^K \circ \tilde{\gamma}^A + \gamma^R \circ \tilde{\Delta}^K - \Sigma^K & \\ i\hbar (\mathbf{v}_F \cdot \nabla - \partial_t) \tilde{x} - [\tilde{\gamma} \circ \Delta + \tilde{\Sigma}]^R \circ \tilde{x} - \tilde{x} \circ [\tilde{\Delta} \circ \gamma - \tilde{\Sigma}]^A &= \\ -\tilde{\gamma}^R \circ \Sigma^K \circ \gamma^A + \tilde{\Delta}^K \circ \gamma^A + \tilde{\gamma}^R \circ \Delta^K - \tilde{\Sigma}^K. & \end{aligned} \quad (2.7)$$

The Retarded and Advanced coherence functions are, of course, related so that it will always be enough to only solve for one or the other, and then use general symmetries to obtain the other.

The solution to the transport equations are obtained by solving for them, starting from an initial value, along their characteristics, which is straight trajectories in space. The trajectories are for any value of \mathbf{p}_F defined by the Fermi velocity $\mathbf{v}_F(\mathbf{p}_F)$. Parametrizing the trajectories as $R = \hat{v}_F \cdot \mathbf{s} + c$, with \hat{v}_F being an unit vector parallel to the Fermi velocity, the transport equations turn into ordinary differential equations along their trajectories. The coherence functions turn out to fulfill certain stability criteria; the equations for γ^R , $\tilde{\gamma}^A$ and x are bounded when integrating them along a trajectory (with $\mathbf{v}_F \cdot \mathbf{s} > 0$), while the ones for $\tilde{\gamma}^R$, γ^A and \tilde{x} are stable in the opposite direction (with $\mathbf{v}_F \cdot \mathbf{s} < 0$).

2.2.1 Bulk solutions

In the bulk we, by definition, have no dependence on the position R . We can then write, if the self-energies is diagonal in spin space and the order parameter is singlet, the equilibrium solution for the coherence function in the clean limit as

$$\gamma^{R,A} = -\frac{\Delta_0}{\varepsilon \pm i\Omega}, \quad (2.8)$$

where $\Omega = \sqrt{|\Delta_0|^2 - \varepsilon^2}$. The distribution functions in equilibrium look like

$$x = \left(1 - \gamma^R \tilde{\gamma}^A\right) \tanh\left(\frac{\varepsilon}{2k_B T}\right).$$

Remember that the “tilded” versions are obtained through the tilde-operation, $\tilde{a}(\varepsilon, \mathbf{p}_F, R) = a(-\varepsilon^*, -\mathbf{p}_F, R)^*$.

2.3 Boundary conditions

As mentioned above, the quasiclassical theory gets into problems when considering boundaries and interfaces. The quasiclassical theory is valid as long as all relevant energy scales are small compared to the Fermi energy and changes happen on a length scale of the order of the coherence length. At interfaces where different materials are connected, changes typically happen on an atomic length scale and with an energy scale comparable to the Fermi energy. This means that the quasiclassical formalism is not valid close to boundaries and interfaces, while far away from the interfaces it is. This leads to the necessity to formulate the interface region in a microscopic theory and then connect it to the ‘asymptotic’ quasiclassic region via boundary conditions. Such boundary conditions were first derived for partially transmitting, spin preserving, interfaces by Zaitsev [66] and Kieselmann [67] and were later generalized to include spin-active interfaces by Millis, Rainer and Sauls [68]. In this way, everything going into the interface region were expressed through a normal state scattering matrix which then is connected to the quasiclassical propagators. While this in theory solves the interface problem they are difficult to solve numerically since they contain unphysical solutions that have to be taken care of. These difficulties are all taken care of if the boundary conditions are formulated in terms of the Riccati coherence functions introduced above [63, 69, 70, 64].

As mentioned, an interface region can be connected to the quasiclassical region, through the normal-state scattering matrix. Let us consider such a scattering matrix [68, 69, 70]

$$\mathcal{S} = \begin{pmatrix} \hat{S}_{11} & \hat{S}_{12} \\ \hat{S}_{21} & \hat{S}_{22} \end{pmatrix}.$$

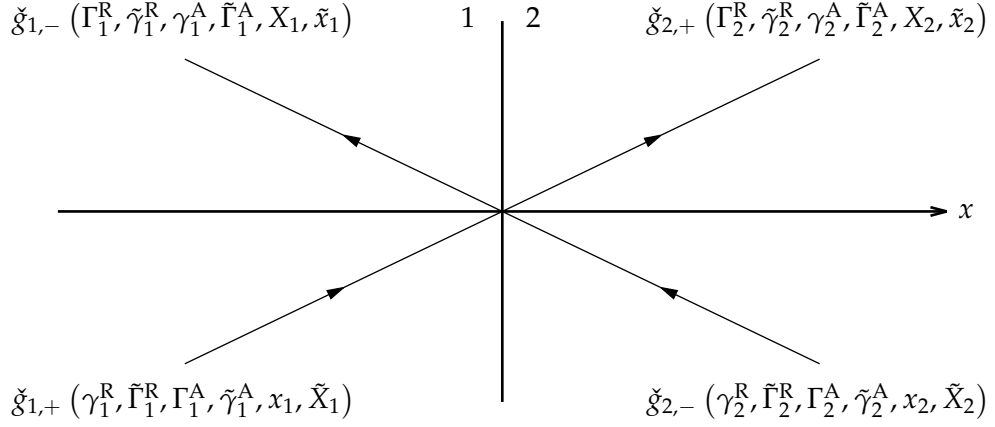


Figure 2.1: The incoming and outgoing trajectories in a scattering region and their respective Green's function, with the dependence of the Green's function on scattered/unscattered coherence functions as indicated. The arrows point in the same direction as the Fermi velocity, \mathbf{v}_F . The label \pm denote if the projection of the Fermi momentum on the x -axis is positive/negative.

The scattering matrix is here written in the combined particle-hole, spin-, and left-right space, i.e. the index 1(2) refers to the left (right) side of the interface. Since this is the normal-state scattering matrix, each of the matrices \hat{S}_{ij} are diagonal in Nambu space,

$$\hat{S}_{ij} = \begin{pmatrix} S_{ij} & 0 \\ 0 & \tilde{S}_{ij} \end{pmatrix},$$

in which the components, in general, are matrices in spin space. We will only discuss specular interfaces, meaning that the momentum parallel to the interface, $\mathbf{p}_{F\parallel}$, is conserved.

In the interface region the coherence and distribution functions can be grouped by whether they are stable integrating from the bulk towards the interface, or from the interface towards the bulk. We will call the ones stable towards the interface unscattered, since they only need as input the bulk value at the start of the trajectory and can be completely determined without any knowledge of the interface region. The ones stable away from the interface are called scattered, and will need an initial value at the interface, which has to be determined from the boundary conditions. We will denote unscattered coherence functions with a small case letter ($\gamma_i^{R,A}, \tilde{\gamma}_i^{R,A}, x_i, \tilde{x}_i$) and scattered with a capital ($\Gamma_i^{R,A}, \tilde{\Gamma}_i^{R,A}, X_i, \tilde{X}_i$). The boundary conditions connect the unknown scattered coherence functions with the known unscattered ones. The trajectories involved in the scattering together with their respective Green's function is shown in fig. 2.1. We also indicate how the Green's functions depend on the scattered and unscattered coherence functions.

In Paper IV we considered a spin-active interface, and investigated effects of spin-

Table 2.1: Scattering amplitudes at an interface, for excitations incident from the 1 side, see fig. 2.1. Amplitudes for excitations incident from the 2 side is obtained through the substitution $1 \leftrightarrow 2$ together with the interchange of barred and unbarred amplitudes. For $r_{ee}^R, r_{hh}^R, r_{eh}^R$ and r_{he}^R we also need to take $\sqrt{\mathcal{R}} \rightarrow -\sqrt{\mathcal{R}}$. The quantity below is defined as $D_{ij}^R = (1 - \mathcal{R}\gamma_j^R\tilde{\gamma}_j^R - \mathcal{D}\gamma_i^R\tilde{\gamma}_j^R)^{-1}$.

$r_{ee}^R = \sqrt{\mathcal{R}} (1 - \gamma_2^R\tilde{\gamma}_2^R) D_{12}^R$	$r_{hh}^R = \sqrt{\mathcal{R}} (1 - \tilde{\gamma}_2^R\gamma_2^R) \tilde{D}_{12}^R$
$t_{ee}^R = \sqrt{\mathcal{D}} (1 - \gamma_2^R\tilde{\gamma}_1^R) D_{21}^R$	$t_{hh}^R = \sqrt{\mathcal{D}} (1 - \tilde{\gamma}_2^R\gamma_1^R) \tilde{D}_{21}^R$
$r_{he}^R = \sqrt{\mathcal{R}} r_{hh}^R \tilde{\gamma}_1^R + \sqrt{\mathcal{D}} \tilde{t}_{hh}^R \tilde{\gamma}_2^R$	$r_{eh}^R = \sqrt{\mathcal{R}} r_{ee}^R \gamma_1^R + \sqrt{\mathcal{D}} \tilde{t}_{ee}^R \gamma_2^R$
$t_{he}^R = -\sqrt{\mathcal{D}} \tilde{r}_{hh}^R \tilde{\gamma}_2^R + \sqrt{\mathcal{R}} t_{hh}^R \tilde{\gamma}_1^R$	$t_{eh}^R = -\sqrt{\mathcal{D}} \tilde{r}_{ee}^R \gamma_2^R + \sqrt{\mathcal{R}} t_{ee}^R \gamma_1^R$

mixing. In the present text we will not discuss this case, but refer the reader to the original paper for details. Here we will consider an interface that preserves spins in the scattering. This makes the scattering matrix scalar in spin-space, and because of inversion symmetry we also have that $S_{ij} = \tilde{S}_{ij}$. We can then write the scattering matrix as

$$\mathcal{S} = \begin{pmatrix} \sqrt{\mathcal{R}} & \sqrt{\mathcal{D}} \\ \sqrt{\mathcal{D}} & -\sqrt{\mathcal{R}} \end{pmatrix}.$$

The boundary conditions can be written in a number of equivalent ways, but our preferred way is how they are written in Ref. [71], which highlight the underlying processes of the boundary conditions in a nice way. In the following passages we summarize their formulation. The boundary conditions are then written as

$$\begin{aligned} \Gamma_1^R &= r_{eh}^R = \sqrt{\mathcal{R}} r_{ee}^R \gamma_1^R + \sqrt{\mathcal{D}} \tilde{t}_{ee}^R \gamma_2^R \\ \tilde{\Gamma}_1^R &= r_{he}^R = \sqrt{\mathcal{R}} r_{hh}^R \tilde{\gamma}_1^R + \sqrt{\mathcal{D}} \tilde{t}_{hh}^R \tilde{\gamma}_2^R \\ X_1 &= r_{ee}^R x_1 r_{ee}^A + \tilde{t}_{ee}^R x_2 \tilde{t}_{ee}^A - \tilde{t}_{eh}^R \tilde{x}_2 \tilde{t}_{eh}^A \\ \tilde{X}_1 &= r_{hh}^R \tilde{x}_1 r_{hh}^A + \tilde{t}_{hh}^R \tilde{x}_2 \tilde{t}_{hh}^A - \tilde{t}_{he}^R x_2 \tilde{t}_{he}^A. \end{aligned} \tag{2.9}$$

The boundary conditions for the trajectories on the other side of the interface are obtained by substituting the indices $1 \leftrightarrow 2$ and interchanging barred and unbarred probability amplitude. We have to be a bit careful here. Because of the way we have written the scattering matrix there will be some minus signs popping up in the expressions for the boundary conditions on the 2 side. So in the expression for Γ_2^R and $\tilde{\Gamma}_2^R$ we also have to take $\sqrt{\mathcal{R}} \rightarrow -\sqrt{\mathcal{R}}$.

The probability amplitudes that the boundary conditions are built of can be understood in a physical sense, $r_{\alpha\beta}^{R,A} (t_{\alpha\beta}^{R,A})$ is the probability amplitude of an incoming β excitation to be reflected (transmitted) as an α excitation. Amplitudes without (with) a bar originate on the 1(2) side of the interface.

In table 2.1 we summarize the possible probability amplitudes at the interface. In principle, these amplitudes are the only thing we will have to calculate for any kind of transport we are interested in. Any extra complication will only come from the calculation of the coherence and distribution functions, but once we have them we know everything about the system.

It is possible to derive relations among the probability amplitudes from considering probability and charge conservation. At this point the relations are quite lengthy so we will refrain from writing them here, but we shall see later when we consider the case of an SN-junction in section 2.6.2 that the relations can be quite insightful.

To simplify numerical calculations when dealing with interfaces we can use general properties of the Riccati equations, reducing the number of iterations that is needed for self-consistency. This is described in Appendix A.2.

2.4 Impurities

Materials found in Nature are usually not pure. Rather they are contaminated with other types of atoms. For that reason it is important to know how our superconductor behaves when being impure, to be able to compare theory with experiments. Another reason why one should be interested in studying impurities in superconductor is that the impurities can induce both other correlations and phases uncommon to find in Nature, but with knowledge of material behavior we can engineer them.

2.4.1 t -matrix equation

For a distribution of impurities dilute enough, we can neglect scattering off multiple impurities, and only include scattering off a single one. The object describing this is the single impurity t -matrix equation,

$$\hat{t}(\varepsilon, \mathbf{p}_F, \mathbf{p}'_F) = \hat{u}(\mathbf{p}_F, \mathbf{p}'_F) + N_F \int \frac{d\Omega_{\mathbf{p}'_F}}{4\pi} \hat{u}(\mathbf{p}_F, \mathbf{p}'_F) \hat{g}(\varepsilon, \mathbf{p}'_F) \hat{t}(\varepsilon, \mathbf{p}'_F, \mathbf{p}'_F), \quad (2.10)$$

here \hat{u} is the impurity potential and N_F the normal state density of states at the Fermi surface.

This equation can be described in diagram[58, 72] form as shown in fig. 2.2. We will be content with studying s -wave, isotropic, impurity scattering, meaning that the impurity potential is independent of momentum. This simplifies eq. (2.10) to

$$\hat{t}(\varepsilon) = \hat{u} + N_F \hat{u} \langle \hat{g}(\varepsilon) \rangle_{\mathbf{p}_F} \hat{t}(\varepsilon),$$

where $\langle \hat{g}(\varepsilon) \rangle_{\mathbf{p}_F} = \int \frac{d\Omega_{\mathbf{p}_F}}{4\pi} \hat{g}(\varepsilon, \mathbf{p}_F)$ is a Fermi surface average of the propagator.

The self-energy for the full distribution of impurities is then given from the t -matrix as

$$\hat{\sigma}(\varepsilon) = n_{imp} \hat{t}(\varepsilon), \quad (2.11)$$

$$\begin{aligned}
\hat{t}(\varepsilon, \mathbf{p}_F, \mathbf{p}'_F) &= \begin{array}{c} \times \\ | \\ \text{---} \end{array} + \begin{array}{c} \times \\ / \quad \backslash \\ \text{---} \end{array} + \begin{array}{c} \times \\ / \quad \backslash \\ \text{---} \end{array} + \dots \\
\hat{u}(\mathbf{p}_F, \mathbf{p}'_F) &\equiv \begin{array}{c} \times \\ | \\ \text{---} \end{array} \quad \hat{g}(\varepsilon, \mathbf{p}_F) \equiv \text{---}
\end{aligned}$$

Figure 2.2: The diagrammatic representation of eq. (2.10), the t -matrix equation.

where n_{imp} is the concentration of impurities. Since the self-energy $\hat{\sigma}$ and the Green's function \hat{g} depend on each other, we will have to solve for them together until we achieve selfconsistency.

2.5 Diffusive limit - the Usadel equation

Before moving on to calculating observables, we should point out that even though the general transport equation for the quasiclassical Green's function is the Eilenberger equation we can in the dirty limit make further simplifications that lead to a diffusion-like equation called the Usadel equation[73, 74]. In this work we will not use this formulation, since we want to be able to consider both the clean limit and of variable degree of disorder, but we will sketch the general idea behind the derivation below, for completeness.

If we are in the dirty limit, where the concentration of impurities is large, the impurity scattering will dominate all other energy scales in the Eilenberger equation. The scattering will randomize the electron trajectories and make the Green's function close to isotropic. By then expanding the Green's function to first order in spherical harmonics, the Eilenberger equation can be shown to reduce to

$$\frac{D}{\pi} \nabla (\check{g} \nabla \check{g}) + [\varepsilon \hat{\tau}_3 \check{1} - \check{\Delta}, \check{g}] = 0, \quad (2.12)$$

where $D = v_F \ell / 3$ is the diffusion constant, which is related to the Fermi velocity, v_F , and the mean free path, ℓ . The dominating energy scale in the diffusive limit is the Thouless energy, given by $E_{th} = \hbar D / L^2$, where L is the size of the system. The diffusive coherence length is given by $\xi_D = \sqrt{D / \Delta_0}$.

The Green's function $\check{g}(R, \varepsilon)$ is in this formulation no longer dependent on the Fermi momentum.

The Usadel equation has successfully been used to, for example, describe problems such as the phase-dependence of the local density of states in a diffusive SNS junction[75, 76], the temperature dependence of the Josephson critical current[77], and the cross-over of the magnetic field-dependence of the critical current from a Fraun-

hofer pattern to a monotonic decay when the width of the SNS junction decreases[78, 79].

2.6 Charge transport

Now we can compute the Green's function everywhere, and we know how to connect it across interfaces. The problem is that the Green's function is not an observable, in its own right. For this we need to compute something that we would actually measure in an experiment. So, for this we turn to transport, and compute both equilibrium and non-equilibrium currents.

In this section we will go through how the observables that we are interested in are expressed in the quasiclassical formulation, and we will also go through a couple of example calculations to show their use.

The charge current is calculated through the Keldysh Green's function[58]

$$j^c = eN_F \int \frac{d\varepsilon}{8\pi i} \int \frac{d\Omega_{\mathbf{p}_F}}{4\pi} \text{Tr} \left[\mathbf{v}_F \hat{\tau}_3 \hat{\delta}^K \right], \quad (2.13)$$

where the Keldysh Green's function can here either depend on an applied bias or a phase difference. In any case the expression for the current looks the same, but the way we have to compute the Green's function differs.

2.6.1 Supercurrent in an s-wave point contact

As a first example we consider the equilibrium current in a clean s-wave point contact. In a point contact the radius of the contact is much smaller than the coherence length and all effects of the point contact on the superconductors may be neglected. This means that we can take the amplitude of the superconducting order parameter to be constant all the way up to the point contact.

Letting the point contact be symmetric so that the magnitude of the order parameter is the same in both of the superconductors, $|\Delta_L| = |\Delta_R| = \Delta_0$, the only thing that differ between them is their relative phase, so $\Delta_L = \Delta_0 e^{i\phi_L}$ and $\Delta_R = \Delta_0 e^{i\phi_R}$. In equilibrium the Keldysh Green's function has the form given by eq. (2.3), while the Retarded and Advanced are written in terms of the coherence functions according to eq. (2.4). Since we consider spin-singlet superconductors, with an interface that not is spin-active, we can write the incoming coherence functions as $\gamma^{R,A} = \gamma_0^{R,A} i\sigma_y$ and $\tilde{\gamma}^{R,A} = \tilde{\gamma}_0^{R,A} i\sigma_y$ (with the same for the outgoing coherence functions). We neglect the effect of the point contact on the superconductors, meaning that $\gamma_0^{R,A}$ and $\tilde{\gamma}_0^{R,A}$ will have their respective bulk values, given by eq. (2.8).

An s-wave superconductor is isotropic, so that there is no dependence on direction, which turns the Fermi surface average in eq. (2.13) into just a difference between an incoming and outgoing trajectory. This make sense from a physical point of view,

since the total current is then just the difference between the current going towards the interface and the current going away from it. The charge current reads

$$j^c = eN_F v_F \int \frac{d\varepsilon}{8\pi i} \text{Tr} \left[\hat{\tau}_3 \left(\hat{g}_+^R - \hat{g}_+^A - \hat{g}_-^R + \hat{g}_-^A \right) \right] \tanh \frac{\varepsilon}{2T},$$

where v_F is the magnitude of the Fermi velocity, and the $+(-)$ denote if the Green's function is incoming (outgoing). Since there is no spin dependence in the problem the trace over the spin- and Nambu-space will just give us a factor 4, so that the current in terms of coherence functions is written as

$$j^c = -\frac{eN_F v_F}{2} \int d\varepsilon \left(\frac{1 - \gamma_0^R r_{he,0}^R}{1 + \gamma_0^R r_{he,0}^R} - \frac{1 - r_{he,0}^A \tilde{\gamma}_0^A}{1 + r_{he,0}^A \tilde{\gamma}_0^A} - \frac{1 - r_{eh,0}^R \tilde{\gamma}_0^R}{1 + r_{eh,0}^R \tilde{\gamma}_0^R} + \frac{1 - \gamma_0^A r_{eh,0}^A}{1 + \gamma_0^A r_{eh,0}^A} \right) \tanh \frac{\varepsilon}{2T}. \quad (2.14)$$

This is a general expression for the equilibrium current across an interface, for the case of a spin-independent Green's function. As long as the coherence functions are determined in a self-consistent manner, it is even valid for the case of impurities or a spatially dependent order parameter.

Plugging in the explicit expressions for the bulk coherence functions from eq. (2.8), and the outgoing coherence functions from eq. (2.9), this simplifies to

$$j^c = -eN_F v_F \int d\varepsilon \text{Im} \left[\frac{D\Delta_0^2 \sin \Delta\phi}{\varepsilon^2 - \Delta_0^2 \left(1 - D \sin^2 \frac{\Delta\phi}{2} \right)} \right] \tanh \frac{\varepsilon}{2T}, \quad (2.15)$$

where $\Delta\phi = \phi_R - \phi_L$ is the relative phase difference between the superconductors. The poles in the current, $\varepsilon_b^\pm = \pm\Delta_0 \sqrt{1 - D \sin^2 \frac{\Delta\phi}{2}}$, define bound states, the so called Andreev bound states, see fig. 2.3 (a). The Andreev bound states are the states that carry the supercurrent.

The integral in eq. (2.15) can be evaluated using residue theory, yielding

$$j^c(T) = e\pi v_F N_F D \Delta_0^2 \frac{\sin \Delta\phi}{\varepsilon_b^+} \tanh \left(\frac{\varepsilon_b^+}{2T} \right).$$

In fig. 2.3 (b) we have plotted the zero temperature supercurrent as a function of phase difference for different transmission coefficient.

In the tunneling limit, ($D \ll 1$), we can expand the expression for the current giving

$$j^c(T) = eN_F v_F \pi D \Delta_0^2 \sin \Delta\phi \tanh \left(\frac{\Delta_0}{2T} \right),$$

to obtain the Ambegaokar-Baratoff[80, 81] result.

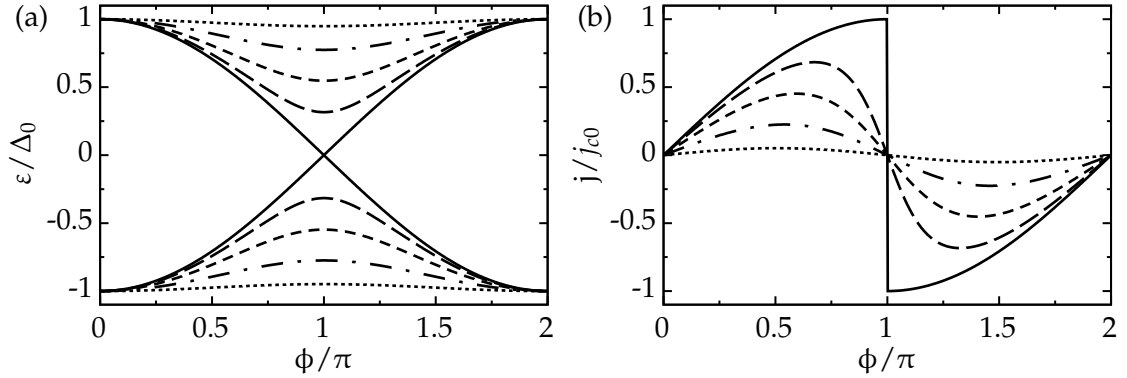


Figure 2.3: (a) The Andreev bound states and (b) the zero temperature supercurrent as a function of phase for a symmetric s-wave point contact. The supercurrent has been normalized with the critical current for a completely transparent point contact, $j_{c0} = 2\pi e v_F N_F \Delta_0$. The different curves correspond to different transmission coefficient of the point contact. The transmission is $D = 1.0, 0.9, 0.7, 0.4, 0.1$ from top to bottom in (b). The curves in (a) with the corresponding line style have the same transparency.

2.6.2 Voltage bias

In general the problem of voltage biasing a superconducting junction is quite involved. Since applying a voltage across a junction will make the phase time-dependent, as stated by the second Josephson relation[82],

$$\hbar \frac{\partial}{\partial t} \phi = 2eV, \quad (2.16)$$

we will have to take into account such effects as multiple Andreev reflection (MAR), where charges at energies below the gap will perform many Andreev reflections in succession to be able to overcome the gap.

But before we get to that, we will start with discussing the simpler problem of a voltage biased superconductor-normal metal junction.

SN junction

Let us consider a system without any spin-dependence, consisting of a normal metal (1) connected to a superconductor (2) via a point contact. This is a problem that has been extensively studied before, see e.g. the seminal paper by Blonder, Tinkham and Klapwijk [83]. Just as in the previous section, we can assume that all incoming coherence functions take their respective bulk values, and can be written as $\gamma^{R,A} = \gamma_0^{R,A} i\sigma_y$ and $\tilde{\gamma}^{R,A} = \tilde{\gamma}_0^{R,A} i\sigma_y$. We will also assume the incoming distribution functions to take their bulk value, and will choose the Fermi level in the superconductor as our reference point, meaning that the distribution functions from the normal side will be shifted by

the applied voltage. This gives us the incoming distribution functions as

$$\begin{aligned} x_1 &= \tanh \frac{\varepsilon - eV}{2T} & x_2 &= (1 + \gamma_0^R \tilde{\gamma}_0^A) \tanh \frac{\varepsilon}{2T} \\ \tilde{x}_1 &= -\tanh \frac{\varepsilon + eV}{2T} & \tilde{x}_2 &= -(1 + \tilde{\gamma}_0^R \gamma_0^A) \tanh \frac{\varepsilon}{2T}. \end{aligned} \quad (2.17)$$

The coherence functions are, in a sense, a measure of how big the superconducting correlations are. In a bulk normal metal these correlations will by necessity vanish, which mean that all incoming coherence functions are zero in the normal metal, while in the superconductor they are given by eq. (2.8).

With a voltage bias the basic calculation follow the same lines as when computing the equilibrium current, starting with eq. (2.13), but since we no longer are in equilibrium we have to consider the full Keldysh Green's function, see eq. (2.5). It is convenient to compute the current on the normal side. As mentioned, all incoming coherence functions vanish there and the Keldysh Green's functions will take a simple form. The Green's function on the incoming trajectory is

$$\hat{g}_{1,+}^K = -2\pi i \begin{pmatrix} x_1 & x_1 r_{he,0}^A \\ r_{he,0}^R x_1 & \tilde{X}_{1,0} + r_{he,0}^R x_1 r_{he,0}^A \end{pmatrix}$$

while on the outgoing one

$$\hat{g}_{1,-}^K = -2\pi i \begin{pmatrix} X_{1,0} + r_{eh,0}^R \tilde{x}_1 r_{eh,0}^A & \tilde{x}_1 r_{eh,0}^A \\ r_{eh,0}^R \tilde{x}_1 & \tilde{x}_1 \end{pmatrix}.$$

The Fermi velocity will only give us a relative minus-sign for the incoming and outgoing trajectory in the Fermi surface average in the current, see eq. (2.13). The difference of the Green's functions is then

$$\hat{g}_{1,+}^K - \hat{g}_{1,-}^K = -2\pi i \begin{pmatrix} x_1 - \left(X_{1,0} + r_{eh,0}^R \tilde{x}_1 r_{eh,0}^A \right) & x_1 r_{he,0}^A - \tilde{x}_1 r_{eh,0}^A \\ r_{he,0}^R x_1 - r_{eh,0}^R \tilde{x}_1 & \left(\tilde{X}_{1,0} + r_{he,0}^R x_1 r_{he,0}^A \right) - \tilde{x}_1 \end{pmatrix}. \quad (2.18)$$

In the present case, without any spin-dependence, the scattered distribution functions are given by

$$\begin{aligned} X_{1,0} &= r_{ee,0}^R x_1 r_{ee,0}^A + \bar{t}_{ee,0}^R x_2 \bar{t}_{ee,0}^A + \bar{t}_{eh,0}^R \tilde{x}_2 \bar{t}_{eh,0}^A \\ \tilde{X}_{1,0} &= r_{hh,0}^R \tilde{x}_1 r_{hh,0}^A + \bar{t}_{hh,0}^R \tilde{x}_2 \bar{t}_{hh,0}^A + \bar{t}_{he,0}^R x_2 \bar{t}_{he,0}^A, \end{aligned} \quad (2.19)$$

and the components of the probability amplitudes that are needed for the current are

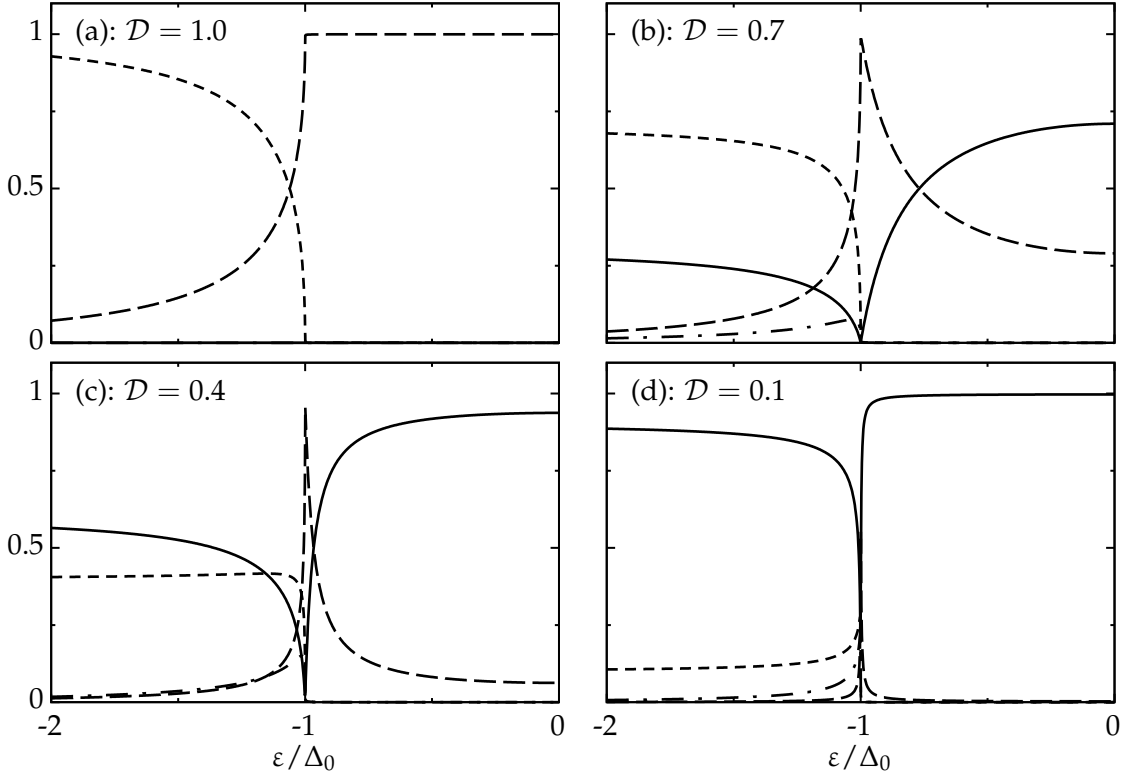


Figure 2.4: The scattering probabilities at an NS interface for different transparency of the interface, as indicated in the figure. The full line are for normal reflection, the long dashed for Andreev reflection, the short dashed for normal transmission and the dash-dotted for transmission with branch conversion. The scattering probabilities are even functions around the Fermi surface, $\varepsilon = 0$.

written as

$$\begin{aligned}
 r_{ee,0}^R &= \sqrt{\mathcal{R}} \frac{1 + \gamma_0^R \tilde{\gamma}_0^R}{D_0^R} & \bar{t}_{ee,0}^R &= \sqrt{\mathcal{D}} \frac{1}{D_0^R} \\
 r_{he,0}^R &= \mathcal{D} \frac{\tilde{\gamma}_0^R}{D_0^R} & \bar{t}_{he,0}^R &= \sqrt{\mathcal{R}\mathcal{D}} \frac{\tilde{\gamma}_0^R}{D_0^R} \\
 r_{hh,0}^R &= \sqrt{\mathcal{R}} \frac{1 + \gamma_0^R \tilde{\gamma}_0^R}{D_0^R} & \bar{t}_{hh,0}^R &= \sqrt{\mathcal{D}} \frac{1}{D_0^R} \\
 r_{eh,0}^R &= \mathcal{D} \frac{\gamma_0^R}{D_0^R} & \bar{t}_{eh,0}^R &= \sqrt{\mathcal{R}\mathcal{D}} \frac{\gamma_0^R}{D_0^R},
 \end{aligned} \tag{2.20}$$

with $D_0^R = 1 + \mathcal{R}\gamma_0^R \tilde{\gamma}_0^R$.

It is also convenient to define scattering probabilities as

$$R_{\alpha\beta} = \epsilon_{\alpha\beta} r_{\alpha\beta,0}^R r_{\alpha\beta,0}^A \quad \text{and} \quad T_{\alpha\beta} = \epsilon_{\alpha\beta} t_{\alpha\beta,0}^R t_{\alpha\beta,0}^A, \tag{2.21}$$

Table 2.2: The connection between the A, B, C, D factors in Ref. [83] and the terms in eq. (2.2). A is the probability of Andreev reflection, B the probability of normal reflection, C the probability of normal transmission, and D the probability of transmission with branch conversion.

BTK	Here
A	R_{he}
B	R_{ee}
C	$\bar{T}_{ee} (1 - \tilde{\gamma}_0^R ^2)$
D	$\bar{T}_{he} (1 - \gamma_0^R ^2)$

where $\epsilon_{\alpha\beta} = \pm 1$ is an extra minus-sign that is needed for the terms with $\alpha = \beta$, coming from when we relate the Advanced scattering amplitude to the complex conjugated Retarded ones.

If we now consider particle current conservation we can, as mentioned above, derive relations among these amplitudes. We get

$$1 = r_{ee,0}^R r_{ee,0}^A - r_{he,0}^R r_{he,0}^A + \frac{t_{ee,0}^R}{1 + \bar{r}_{eh,0}^R \tilde{\gamma}_0^R} \frac{t_{ee,0}^A}{1 + \gamma_0^A \bar{r}_{eh,0}^A} (1 + \tilde{\gamma}_0^R \gamma_0^A) - \frac{t_{he,0}^R}{1 + \gamma_0^R \bar{r}_{he,0}^R} \frac{t_{he,0}^A}{1 + \bar{r}_{he,0}^A \tilde{\gamma}_0^A} (1 + \gamma_0^R \tilde{\gamma}_0^A),$$

which can be shown to be

$$\begin{aligned} 1 &= r_{ee,0}^R r_{ee,0}^A - r_{he,0}^R r_{he,0}^A + \bar{t}_{ee,0}^R \bar{t}_{ee,0}^A (1 + \tilde{\gamma}_0^R \gamma_0^A) - \bar{t}_{he,0}^R \bar{t}_{he,0}^A (1 + \gamma_0^R \tilde{\gamma}_0^A) \\ &= R_{ee} + R_{he} + \bar{T}_{ee} (1 - |\tilde{\gamma}_0^R|^2) + \bar{T}_{he} (1 - |\gamma_0^R|^2). \end{aligned} \quad (2.22)$$

The terms in this expression correspond to the A, B, C, D factors in the 1982 BTK[83] paper, see Table 2.2. We can note that while Andreev reflection is a two-particle process, both normal transmission and transmission with branch conversion are single-particle processes. These probabilities are plotted in fig. 2.4, for different transmission of the interface. For a high transparency the dominating process below the gap is Andreev reflection, with it being the only available subgap process for a completely transparent interface. With an increased reflection at the interface the probability of Andreev reflection is reduced while the normal reflection probability increases. With a non-zero reflection we also get a finite probability to branch convert in the transmission, meaning that an incoming electron is transmitted into the superconductor as a hole.

If we now use the Green's function difference, eq. (2.18), in the equation for the charge current, eq. (2.13), we get

$$j^c = -\frac{eN_F v_F}{2} \int d\epsilon [(1 - R_{ee} + R_{he})x_1 - (\bar{T}_{ee} + \bar{T}_{he})x_2 + (1 - R_{hh} + R_{eh})\tilde{x}_1 - (\bar{T}_{hh} + \bar{T}_{eh})\tilde{x}_2].$$

The symmetry of this expression is a consequence of a redundancy of our formalism, since we work in the extended 4×4 Hilbert space of Nambu-spin space. We can indeed, use particle-hole symmetry to show that the “tilded” terms will only double the untilded ones. To do this we simply take $\varepsilon \rightarrow -\varepsilon$ on these terms and obtain that e.g $\tilde{x}_{1/2}(-\varepsilon) = x_{1/2}(\varepsilon)$ and $R_{hh}(-\varepsilon) = R_{ee}(\varepsilon)$.

The current then take the simple form

$$j^c = -eN_F v_F \int d\varepsilon [(1 - R_{ee} + R_{he})x_1 - (\bar{T}_{ee} + \bar{T}_{he})x_2].$$

The second term in this expression is an odd function in energy, so it will vanish under the integration, giving us

$$j^c = -eN_F v_F \int d\varepsilon (1 - R_{ee} + R_{he}) x_1. \quad (2.23)$$

In this expression it can clearly be seen that while normal reflection reduces the current, Andreev reflection (R_{he}) will actually increase it. This is due to the fact that in Andreev reflection, twice the charge is transferred to the superconductor[19].

At zero temperature a voltage derivative of the distribution function will give us a delta function centered around $\varepsilon = V$, so that the energy integral easily can be computed, giving us the conductance as

$$G^c(T = 0) = 2eN_F v_F (1 - R_{ee}(V) + R_{he}(V)). \quad (2.24)$$

In fig. 2.5 we plot the zero temperature conductance of the point contact as a function of applied voltage, for varying transparency of the interface. When the transparency increases the subgap conductance increases, and finally for a completely transparent interface the conductance below the gap is twice the normal conductance, signaling that we, indeed, only transfer charges via Andreev reflection at this point. When the transparency decreases the conductance decreases as well, and in the tunneling limit ($\mathcal{D} \ll 1$) we can show by expanding the current in terms of the transparency and only keeping terms to linear order that the conductance is directly proportional to the density of states of the superconductor

$$G^c(T = 0, \mathcal{D} \ll 1) = 2eN_F v_F \mathcal{D} N(V), \quad (2.25)$$

where $N(\varepsilon)$ is said density of states. This we can also see in fig. 2.5, the more the transparency decreases, the closer the conductance get to the expected shape of the superconducting density of states. This is why a tunnel contact is very useful, since it provides a way to directly probe the density of states of the material we are studying [84, 85].

For increasing voltages above the gap the current approaches a linear behavior with the same slope as in the normal state, but since Andreev reflection increases the current

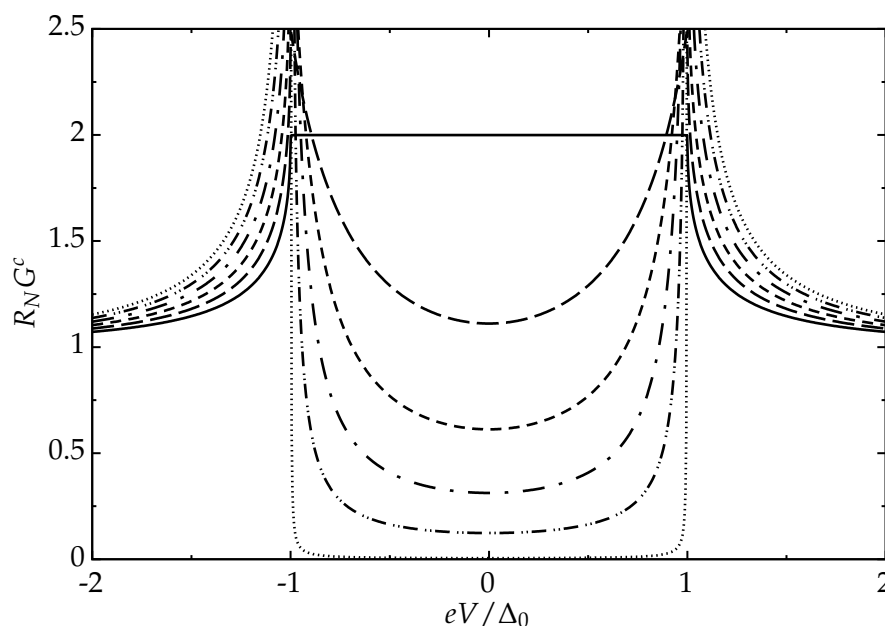


Figure 2.5: The zero temperature conductance as a function of applied voltage for an NS interface, for different transparencies. The transparency is $\mathcal{D} = 1.0, 0.8, 0.6, 0.4, 0.2, 0.01$ from top to bottom. The conductance is normalized by the normal state resistance of the interface, $R_N^{-1} = 2e^2 N_F v_F \mathcal{D}$

we can define a so called excess current as the difference of the high-voltage current in the superconducting state and the normal state

$$j_{exc} = \lim_{V \rightarrow \infty} (j_{NS} - j_{NN}), \quad (2.26)$$

where j_{NS} is the current in the superconducting state, and j_{NN} the current for the corresponding case in the normal state. The excess current has the limiting values[86] of $eR_N j_{exc} = 4\Delta_0/3$ in the transparent case, and in the tunneling limit is proportional to $eR_N j_{exc} \propto \mathcal{D}$. Here $R_N^{-1} = 2e^2 N_F v_F \mathcal{D}$ is the normal state resistance of the interface.

SS junction

If we voltage bias a system consisting of multiple superconductors we will be in trouble. This can be seen from the second Josephson relation[82] which says that the applied voltage is related to the time derivative of the phase

$$\frac{\partial}{\partial t} \phi = 2eV. \quad (2.27)$$

So applying a voltage to a junction between two superconductors, will make the phase time-dependent. This of course also happened in the SN case considered above, but

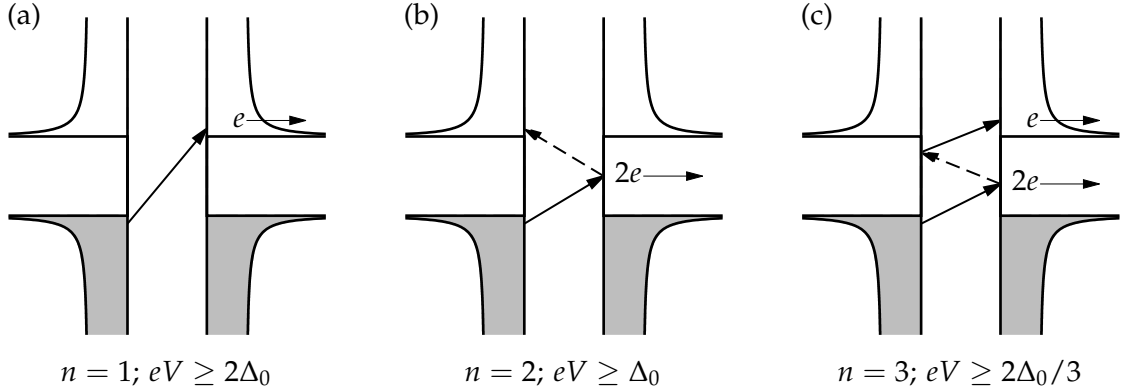


Figure 2.6: Schematic representation of the lowest orders of MAR between two s -wave superconductors in a symmetric point-contact. The n :th order process is allowed as the voltage is $eV = 2\Delta_0/n$. By making (at least) $n - 1$ Andreev reflections an incoming electron at an energy ε below the gap reaches an empty final state at an energy $\varepsilon + neV$ above the gap. In this process a charge ne is transferred to the other superconductor, with a probability $\propto \mathcal{D}^n$ for low transparencies. Note that the case sketched in the figure describe the case of transparent interfaces, for a decreased transparency there is also the possibility to back-scatter.

with only one superconductor in the game we are safe, since the phase, in itself, not is an observable. With two or more superconductors involved we all of a sudden have to consider phase differences varying in time, and phase differences are observables.

With a time dependent phase the convolutions in e.g. eq. (2.6), have to be taken care of more carefully. That level of detail is outside the scope of this thesis but we will sketch the basic physical picture behind what happens in this case. For the calculation of the current-voltage characteristics in Paper II we used the method described by Cuevas *et al.* in Ref. [87].

Let us now imagine a junction between two superconductor. All quasi-particle states below the Fermi level are filled, while the ones above are empty, and around the Fermi level there is an energy gap of $2\Delta_0$. The excitation gap will prevent a current from flowing between the superconductors (apart from the equilibrium current, as discussed in Chapter 2.6.1).

Applying a voltage $eV > 2\Delta_0$, quasi-electrons from the filled states below the gap are accelerated and can reach the empty states above. This process will transfer a single charge between the superconductor. If the voltage is $2\Delta_0 > eV > \Delta_0$, the quasi-electron cannot reach the empty states, but just as in the NS case described above it can be Andreev-reflected as a quasi-hole. This quasi-hole traces back the path of the electron, gaining another eV in energy, and reaches the empty states above the gap. The Andreev reflection transfers a Cooper pair between the superconductors. If $\Delta_0 > eV > 2\Delta_0/3$, two Andreev reflections have to be made before reaching the empty states, transfer-

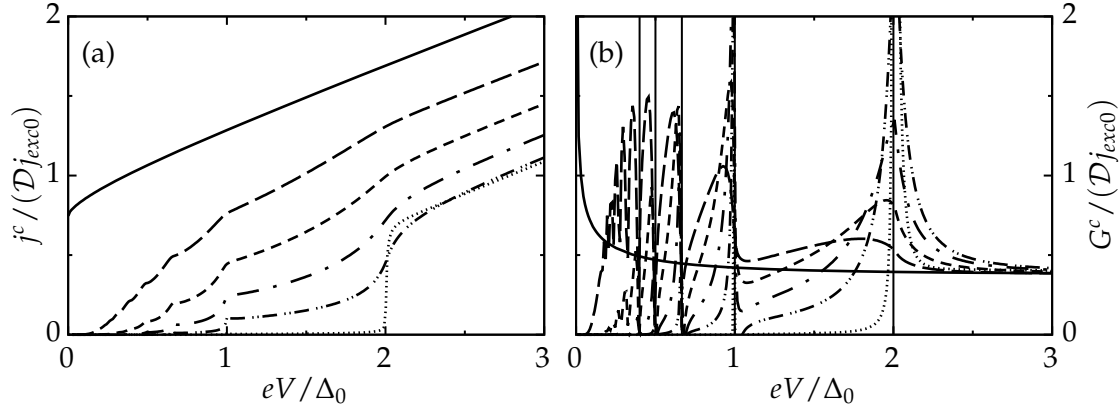


Figure 2.7: (a) the current and (b) the conductance as a function of applied voltage for a symmetric superconducting point-contact. The transparency of the point-contact is $\mathcal{D} = 1.0, 0.8, 0.6, 0.4, 0.2, 0.01$ from top to bottom in (a). The curve with the corresponding line-style in (b) has the same transparency. Both the current and the conductance is given in units of the excess current for a transparent channel, $j_{exc0} = 16ev_F N_F \Delta_0 / 3$. In (b) the vertical, solid, lines shows the position for the voltage $eV = 2\Delta_0/n$, with $n = 1 \dots 5$.

ring three quasi-electrons between the superconductors, and so on for higher order. These processes, where multiple charges are transferred between two superconductors by performing a series of Andreev reflections, are called multiple Andreev reflection (MAR).

In fig. 2.6 we schematically show the lowest order MAR:s. A new MAR channel opens as the voltage is $eV = 2\Delta_0/n$, and the process for the n :th channel transfers a charge ne . Including the effect of non-ideal interfaces the total current for the process will decrease, since the current for the n :th process, roughly, will be $\propto \mathcal{D}^n$ for lower transparencies.

The opening of a new MAR channel will be visible in the current-voltage characteristics as so-called sub-gap-structure (SGS). The SGS will look somewhat like steps in the current that appears as the voltage reaches the threshold voltages, $eV = 2\Delta_0/n$. In fig. 2.7 we plot the current-voltage characteristics of a symmetric, s -wave, superconducting point-contact. As can be seen the current shows some distinctive SGS, which is perhaps even better seen in the conductance. In the conductance the SGS is visible as a series of peaks and dips at the voltages $eV = 2\Delta_0/n$. The excess current in a superconductor-superconductor junction turns out to be twice the excess current for a superconductor-normal metal junction, so $eR_N j_{exc} = 8\Delta_0/3$ with $R_N^{-1} = 2e^2 N_F v_F \mathcal{D}$.

2.7 Spin transport

In systems where we create a difference between the current for spin up and down excitations we can define a spin current as the difference between the two. In superconducting systems it has been experimentally shown that these spin-polarized currents can be long-range[88, 89], exceeding other length-scales, e.g. the superconducting coherence length and normal state spin-diffusion length.

In this Chapter we will show a simple example how a spin-polarized current enters in a superconductor.

2.7.1 SN junction in a Zeeman field

Let us consider the same superconductor-normal metal junction as we considered above, but with the extra ingredient that we let the superconductor be under the influence of a constant, in-plane, background Zeeman field.

In a superconductor there is spin-rotational invariance which means that the reasonable choice for quantization axis is along the Zeeman field. So let's take the Zeeman field to be along the z -axis, this will make the two spin-bands in the superconductor inequivalent since they will be subject to plus or minus a constant shift [90], $h = \frac{1}{2}g\mu_B H$, set by the Zeeman field. Here μ_B is the Bohr magneton and g the gyromagnetic factor. This will give the bulk coherence functions as

$$\gamma^R = \begin{pmatrix} \gamma_{\uparrow}^R & 0 \\ 0 & \gamma_{\downarrow}^R \end{pmatrix} i\sigma_y, \quad \tilde{\gamma}^R = \begin{pmatrix} \tilde{\gamma}_{\uparrow}^R & 0 \\ 0 & \tilde{\gamma}_{\downarrow}^R \end{pmatrix} i\sigma_y, \quad (2.28)$$

where

$$\gamma_{\uparrow\downarrow}^R = -\frac{\Delta_0}{\varepsilon_{\uparrow\downarrow} + i\sqrt{\Delta_0^2 - \varepsilon_{\uparrow\downarrow}^2}} \quad \text{and} \quad \tilde{\gamma}_{\uparrow\downarrow}^R = \frac{\Delta_0}{\varepsilon_{\uparrow\downarrow} + i\sqrt{\Delta_0^2 - \varepsilon_{\uparrow\downarrow}^2}}, \quad (2.29)$$

with $\varepsilon_{\uparrow\downarrow} = \varepsilon \mp \frac{h}{2}$ giving the shift to lower (higher) energies for the two different spin bands. To be able to neglect orbital effects, we will also require that our superconductor is a thin film, with a thickness much smaller than the magnetic penetration depth.

We then repeat the calculation that we did above, but now we have to keep all the spin matrices since there is a spin-dependence. In the end we will get the same scattering probabilities as above in Eq. (2.20), except that they will be different for the two spin bands, since e.g. $\gamma_{\uparrow}^R \neq \gamma_{\downarrow}^R$, and similarly we can define spin dependent scattering probabilities. The current will have four different components, reflecting our extended 4×4 Hilbert space. These components look like

$$\begin{aligned} \hat{j}_{e,\uparrow} &= (1 - R_{ee,\uparrow})x_1 + R_{eh,\uparrow}\tilde{x}_1 - \bar{T}_{ee,\uparrow}x_{2,\uparrow} + \bar{T}_{eh,\uparrow}\tilde{x}_{2,\uparrow} \\ \hat{j}_{e,\downarrow} &= (1 - R_{ee,\downarrow})x_1 + R_{eh,\downarrow}\tilde{x}_1 - \bar{T}_{ee,\downarrow}x_{2,\downarrow} + \bar{T}_{eh,\downarrow}\tilde{x}_{2,\downarrow} \\ \hat{j}_{h,\downarrow} &= (1 - R_{hh,\downarrow})\tilde{x}_1 + R_{he,\downarrow}x_1 - \bar{T}_{hh,\downarrow}\tilde{x}_{2,\downarrow} + \bar{T}_{he,\downarrow}x_{2,\downarrow} \\ \hat{j}_{h,\uparrow} &= (1 - R_{hh,\uparrow})\tilde{x}_1 + R_{he,\uparrow}x_1 - \bar{T}_{hh,\uparrow}\tilde{x}_{2,\uparrow} + \bar{T}_{he,\uparrow}x_{2,\uparrow}, \end{aligned} \quad (2.30)$$

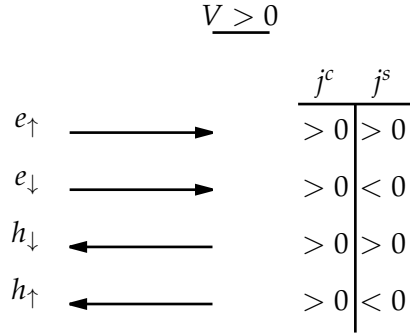


Figure 2.8: A simple illustration showing the different components contributing to the transport, and whether they give a positive or negative contribution to the charge and spin current. The arrow points in the same direction as the propagation direction of the quasi-particle. The example is for a positive voltage, for a negative voltage propagation direction arrows and current signs would all be reversed.

where we have assumed that there is no spin dependence in the normal metal. The spin dependence in the distribution functions in the superconductor comes from the spin-dependence in the coherence functions. Even though the terms are at this instance written for the case of a Zeeman split superconductor, they are in fact general for all cases where we can define a single quantization axis. In that case we can always rotate our basis to be in σ_z , in which case it reduces to what is written above.

From these terms we can define spin up and down currents as

$$\begin{aligned} j_\uparrow &= \hat{j}_{e,\uparrow} + \hat{j}_{h,\downarrow} \\ j_\downarrow &= \hat{j}_{e,\downarrow} + \hat{j}_{h,\uparrow}. \end{aligned} \quad (2.31)$$

That we pair the terms in this particular way for the different spin parts has to do with the fact that electrons and holes have the same spin, but propagate in opposite direction with respect to each other and thereby contribute in opposite way to the spin current. In fig. 2.8 we show with a small illustration how the different electron and hole terms contribute to the total current. As seen from the figure the most logical way to pair the terms is as done above in Eq. (2.31). From this pairing we get the total charge and spin currents as

$$\begin{aligned} j^c &= -eN_F v_F \int \frac{d\varepsilon}{4} \int \frac{d\Omega_{\mathbf{p}_F}}{4\pi} [j_\uparrow + j_\downarrow] \\ j^s &= -eN_F v_F \int \frac{d\varepsilon}{4} \int \frac{d\Omega_{\mathbf{p}_F}}{4\pi} [j_\uparrow - j_\downarrow]. \end{aligned} \quad (2.32)$$

Using the same type of symmetries as for the spin-independent case earlier, e.g.

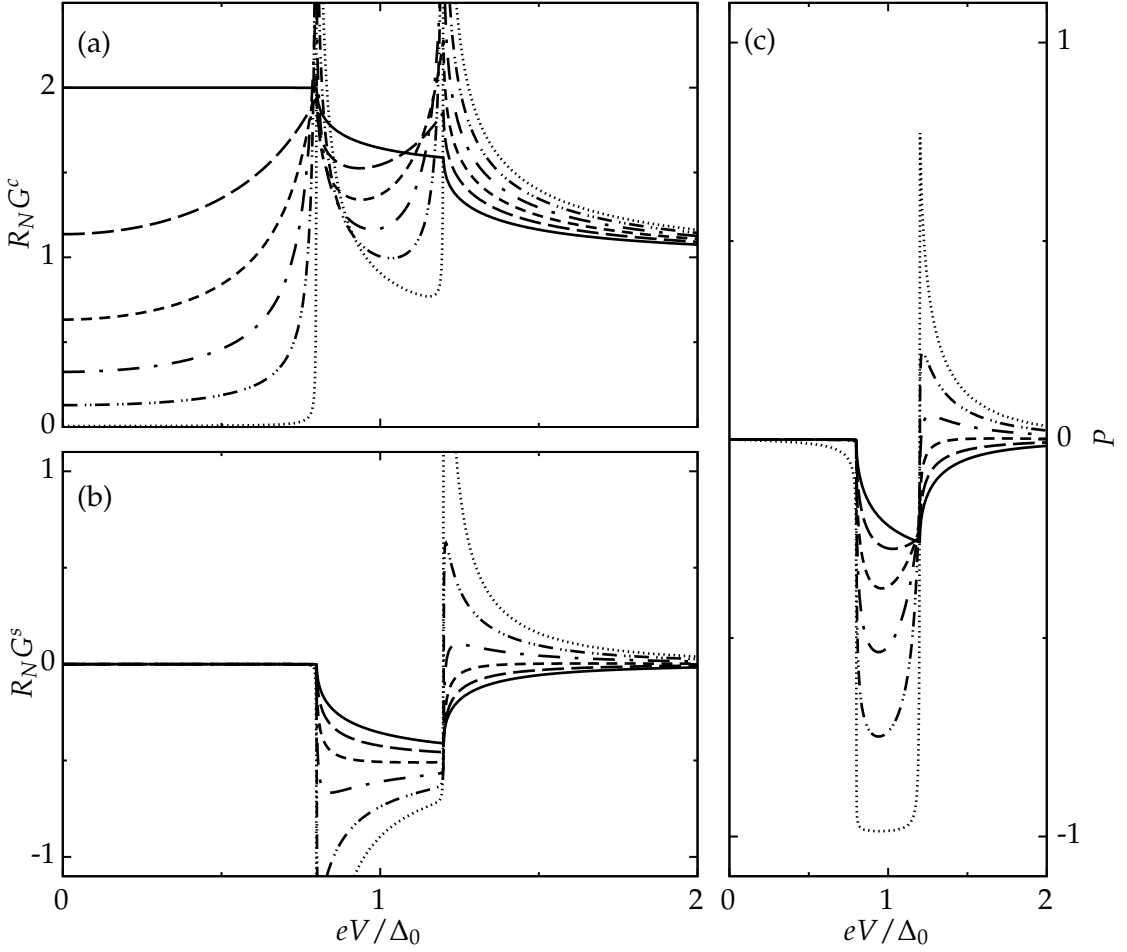


Figure 2.9: (a) The charge conductance, (b) the spin conductance and (c) the polarization for the same point contact as in fig. 2.5, but with an external exchange field of magnitude $h = 0.4\Delta_0$. The transparency for the different curves are from top to bottom in (a): $\mathcal{D} = 1.0, 0.8, 0.6, 0.4, 0.2, 0.01$. The curves with the same line styles in the other plots have the same transparency. The charge conductance is an even function in the voltage, while both the spin conductance and the polarization are odd.

$R_{eh,\sigma}(\varepsilon) = R_{he,-\sigma}(-\varepsilon)$, the spin resolved currents can be written in a quite simple form

$$\begin{aligned}
 j_{\uparrow} &= 2 (1 - R_{ee,\uparrow} + R_{he,\downarrow}) \left[\tanh \left(\frac{\varepsilon + eV}{2T} \right) - \tanh \varepsilon/2T \right] \\
 j_{\downarrow} &= 2 (1 - R_{ee,\downarrow} + R_{he,\uparrow}) \left[\tanh \left(\frac{\varepsilon + eV}{2T} \right) - \tanh \varepsilon/2T \right].
 \end{aligned} \tag{2.33}$$

At zero temperature we can again write the conductance in closed-form as

$$\begin{aligned} G^c(T=0) &= eN_F v_F [2 - R_{ee,\uparrow}(V) - R_{ee,\downarrow}(V) + R_{he,\uparrow}(V) + R_{he,\downarrow}(V)] \\ G^s(T=0) &= eN_F v_F [R_{ee,\downarrow}(V) - R_{ee,\uparrow}(V) + R_{he,\downarrow}(V) - R_{he,\uparrow}(V)], \end{aligned} \quad (2.34)$$

and in the tunneling limit as

$$\begin{aligned} G^c(T=0, \mathcal{D} \ll 1) &= eN_F v_F \mathcal{D} (N_{\uparrow}(V) + N_{\downarrow}(V)) \\ G^s(T=0, \mathcal{D} \ll 1) &= eN_F v_F \mathcal{D} (N_{\uparrow}(V) - N_{\downarrow}(V)), \end{aligned} \quad (2.35)$$

where $N_{\uparrow\downarrow}$ are the density of states for the two spin directions. This case was studied by Meservey and Tedrow[91, 90], and they could observe the splitting of the density of states for the different spins of the quasi-particles.

A way of quantifying the spin current is to also look at the spin-polarization

$$P = \frac{G^s}{G^c}. \quad (2.36)$$

If the conductance is carried entirely by one of the spins, the polarization takes the value $P = \pm 1$. If spin up dominates the polarization is positive and if spin down dominates negative.

In fig. 2.9 we plot the charge and spin conductance as well as the polarization for the same point contact that we previously considered for the case without Zeeman field. As can be clearly seen the Zeeman field induces a spin conductance due to the in-equivalent density of states for the different spins. The polarization of the current approaches unity as the transparency goes towards zero in a region of width h around the gap edges, which means that a superconductor in a Zeeman field can be used to produce spins with a certain spin to a high degree of accuracy. This is an effect that has been studied previously with spintronics in mind[92, 93].

2.8 Current fluctuations

In this section we will see how the current fluctuations can be formulated in the quasiclassical theory and show in a more extended fashion how we derive the expression for the spin-dependent fluctuations for a superconductor-normal metal junction that then was used in Paper IV. This derivation closely follows the one in Ref. [71].

When deriving boundary conditions or observables in the quasiclassical approximation, it is useful to split the full Green's function into a sum of slowly varying envelope functions and rapidly oscillating functions. The slowly varying envelope functions are then related to the quasiclassical propagator, while the rapidly varying functions are unnecessary at a quasiclassical level. Normally we can just throw these rapidly varying functions away, but at interfaces they are important and we have to take care of them explicitly. This is what is done when deriving the boundary conditions that was

presented in section 2.3. So far so good, but since the current fluctuations is a “second order” correlator, we will once again have to deal with them.

The current-current correlator has in the quasiclassical approximation been shown [46, 71] to have the zero frequency form

$$S = e^2 N_F v_F \int \frac{d\varepsilon}{32\pi^2} \frac{d\Omega_{\mathbf{p}_F}}{4\pi} \text{Tr} \left[\hat{g}_{1,+}^{\leftarrow} \hat{\tau}_3 \hat{g}_{1,+}^{\rightarrow} \hat{\tau}_3 - \hat{d}_{1,+}^{\leftarrow} \hat{\tau}_3 \hat{d}_{1,-}^{\rightarrow} \hat{\tau}_3 + (+ \leftrightarrow -) \right], \quad (2.37)$$

or equivalently on the other side of the interface. The lesser(greater) Green’s functions as well as the “drones” are related to the Keldysh ones via

$$\hat{g}^{\lessgtr} = \hat{g}^K \mp (\hat{g}^R - \hat{g}^A) \quad \hat{d}^{\lessgtr} = \hat{d}^K \mp (\hat{d}^R - \hat{d}^A).$$

The drones are related to interference effects of the rapidly varying wave function. As mentioned above, this information is not relevant at the quasiclassical level, so we naturally want to get rid of the dependence on the drones. The derivation of the boundary conditions[68] for the quasiclassical Green’s functions $\check{g}_{1(2)\pm}$ on the two sides of the interface can also be used to give us relations between the drones and the quasiclassical propagators[71],

$$\begin{aligned} \check{d}_{1s} &= \frac{1}{2\sqrt{\mathcal{R}}} [(1 + \mathcal{R})\check{g}_{1s} - \mathcal{D}\check{g}_{2s}] \\ \check{d}_{2s} &= \frac{1}{2\sqrt{\mathcal{R}}} [\mathcal{D}\check{g}_{1s} - (1 + \mathcal{R})\check{g}_{2s}] \\ \check{d}_{1a} &= \frac{1}{4\pi i} [\check{g}_{1s}\check{d}_{1s} - \check{g}_{2s}\check{d}_{2s}], \end{aligned} \quad (2.38)$$

where we have defined symmetric and anti-symmetric Green’s functions and drones on both sides of the interface according to

$$\begin{aligned} \check{g}_{1(2)s} &= \check{g}_{1(2),+} + \check{g}_{1(2),-} \\ \check{d}_{1(2)s/a} &= \check{d}_{1(2),+-} \pm \check{d}_{1(2),-+}. \end{aligned} \quad (2.39)$$

From the relations in eq. (2.38) we can then derive explicit relations for the drones in terms of quasiclassical propagators by expressing the incoming and outgoing Green’s function in terms of scattered and unscattered functions. Doing this, we reach that the Retarded and Advanced components of the symmetric and anti-symmetric drones can be written as

$$\begin{aligned} \hat{d}_{1s}^R &= -2\pi i \begin{pmatrix} r_{ee}^R & 0 \\ 0 & -r_{hh}^R \end{pmatrix} & \hat{d}_{1a}^R &= 2\pi i \begin{pmatrix} r_{ee}^R & 0 \\ 0 & r_{hh}^R \end{pmatrix} \\ \hat{d}_{1s}^A &= 2\pi i \begin{pmatrix} r_{ee}^A & 0 \\ 0 & -r_{hh}^A \end{pmatrix} & \hat{d}_{1a}^A &= 2\pi i \begin{pmatrix} r_{ee}^A & 0 \\ 0 & r_{hh}^A \end{pmatrix} \end{aligned} \quad (2.40)$$

while the Keldysh parts look like

$$\begin{aligned}\hat{d}_{1s}^K &= -2\pi i \begin{pmatrix} (r_{ee}^R + r_{ee}^A)x_1 & B \\ \tilde{B} & (r_{hh}^R + r_{hh}^A)\tilde{x}_1 \end{pmatrix} \\ \hat{d}_{1a}^K &= 2\pi i \begin{pmatrix} (r_{ee}^R - r_{ee}^A)x_1 & B \\ -\tilde{B} & -(r_{hh}^R - r_{hh}^A)\tilde{x}_1 \end{pmatrix}\end{aligned}\quad (2.41)$$

where

$$B = r_{ee}^R r_{he}^A x_1 - r_{eh}^R r_{hh}^A \tilde{x}_1 - \bar{t}_{ee}^R x_2 \bar{t}_{he}^A + \bar{t}_{eh}^R \tilde{x}_2 \bar{t}_{hh}^A. \quad (2.42)$$

If we now use these expressions in eq. (2.37), it turns out that we only get a few non-zero terms. Some that depend on the distribution functions explicitly, and some that do not. So the noise will be expressed as

$$S = e^2 N_F v_F \int \frac{d\varepsilon}{32\pi^2} \int \frac{d\Omega_{\mathbf{p}_F}}{4\pi} \text{Tr} [S^K + S^{RA}]. \quad (2.43)$$

Both of these terms consists of only four terms each, all other terms have zeroes on the diagonal and will vanish under the trace. The terms look like

$$\begin{aligned}S^K &= -\frac{1}{2} \left[\frac{1}{2} \hat{d}_{1s}^K \hat{t}_3 \hat{d}_{1s}^K \hat{t}_3 - \frac{1}{2} \hat{d}_{1a}^K \hat{t}_3 \hat{d}_{1a}^K \hat{t}_3 - \hat{g}_{1,+}^K \hat{t}_3 \hat{g}_{1,+}^K \hat{t}_3 - \hat{g}_{1,-}^K \hat{t}_3 \hat{g}_{1,-}^K \hat{t}_3 \right] \\ S^{RA} &= \frac{1}{2} \left[\frac{1}{2} \hat{d}_{1s}^{RA} \hat{t}_3 \hat{d}_{1s}^{RA} \hat{t}_3 - \frac{1}{2} \hat{d}_{1a}^{RA} \hat{t}_3 \hat{d}_{1a}^{RA} \hat{t}_3 - \hat{g}_{1,+}^{RA} \hat{t}_3 \hat{g}_{1,+}^{RA} \hat{t}_3 - \hat{g}_{1,-}^{RA} \hat{t}_3 \hat{g}_{1,-}^{RA} \hat{t}_3 \right],\end{aligned}\quad (2.44)$$

where the superscript RA just stands for that function being the difference between a Retarded and an Advanced function, i.e. $A^{RA} = A^R - A^A$. After working out the different terms we arrive at

$$S^{RA} = (2\pi)^2 \left[4 + \{r_{he}^R, r_{he}^A\} + \{r_{eh}^R, r_{eh}^A\} - \{r_{ee}^R, r_{ee}^A\} - \{r_{hh}^R, r_{hh}^A\} \right], \quad (2.45)$$

for the spectral part, while the Keldysh part is

$$S^K = -(2\pi)^2 [s_1 + s_2 + s_3 + s_4 + s_5 + s_6 + \tilde{s}_1 + \tilde{s}_2 + \tilde{s}_3 + \tilde{s}_4], \quad (2.46)$$

where

$$\begin{aligned}s_1 &= \left(1 + \{r_{he}^R, r_{he}^A\} - \{r_{ee}^R, r_{ee}^A\} - \{r_{ee}^R r_{he}^A, r_{he}^R r_{ee}^A\} + r_{he}^R r_{he}^A r_{he}^R r_{he}^A + r_{ee}^R r_{ee}^A r_{ee}^R r_{ee}^A \right) x_1^2, \\ s_2 &= \bar{t}_{he}^R x_2 \bar{t}_{he}^A \bar{t}_{he}^R x_2 \bar{t}_{he}^A + \bar{t}_{ee}^R x_2 \bar{t}_{ee}^A \bar{t}_{ee}^R x_2 \bar{t}_{ee}^A - \left\{ \bar{t}_{ee}^R x_2 \bar{t}_{he}^A, \bar{t}_{he}^R x_2 \bar{t}_{ee}^A \right\}, \\ s_3 &= \left(\{r_{he}^R r_{he}^A, \bar{t}_{he}^R x_2 \bar{t}_{he}^A\} + \{r_{ee}^R r_{ee}^A, \bar{t}_{ee}^R x_2 \bar{t}_{ee}^A\} + \{r_{he}^R r_{ee}^A, \bar{t}_{ee}^R x_2 \bar{t}_{he}^A\} + \{r_{ee}^R r_{he}^A, \bar{t}_{he}^R x_2 \bar{t}_{ee}^A\} \right) x_1, \\ s_4 &= - \left(\{r_{he}^R r_{ee}^A, \bar{t}_{eh}^R \tilde{x}_2 \bar{t}_{hh}^A\} + \{r_{ee}^R r_{he}^A, \bar{t}_{hh}^R \tilde{x}_2 \bar{t}_{eh}^A\} + \{r_{ee}^R r_{ee}^A, \bar{t}_{eh}^R \tilde{x}_2 \bar{t}_{eh}^A\} + \{r_{he}^R r_{he}^A, \bar{t}_{hh}^R \tilde{x}_2 \bar{t}_{hh}^A\} \right) x_1, \\ s_5 &= \left(\{r_{he}^R r_{ee}^A, r_{eh}^R r_{hh}^A\} + \{r_{ee}^R r_{he}^A, r_{hh}^R r_{eh}^A\} - \{r_{ee}^R r_{ee}^A, r_{eh}^R r_{eh}^A\} - \{r_{he}^R r_{he}^A, r_{hh}^R r_{hh}^A\} \right) x_1 \tilde{x}_1, \\ s_6 &= \left\{ \bar{t}_{he}^R x_2 \bar{t}_{ee}^A, \bar{t}_{eh}^R \tilde{x}_2 \bar{t}_{hh}^A \right\} + \left\{ \bar{t}_{ee}^R x_2 \bar{t}_{he}^A, \bar{t}_{hh}^R \tilde{x}_2 \bar{t}_{eh}^A \right\} - \left\{ \bar{t}_{ee}^R x_2 \bar{t}_{ee}^A, \bar{t}_{eh}^R \tilde{x}_2 \bar{t}_{eh}^A \right\} - \left\{ \bar{t}_{he}^R x_2 \bar{t}_{he}^A, \bar{t}_{hh}^R \tilde{x}_2 \bar{t}_{hh}^A \right\},\end{aligned}\quad (2.47)$$

where $\{A, B\} = AB + BA$ represents a usual anti-commutator. These different terms correspond to fluctuations between different channels of quasi-particles injected from the two sides of the interface. For example, the term s_4 describe fluctuations between a quasi-electron injected from the normal metal and a quasi-hole injected from the superconductor.

This expression for the noise, of course, obeys the fluctuation-dissipation theorem relating the noise with the conductance when the bias approaches zero

$$S_{V \rightarrow 0} = 4k_B T G, \quad (2.48)$$

where $G = dI/dV$, is the conductance. As mentioned in the Introduction, we do not learn anything new from the thermal noise, so in this work we will only consider low-temperature results, where the thermal noise can be neglected.

In the normal state the zero-temperature noise reduces to the result alluded to in the Introduction

$$S = 4e^3 N_F v_F \mathcal{R} \mathcal{D} V, \quad (2.49)$$

showing the vanishing of the noise for the cases $\mathcal{D} = 1$ and $\mathcal{D} = 0$.

Once both the conductance and its fluctuations are known it is very useful to define their quotient, the so-called differential Fano factor,

$$F = \frac{1}{2eG} \frac{dS}{dV}. \quad (2.50)$$

From the differential Fano factor we can, in the tunneling limit, tell what the effective charge of the current carrier has. The differential Fano factor can either be measured [94] or be extracted from a noise measurement.

2.8.1 Noise from an SN junction

Let us once again turn to our favorite example, the superconductor-normal metal junction, without any spin-dependence.

The expression for the noise written out above in eq. (2.47) simplify slightly when we use that all of the coherence functions are of the form $\gamma^R = \gamma_0^R i\sigma_y$ and that the Advanced components are related to the Retarded ones,

$$\begin{aligned} S^{RA} &= 4(2 + R_{he} + R_{eh} - R_{ee} - R_{hh}) \\ s_1 &= 2x_1^2 (1 + R_{he} - R_{ee})^2 \\ s_2 &= 2x_2^2 (\bar{T}_{he} - \bar{T}_{ee})^2 \\ s_3 &= 4x_1 x_2 |r_{he} \bar{t}_{he}^* + r_{ee} \bar{t}_{ee}^*|^2 \\ s_4 &= -4x_1 \tilde{x}_2 |r_{ee} \bar{t}_{eh}^* - r_{he} \bar{t}_{hh}^*|^2 \\ s_5 &= -4x_1 \tilde{x}_1 |r_{he} r_{hh}^* + r_{ee} r_{eh}^*|^2 \\ s_6 &= -4x_2 \tilde{x}_2 |\bar{t}_{he} \bar{t}_{hh}^* + \bar{t}_{ee} \bar{t}_{eh}^*|^2, \end{aligned} \quad (2.51)$$

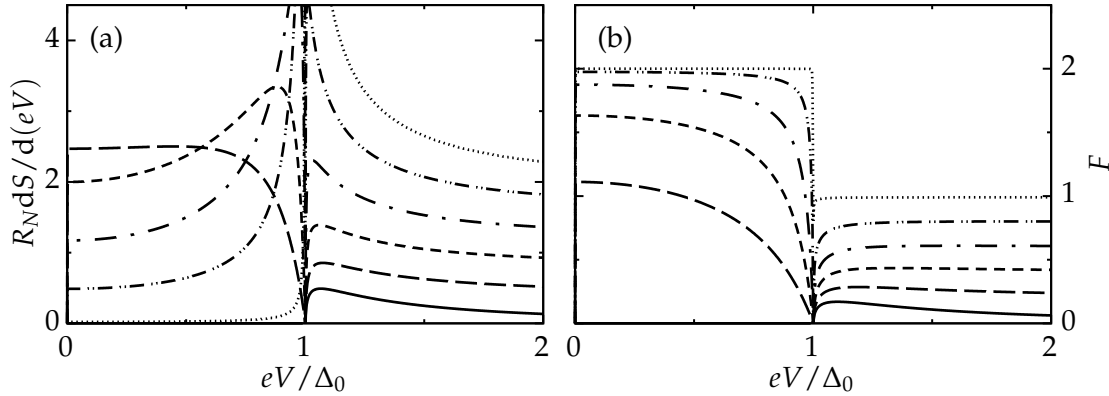


Figure 2.10: (a), The zero temperature differential noise, and (b), the differential Fano factor as a function of applied voltage for an NS interface, for different transparencies. The transparency is $\mathcal{D} = 1.0, 0.8, 0.6, 0.4, 0.2, 0.01$ from bottom to top at $eV > \Delta_0$. The conductance is normalized by the normal state resistance of the interface, $R_N = 2e^2 N_F v_F \mathcal{D}$. Both the differential noise and Fano factor is odd functions in the applied voltage.

where the scattering amplitudes that we need is already written down above in eq. (2.20), and we have suppressed the R index to not overstuff the notation. This agrees with what was obtained in Ref. [71]. If we write the distribution functions instead in terms of Fermi functions, the parts of the Keldysh noise without a Fermi function will cancel the spectral part.

To more clearly show some of the features in the noise we plot the differential noise, that is dS/dV , in fig. 2.10(a) for the same junction as was previously considered for the conductance. In 2.10(b) we also plot the differential Fano factor. In the differential noise we can first of all notice that for perfect transmission and perfect reflection the subgap noise vanishes. This is to be expected, since for those cases there is only one open channel meaning that there is no other channels to fluctuate with. This is the same as in the normal state [45].

Turning instead to the differential Fano factor, and especially focus on the low transparency limit, we can see something interesting. As the transparency decreases the differential Fano factor assumes a step function like behavior. Above the gap it is unity, and below the gap it is twice as much. This is, once again, a sign of the fact that below the gap the only available way to transfer charge is Andreev reflection, thereby transferring twice the charge. This makes the noise a really useful tool in experiments when trying to figure out how charges are transported. For example in the case of MAR, it could be shown[55] from the noise that multiple charges were transferred in the process.

Superconductor-nanowire junctions

3

In Papers I and II a combined theoretical and experimental study was made on the proximity effect in InAs nanowires connected to superconductors. In this Chapter we will outline the model we used to describe the experiments and also show some of the results and comment on the applicability of the model. The nanowires were grown in Lund and the experiments were performed by Simon Abay, and are presented in his PhD thesis[95], while we performed the theoretical modeling.

3.1 Experiment

In order to characterize the nanowires, measurements were made on a broad range of nanowires. The nanowire junctions could be grouped into three different basic types, (i) with only two leads, (ii) with multiple leads, and (iii) with suspended nanowires.

These types of devices are useful for different purposes; type (i) could be made extremely short, type (ii) could be used to measure length-dependent properties on the same nanowire, and with type (ii) a local gate could be applied underneath the wire to tune the number of conducting modes.

3.1.1 Normal state characteristics

First, a characterization of normal-state properties was made. From the multiple-lead devices the length dependence of the nanowire resistance could be measured, which together with the expression for the Drude conductivity give us an estimate of the mean-free path of the nanowires. The nanowires with multiple leads also allowed us to take advantage of the ability to make two- and four-point measurements[96] on the same

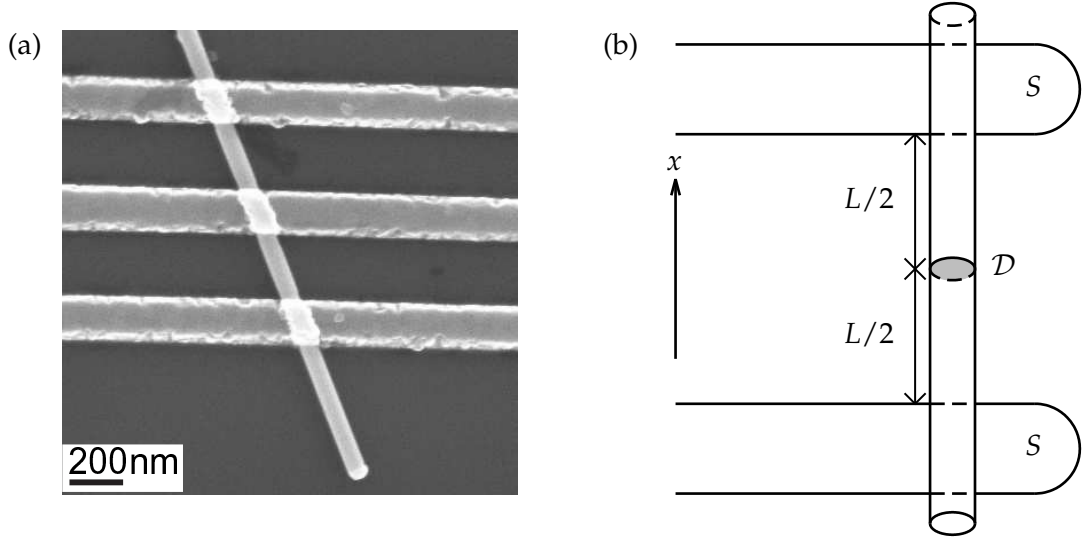


Figure 3.1: (a) An SEM image of a typical device. In the image the nanowire is contacted by three superconducting leads. (b) A theoreticians view of the same junction. A disordered nanowire of length L is connected to superconducting leads. Crystalline defects are modeled with a lumped scatterer situated in the middle of wire, having the effective transparency \mathcal{D} .

section of the nanowire, to estimate the number of conducting modes in the wires to range between 50 and 100.

From the similar behavior of the different nanowires we conclude that the values obtained from the normal-state measurements can be used for all nanowires. This also makes sense from the fact that the nanowires were taken from the same growth-batch, meaning that they were grown in the same environment.

3.2 Theoretical model

The experiments were made on a wide range of nanowires, with lengths ranging from 30 nm all the way up to 600 nm . This spread in lengths would put the shortest in the ballistic short-junction limit, with a length much shorter than both the superconducting coherence length and the mean free path, ($L \ll \ell, \xi_0 = \hbar v_F / 2\pi k_B T_c$), while the longest were in the diffusive long-junction limit, with a length longer than the mean free path and the diffusive coherence length, ($L > \ell, \xi_D = \sqrt{\ell \xi_0}$). The majority of the wires, on the other hand, lie somewhere in between, in a cross-over regime. Furthermore, all of the junctions in the study exhibit the Josephson effect, implying that the transport is fully coherent and will require treatment in the full coherent MAR theory [97, 98, 99, 100]. To fit all of these observations into a single model, we use a simple theory which allows us to go from the ballistic to the diffusive regime. In fig. 3.1 we show an SEM

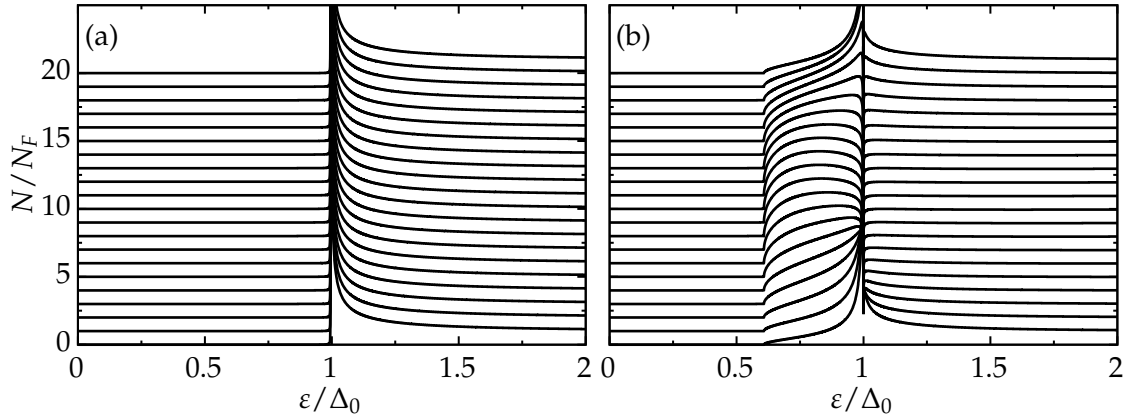


Figure 3.2: The local density of states going from one side of the nanowire to the other. The mean free path of the nonwires are obtained from normal state measurements, and the lengths are (a) $L = 0.7\ell$ and (b) $L = 3.7\ell$. The temperature has been taken to $T = 0.01T_c$. The different curves have been vertically offset for clarity.

image of an actual wire and also schematically how we model it. We assume that the nanowire is connected to the superconducting leads by highly transmissive contacts, which from the experimental fact that the contact resistance is much smaller than the total wire resistance may be taken to be perfectly transparent. The strong confinement in the transverse direction of the nanowire, which results in only a few conducting modes, allows us to simplify the problem by only considering a single mode. The current from that mode is then multiplied with the total number of modes to obtain the total current carried by the nanowire.

All effects of crystal defects are collected into and described by a single transmission coefficient \mathcal{D} that we model as an interface in the center of the nanowire. We also assume that the nanowire will have some disorder due to simple elastic scattering of impurities and crystal imperfections, which we model in the Born approximation with a scattering rate $\Gamma = \hbar v_F/\ell$, given by the nanowire mean free path, ℓ . The voltage is assumed to drop at the scattering center, which then is where we compute the currents.

If we neglect the inverse proximity effect, that is the influence of the nanowire on the superconductors, the superconducting order parameter can be taken to be constant all the way up to the interface to the nanowire. The equilibrium current is calculated along the line of the point-contact calculation above, see Chapter 2.6.1, except that the incoming coherence functions at the scattering center are not the bulk solutions but rather they are solved for from the superconductor-nanowire interface and along their trajectory to the scattering center. The solution along the trajectory can efficiently be done with a “stepping method”, as outlined in Appendix A.3.

The impureness of the nanowire mean that we along the trajectory also have to solve for the impurity self-energy. The impurities are taken into account by solving the single

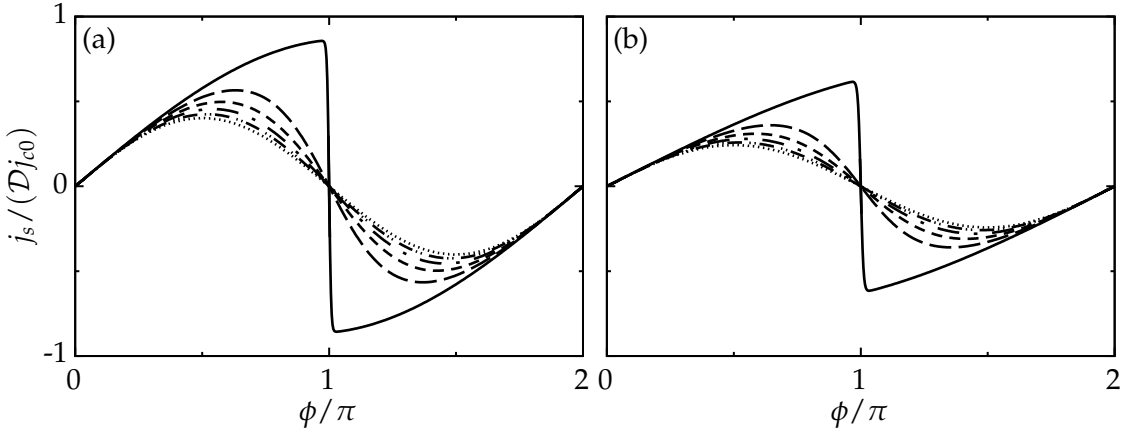


Figure 3.3: The supercurrent across the nanowire as a function of the phase difference for varying transparency of the middle constriction. The lengths of the nanowires are (a) $L = 0.7\ell$ and (b) $L = 3.7\ell$. From top to bottom curve the transparencies are $\mathcal{D} = 1.0, 0.8, 0.6, 0.4, 0.2, 0.01$. The current has been normalized by the critical current of a transparent, clean, point-contact $j_{c0} = 2\pi e v_F N_F \Delta_0$ and once again by the transparency \mathcal{D} . The current is calculated at the temperature $T = 0.01T_c$.

impurity t -matrix, see eq. (2.4.1), which in the Born approximation, simplifies to the self-consistency equations

$$\hat{\sigma}(\varepsilon, x) = \Gamma \langle \hat{g}(\mathbf{p}_F, \varepsilon, x) \rangle_{\mathbf{p}_F}, \quad (3.1)$$

where $\langle \cdot \rangle_{\mathbf{p}_F}$ here stands for an average over the directions $\pm \mathbf{p}_F$, and Γ is the scattering rate given by the mean-free path of the nanowires.

Once we have the coherence functions at the scattering center, the equilibrium current is given by eq. (2.14), and the maximum of this current is then the critical current. For the current-voltage characteristics we follow the theory outlined in Ref. [87]. From the high voltage part of the current-voltage characteristics we can then obtain the excess current, j_{exc} , as the deviation from the normal transport result.

3.2.1 Results

From the model described above we can compute the critical current and excess current of the nanowires as a function of length of the nanowire, transparency of the middle constriction and temperature. These results can then be used to fit the behavior of the nanowire junctions.

In the rest of this section we will show how our results look like for a pair of typical junctions. We choose to focus on two different junctions, one in the point-contact limit and one in the intermediate cross-over regime. As explained above, the normal state measurements give us a mean-free path, which we then assume is the same for all

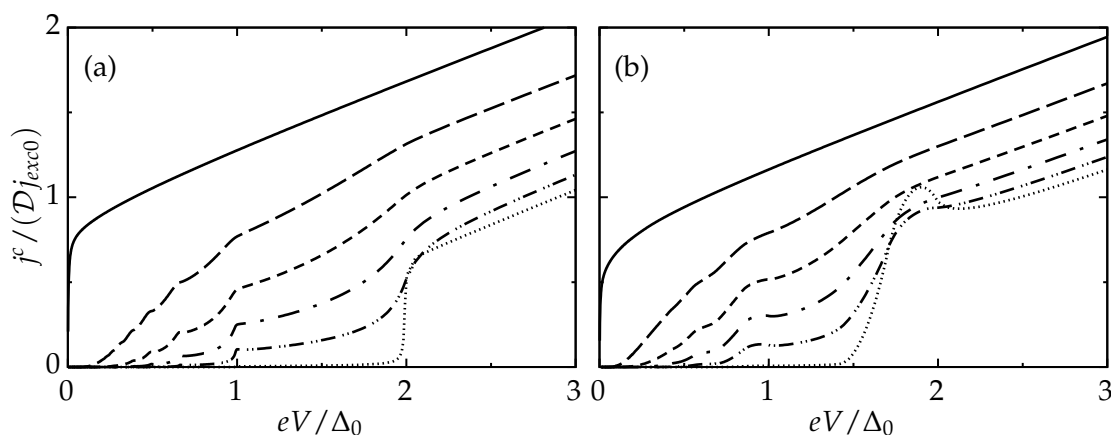


Figure 3.4: The current across the nanowire as a function of the applied voltage for varying transparency of the middle constriction. The lengths of the nanowires are (a) $L = 0.7\ell$ and (b) $L = 3.7\ell$. From top to bottom curve the transparencies are $D = 1.0, 0.8, 0.6, 0.4, 0.2, 0.01$. The current has been normalized by the excess current of a transparent, clean, point contact $j_{exc0} = 16e v_F N_F \Delta_0 / 3$ and once again by the transparency D . The current is calculated at the temperature $T = 0.01 T_c$.

nanowires. It is this length-scale compared to the nanowire length and the coherence length that tell us if we are in the long or short junction regime.

As a start we show the density of states for the two wires in fig. 3.2 when traversing it from one end to the other. As can be seen, the density of states in the shorter wire looks like the density of states of the superconductor. This is to be expected from a junction in the clean, short-junction limit. For the longer nanowire in fig. 3.2(b), on the other hand, the longer length compared to the mean free path puts it more in the diffusive limit. This can be seen from the opening of the so called mini-gap, see e.g. Ref. [101], which is seen as a smaller gap in the normal metal density of states that is independent of the position, even though the exact shape of the density of states is not.

Next, in fig. 3.3, we show the equilibrium current for these nanowires as a function of the phase difference between the two superconductors, for varying transparency of the middle constriction. Comparing the current-phase relation for the two cases we can see the cross-over between short to long junction, with the change of the current-phase relation into a more “saw-tooth” like behavior, for the transparent case. The current-phase relation is known to undergo this change for long junctions[102].

Finally, we can also obtain the current-voltage characteristics, see fig. 3.4. The shorter wire displays subharmonic-gap-structure similar to the typical BCS point contact result with current steps at voltages $eV = 2\Delta_0/n$ (n is an integer). With increasing length these steps are shifted to lower voltages, and instead of the gap more corresponds with the mini-gap. Interestingly, the increasing length also leads to areas of

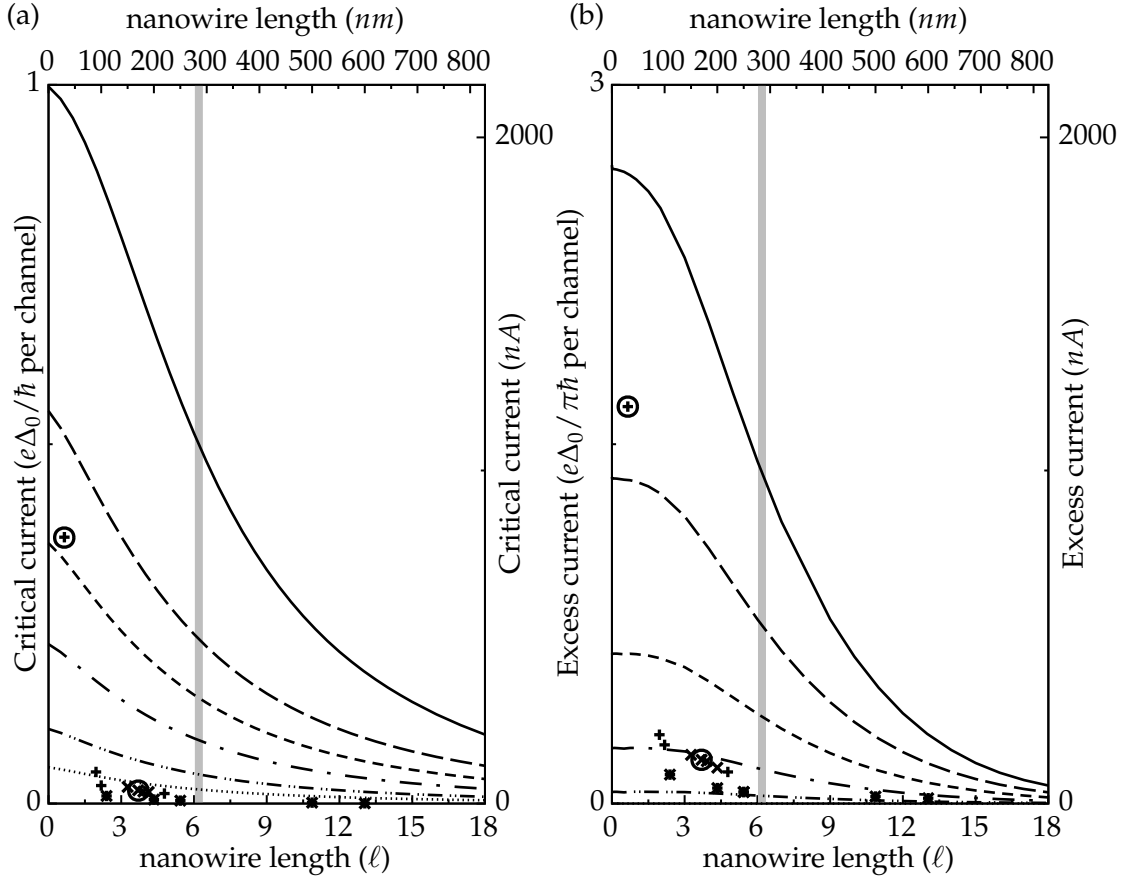


Figure 3.5: (a) The computed critical current and (b) excess current as a function of the junction length, for varying transparency of the middle constriction. From top to bottom curve the transparencies are $\mathcal{D} = 1.0, 0.8, 0.6, 0.4, 0.2, 0.1$. The units of the critical current and the excess current are on the left axis given in term of the single mode result and on the right axis in nA assuming the same transparency for all modes. The nanowire length is given in units of mean free paths on the bottom axis and in nm on the top. The vertical gray line in both plots indicate the point where the Thouless energy, $E_{th} = \hbar D_{diff}/L^2$, equals the superconducting gap; this point separates short junctions ($E_{th} \gg \Delta_0$) from the long ($E_{th} \ll \Delta_0$). The pluses (+), crosses (\times), and stars (*) are experimental data stemming from three different device types. Most of our experimental data are in the intermediate regime. The experimental points that are circled, are the two that we show the theoretical fits for.

negative differential conductance, most clearly seen in the low transparency limit as a peak in the current for voltages close to twice the gap. This has previously been seen in both experiment[103, 104] and theory[105]. It can be explained by resonant tunneling through the Andreev states that appear in the density of state of the normal region

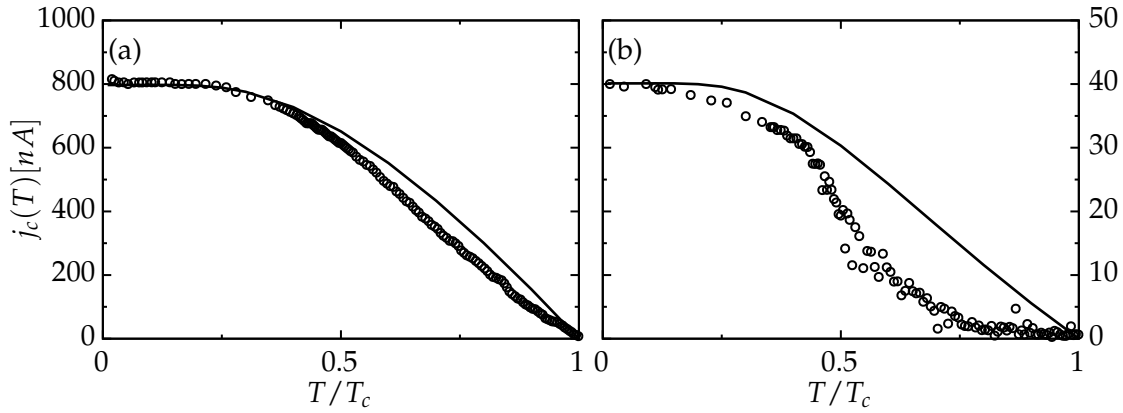


Figure 3.6: The computed temperature dependence of the critical current together with experimental values. The nanowire length (a) $L = 0.65\ell \approx 30\text{nm}$ and (b) $L = 3.7\ell \approx 170\text{nm}$ and the transparency is $\mathcal{D} = 0.64$ for (a) and $\mathcal{D} = 0.065$ for (b). The transparency is chosen from the length dependence fit for the critical current in fig. 3.5.

when the length increases.

3.3 Comparison with experiments

We now turn to comparing the theoretical results with the experimental ones. To do so, we have computed the critical current and the excess current for a number of different transparencies as a function of nanowire length. This can be seen in fig. 3.5, where we also show the experimental data in the same plot.

From this we can see that most of the nanowires lie in the intermediate, cross-over regime. There is one outlier which can be said to be in the short-junction regime. The two nanowires that we showed numerical calculations for are the ones that are circled in fig. 3.5. We can also learn from this that there is a mismatch between the transparency we can fit for the excess current and the critical current. Except for the shortest nanowire, where the fit is pretty good, there is generally a factor ~ 4 discrepancy between the transparency obtained from the excess current and the one obtained from the critical current. This kind of reduction in the critical current is usually observed in nanowires, and is also common in 2DEG InAs Josephson junctions[106]. This is a phenomenon that is not well understood but could be a result of premature switching or some depairing mechanism such as magnetic scattering.

The transparencies obtained from the length dependence are then used when computing the temperature dependence of the critical current. The theory and experiments agree well for the shorter device, but the longer device shows a decay for higher temperatures which is not captured by the theory. Diffusive junctions with resistive interfaces have theoretically been shown[107] to exhibit similar features, which was then

explained by an enhanced electron-hole dephasing in the normal region due to a longer dwell-time there. Even though the nanowire junctions were shown to have very low interface transmission, such a theory might better capture that feature of the experiments.

Another shortcoming of our model, is that we assumed all conducting modes to have the same transparency. A more correct description would be to average over modes with a distribution of transparencies.

4

Magnetic impurities

In Papers III and IV we consider a model describing a superconductor with a random distribution of magnetic impurities on top of it. In Paper III we consider thermodynamical properties of this system, such as the order parameter behavior and the density of states, and in Paper IV we investigate how the impurities affect the transport when tunneling into the superconductor.

In this Chapter we will go through the model, and show some of the key results from both the thermodynamics and transport sides.

4.1 Impurity self-energy

The system we wish to describe consists of an s -wave spin-singlet superconductor with a distribution of magnetic impurities on top of it. We will take the impurity spins to be classical, similarly to what was done in the 1960s independently by Yu, Shiba and Rusinov[27, 28, 29].

The two cases we wish to consider are on one hand completely random impurities and on the other hand completely aligned impurities. The thickness of the film is smaller than the London penetration depth, so that screening currents created by the magnetic field induced by the aligned impurity spins can be neglected. But the Zeeman shift created by the impurity spins can still be substantial, which is an effect normally not considered in these types of systems. We will take this into account by not only considering the local scattering off the impurity but also add an extra term to the impurity self-energy for the case of aligned impurities describing the non-local effect of the impurity Zeeman field.

We model the local effect of the impurities with the impurity potential

$$\hat{u} = \begin{pmatrix} v & 0 \\ 0 & -\sigma_y v \sigma_y \end{pmatrix}, \quad v = v_0 + \alpha v_S \mathbf{m} \cdot \boldsymbol{\sigma}, \quad (4.1)$$

where $\boldsymbol{\sigma}$ is the quasiparticle spin, and \mathbf{m} is a unit vector pointing in the same direction as the impurity spin. The impurity scattering is parameterized by a scalar part, v_0 , and an exchange part. The exchange part consists of a parameter α describing the tunneling amplitude of a quasi-particle onto the impurity site, and the parameter v_S which is proportional to the magnetic moment of the impurity. The tunneling amplitude $|\alpha| < 1$ can take both positive and negative values depending on the nature of the impurities. Negative α describes ferromagnetic coupling while positive antiferromagnetic.

Because of the spin-rotational symmetry of the clean superconductor, we can expect the aligned impurities to split the solutions for spin up and down into separate bands, just as in the Zeeman case considered before, see Chapter 2.7.1. We are also free to choose the impurity spin to point in the, to us, most convenient direction, to which end we choose $\mathbf{m} = (0, 0, 1)$. For the case of random impurities we need to average over impurity spin direction, that is expressing the impurity spin direction in spherical coordinates and then averaging over the solid angle.

We include the impurity effects through the self-consistent single impurity t -matrix approximation, as described in section 2.4.1. Solving the t -matrix for the two cases and averaging over the impurity spin direction we can notice that all terms in the t -matrix which are odd in the impurity spin vanish, while the even terms survive. This allows us to write the impurity self-energy solution for the two cases compactly as a sum of two terms, one term even in the impurity spin and the other one odd,

$$\hat{\sigma}_{imp} = \hat{\sigma}_{imp}^e + \hat{\sigma}_{imp}^o, \quad (4.2)$$

where

$$\begin{aligned} \sigma_{imp}^e &= \Gamma \frac{A^e \hat{\tau}_0 + B^e \hat{g} + C^e \hat{\tau}_3 \hat{g} \hat{\tau}_3}{Z} \\ \sigma_{imp}^o &= \Gamma \sigma_z \frac{A^o g \hat{\tau}_3 + B^o g \hat{\tau}_3 \hat{g} + C^o \hat{\tau}_0}{Z}. \end{aligned} \quad (4.3)$$

Here \hat{g} is the full Green's function and g the upper-left 2×2 component of the Green's function, as defined in eq. (2.3). Written like this it is quite clear that averaging over spin-direction would remove the odd terms, since those are the only ones that depend on the spin-direction. The other terms are defined according to

$$\begin{aligned} Z &= (1 + u_0^2 - \alpha^2 u_S^2)^2 - (2\alpha u_S g / \pi)^2 \\ A^e &= u_0 (1 + u_0 - \alpha^2 u_S^2) & A^o &= 2\alpha u_0 u_S / \pi \\ B^e &= [u_0^2 + (u_0^2 - \alpha^2 u_S^2)^2] / \pi & B^o &= 2\alpha u_S (u_0^2 - \alpha^2 u_S^2) / \pi^2 \\ C^e &= \alpha^2 u_S^2 / \pi & C^o &= \alpha u_S (1 + u_0^2 - \alpha^2 u_S^2). \end{aligned} \quad (4.4)$$

We have here introduced a set of effective parameters describing the impurity subsystem,

$$u_{0,S} = \pi N_F v_{0,S}, \quad \Gamma = \frac{n_{imp}}{\pi N_F}, \quad (4.5)$$

where N_F is the normal state density of state and n_{imp} the concentration of impurities. The random impurity case is obtained by removing the terms odd in impurity spin while for the aligned impurity case we keep all of them.

To take into account the background Zeeman field created by the aligned impurities we will add a second term to the self-energy which has the form of a Zeeman term,

$$\hat{\sigma}_{non-loc} = \Gamma A^{nl} \hat{\sigma}_z, \quad (4.6)$$

with $A^{nl} = \beta u_S$. The parameter $\beta \sim 1$ is a dimensional fitting parameter depending on the actual distribution of the impurities.

The total self-energy for the two cases read

$$\hat{\sigma} = \begin{cases} \hat{\sigma}_{imp}^e & \text{random} \\ \hat{\sigma}_{imp}^e + \hat{\sigma}_{imp}^o + \hat{\sigma}_{non-loc} & \text{aligned.} \end{cases} \quad (4.7)$$

The zeroes of the denominator in eq. (4.3) define bound states that are bound to the impurity sites, but if we assume that the impurities fulfill the Mott criterion[108, 109], $n_{min}^{1/3} \xi_0 = 1/5$, with $\xi_0 = \hbar v_F / 2\pi k_B T_c$ being the superconducting coherence length, the impurity states delocalize and form extended bands. Expressing this criterion in terms of parameters from our model gives us the minimum density for delocalization as $\Gamma_{min} / 2\pi k_B T_c = 1/2 (k_B T_c / E_F)^2 T_c / T_{c0}$. We are working in the quasiclassical approximation, which assumes that $k_B T_c \ll E_F$ meaning that the impurity states will always delocalize for the impurity concentration we will consider. The position of the bound states is given by

$$\varepsilon_b = \pm \Delta \frac{1 + u_0^2 - \alpha^2 u_S^2}{\sqrt{(1 + u_0^2 - \alpha^2 u_S^2)^2 + 4\alpha^2 u_S^2}}, \quad (4.8)$$

which we plot in fig. 4.1, for some different cases. As can be seen the bound state can be located anywhere in gap for all values of both the scalar part and the exchange part of the potential. It has, in fact, been shown[110] that the scalar part of the impurity potential only enters through the position of the bound state. By introducing an effective exchange scattering amplitude, that is a function of both the scalar part and the exchange part, this is totally taken into account. For this reason we could with good conscience put $u_0 = 0$ for all results in Paper III and Paper IV.

Once we know the impurity self-energies, let us write it component-wise on the same form as the Green's function

$$\hat{\sigma} = \begin{pmatrix} \sigma_{11} & \sigma_{12} i \sigma_y \\ i \sigma_y \sigma_{21} & -\sigma_y \sigma_{22} \sigma_y \end{pmatrix}, \quad (4.9)$$

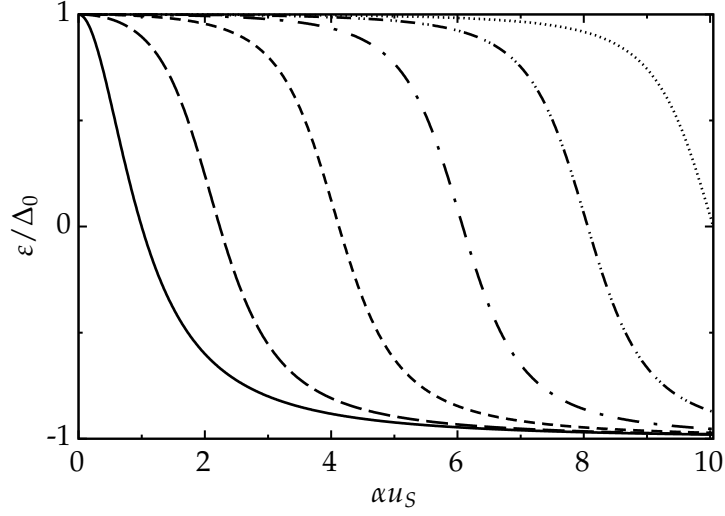


Figure 4.1: The position of the bound states for one of the spin projections as a function of strength of the exchange part of the impurity potential. From the top to bottom curve $u_0 = 10, \dots, 0$. The position of the bound state for the other spin projection is mirrored around the Fermi surface, $\varepsilon = 0$. For random impurity spins, the bound states are spin degenerate.

where the components, σ_{ij} , are 2×2 , diagonal, matrices in spin-space, e.g. $\sigma_{11} = \text{diag}(\sigma_{11,\uparrow}, \sigma_{11,\downarrow})$. When the impurity self-energy is inserted in the Eilenberger equation, eq. (2.2), we can write down the bulk Green's function solution in terms of renormalized energy and order parameter quantities

$$\hat{g} = -\pi \begin{pmatrix} \frac{1}{2}(\underline{\varepsilon} + \underline{\tilde{\varepsilon}}) & -\underline{\Delta}i\sigma_y \\ -i\sigma_y\underline{\tilde{\Delta}} & -\frac{1}{2}\sigma_y(\underline{\varepsilon} + \underline{\tilde{\varepsilon}})\sigma_y \end{pmatrix} / \sqrt{\underline{\Delta}\underline{\tilde{\Delta}} - \frac{1}{4}(\underline{\varepsilon} + \underline{\tilde{\varepsilon}})^2}, \quad (4.10)$$

where

$$\begin{aligned} \underline{\varepsilon} &= \varepsilon - \sigma_{11} \\ \underline{\Delta} &= \Delta_0 + \sigma_{12} \\ \underline{\tilde{\Delta}} &= \Delta_0 + \sigma_{21} \\ \underline{\tilde{\varepsilon}} &= \varepsilon - \sigma_{22}. \end{aligned} \quad (4.11)$$

Since the Green's function depends on the self-energies, which in itself depends on the Green's function, in such a way that it is impossible to write the solution on a closed form, we will have to resort to numerics and solve eq. (4.10) together with eq. (4.11) until we reach self-consistency, but not only this, the order parameter, Δ_0 , also depends on the impurity self-energy, which means that we also have to solve for that together with the previously mentioned equations. To that end, let us now derive a self-consistency equation for the order parameter.

4.2 Gap equation

The gap equation can be written as a sum over Matsubara frequencies

$$\Delta_0 = \frac{\lambda N_F}{2} k_B T \sum_{|\varepsilon_n| < \varepsilon_c} \int \frac{d\Omega_{\mathbf{p}_F}}{4\pi} \text{Tr}[f(\varepsilon_n, \mathbf{p}_F)], \quad (4.12)$$

where $\lambda < 0$ is the electron-phonon coupling constant, ε_c a high-energy cut-off on the order of the Debye frequency, and $f(\varepsilon_n, \mathbf{p}_F)$ the off-diagonal part of the Green's function, see eq. (2.3). Here we would like to remove the unphysical high-energy cut-off and the coupling constant, in favor of the clean limit transition temperature, T_{c0} . This is done by linearizing the clean case gap equation, which give us a relation between the coupling constant and the clean transition temperature[58, 111]

$$\frac{1}{\lambda N_F} = \ln \frac{T}{T_{c0}} + \pi k_B T \sum_{|\varepsilon_n| < \varepsilon_c} \frac{1}{|\varepsilon_n|}. \quad (4.13)$$

The gap equation then reads

$$\Delta_0 \ln \frac{T}{T_{c0}} = 2\pi k_B T \sum_{\varepsilon_n > 0} \left[\frac{\Delta_{\uparrow}}{2\sqrt{\Delta_{\uparrow}\tilde{\Delta}_{\uparrow} - \frac{1}{4}(\varepsilon_{\uparrow} + \tilde{\varepsilon}_{\uparrow})^2}} + \frac{\Delta_{\downarrow}}{2\sqrt{\Delta_{\downarrow}\tilde{\Delta}_{\downarrow} - \frac{1}{4}(\varepsilon_{\downarrow} + \tilde{\varepsilon}_{\downarrow})^2}} - \frac{\Delta_0}{\varepsilon_n} \right]. \quad (4.14)$$

If we linearize the gap equation, eq. (4.14), for small Δ_0 , we will obtain an equation for the transition temperature

$$\ln \frac{T_c}{T_{c0}} = \psi\left(\frac{1}{2}\right) - \frac{1}{2}\psi\left(\frac{1}{2} + \frac{\Gamma^+}{2\pi k_B T_c}\right) - \frac{1}{2}\psi\left(\frac{1}{2} + \frac{\Gamma^-}{2\pi k_B T_c}\right), \quad (4.15)$$

where

$$\Gamma^{\pm} = \Gamma \frac{2\pi C^e}{z} \pm i\Gamma \left(\frac{C^o}{z} + A^{nl} \right), \quad z = (1 + u_0^2 - \alpha^2 u_5^2)^2 + 4\alpha^2 u_5^2 \quad (4.16)$$

and $\psi(z)$ is the digamma function for complex values. This looks very much like the Abrikosov-Gor'kov formula[22], for an superconductor with magnetic impurities in the Born limit. It looks even more similar for the case of random impurity spins, since we then have that $\Gamma^+ = \Gamma^- = 2\pi\Gamma C^e/z = \Gamma_{eff}$ and eq. (4.15) reduces to

$$\ln \frac{T_c}{T_{c0}} = \psi\left(\frac{1}{2}\right) - \psi\left(\frac{1}{2} + \frac{\Gamma_{eff}}{2\pi k_B T_c}\right), \quad (4.17)$$

which has the exakt same form as the Abrikosov-Gor'kov result, but with an effective pair-breaking parameter Γ_{eff} .

By assuming a large scattering, we can even derive the point at which the scattering is big enough to completely kill the superconductivity. For large scattering rates,

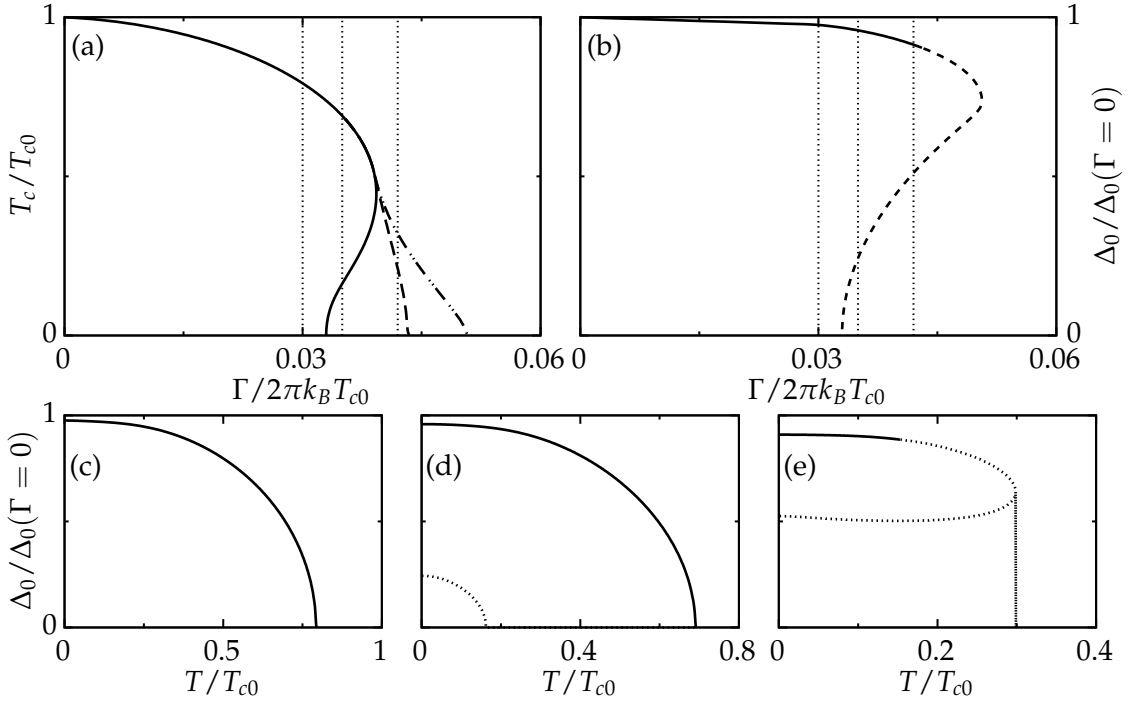


Figure 4.2: Effect of the magnetic impurities on thermodynamic properties. The impurities are aligned, $\alpha > 0$ and $u_s = 4$. In (a) the critical temperature is plotted as a function of the impurity density. The full line is obtained through solving eq. (4.15), the dashed-dotted by solving for the temperature when $\Delta_0 = 0$ in eq. (4.14), and the dashed by finding the temperature when the Free energy difference is zero $\delta\Omega = 0$, see eq. B.3. The maximum impurity density given by eq. (4.18) gives the point where the full line hits zero. In (b) the order parameter at the temperature $T = 0.01 T_{c0}$ is plotted against the impurity density. The full line is the physical solution, while the dashed is unphysical. Finally, in (c)-(e) the order parameter is plotted against the temperature for the impurity densities that are indicated by the vertical dotted lines in (a) and (b), with a growing impurity density from left to right. The order parameter solutions that are dotted are unphysical.

$\Gamma \gg 1$, the digamma function can be approximated with logarithms which gives us the maximum scattering rate as

$$\Gamma_{max} = \frac{1}{4e^{\gamma_{em}}} \frac{z}{\sqrt{(2\pi C^e)^2 + (C^o + zA^{nl})^2}}, \quad (4.18)$$

where $\gamma_{em} = 0.577\dots$ is the Euler-Mascheroni constant. Just as before the second term of the denominator vanishes for the random impurity case.

One should be aware that in linearizing eq. (4.15) we assume that the superconducting phase transition is second order, with a continuous change of the order parameter as

the temperature approaches the superconducting transition temperature. If the phase transition, on the other hand, is first order the transition from the superconducting state to the normal one is not continuous, but rather an abrupt jump, with a sudden appearance of an order parameter with a finite magnitude as the temperature is lowered to the superconducting transition temperature. The order parameter is then never small and we cannot linearize our equations in it. Since we have an effective Zeeman field induced in our system in the case of aligned impurities, we can expect that the phase transition may change from second order to first, which is known to happen for the case of an externally applied Zeeman field[112, 113, 114, 115].

The gap equation is in the aligned impurity case prone to having multiple solutions. For this reason we in Paper III also derive an expression for the difference of the Gibbs free energies in the normal state and the superconducting state to determine the physically relevant one. When the free energy difference is positive it is energetically favorable to be in the normal state instead of in the superconducting one. It turns out that there is always at most one solution that is energetically favorable, and sometimes not even that. The expression for the Gibbs free energy difference is quite lengthy, but for completeness we give a short description on how to derive it and present the result in Appendix B.

To give a taste of how the order parameter and critical temperature behave we plot them for the case of aligned impurity spins in fig. 4.2. For small impurity densities the result is the expected, there is a single solution for the order parameter, slightly reduced in magnitude but the phase transition to the normal state is still second order. Then, suddenly, for a bit higher densities, see fig. 4.2(d), a second solution suddenly appears. This second solution has a Gibbs free energy difference which is larger than the first one, making the first solution the one that is energetically favorable. It, in fact, turns out that the second solution even has a free energy difference that is bigger than zero, making even the normal state more energetically favorable than this solution. And finally, in fig. 4.2(e), the phase transition changes from second order to first, and the transition from the superconducting to the normal state is abrupt. Notice that this happens even before the order parameter drops to zero when solving the gap equation, eq. (4.14). This point is found from calculating when the free energy difference changes sign, signaling that the normal state is more energetically favorable.

4.3 Density of states

Now that we can compute the order parameter, we can also compute the density of state through the Retarded Green's function

$$\frac{N(\varepsilon)}{N_F} = -\frac{1}{2\pi} \text{Im} \left\{ \int \frac{d\Omega_{\mathbf{p}_F}}{4\pi} \text{Tr} \left[\hat{\tau}_3 \hat{g}^R(\varepsilon, \mathbf{p}_F) \right] \right\}. \quad (4.19)$$

In fig. 4.3 we plot the density of states for some representative cases to show the impact of the exchange interaction u_S and the impurity density Γ on the density of

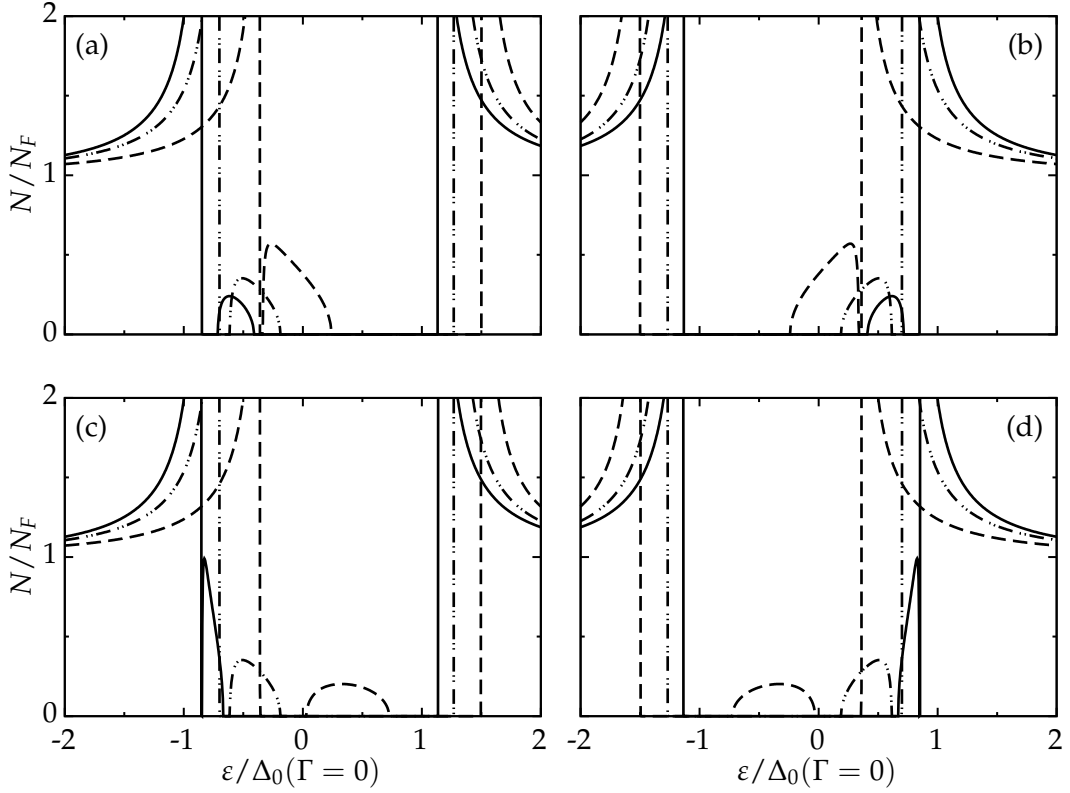


Figure 4.3: The spin-resolved density of states for the case of ferromagnetically ordered impurities with $\alpha > 0$ and the temperature $T = 0.01T_{c0}$. (a) and (b) are for the case of growing $\Gamma/2\pi k_B T_{c0} = 0.01, 0.02, 0.04$ with fixed $u_S = 4$. (c) and (d) are for the case of growing $u_S = 2, 4, 8$ with fixed $\Gamma/2\pi k_B T_{c0} = 0.02$. (a) and (c) show the density of states for spin up, while (b) and (d) show the density of states for spin down.

states. As can clearly be seen u_S sets the position of the impurity band inside the gap, while Γ sets the width of the band. At the same time both of them contribute to the Zeeman splitting. For the case of random impurity spins, the Zeeman splitting would vanish and there would always be two bands mirrored around the Fermi surface inside the gap for both spins.

4.4 Transport

Let us now turn to what was discussed in Paper IV, current and noise properties when tunneling into a superconductor with a distribution of magnetic impurities.

Since our problems separate into different spin bands, we can describe the transport in the exact same way as we described it in the case of just a Zeeman field before, see Chapter 2.7.1.

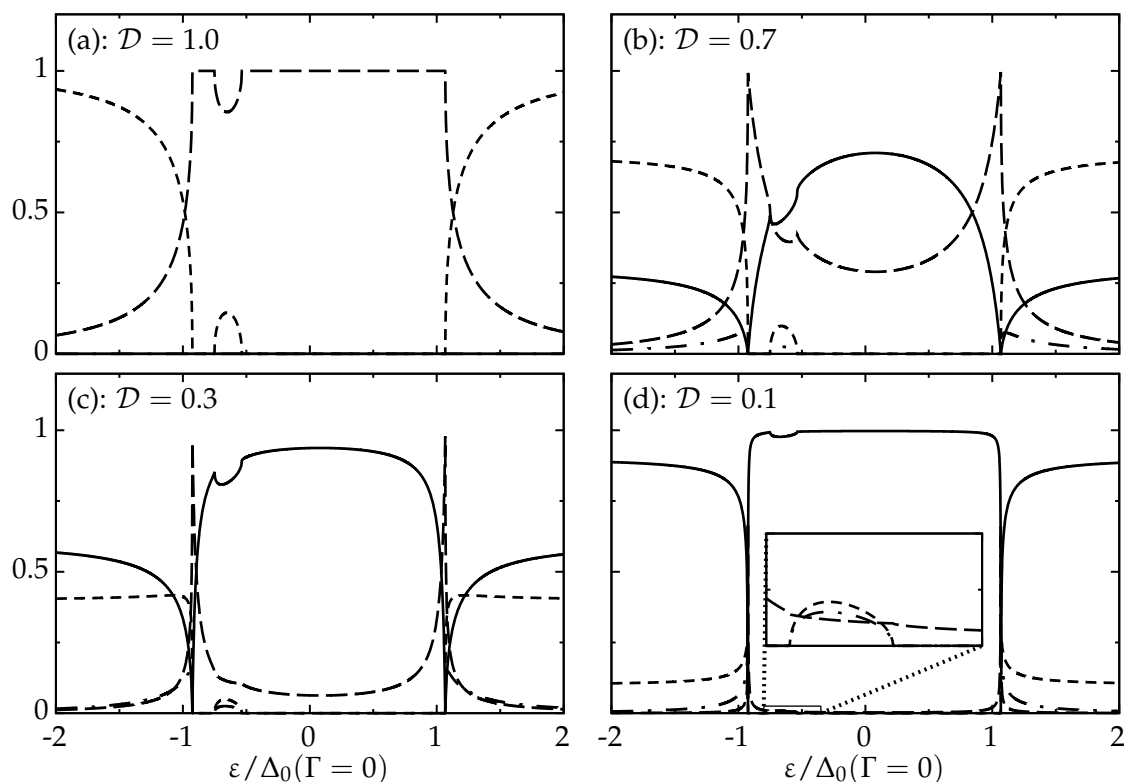


Figure 4.4: The scattering probabilities for a spin up quasi-particle at an NS interface. The different plots are for different transparency of the interface, as indicated in the figure. The impurity spins are ferromagnetically aligned with $\alpha > 0$ and the other parameters for the system are: $\Gamma/2\pi k_B T_{c0} = 0.005$, $u_S = 4$ and $T = 0.01 T_{c0}$. The full line are for normal reflection, the long dashed for Andreev reflection, the short dashed for normal transmission and the dash-dotted for transmission with branch conversion. The inset in (d) shows a zoom for energies around the impurity band. The effective Zeeman shift given by the aligned impurities can clearly be seen in all of the plots, with the current parameters it is given by $\sim 0.02 \times 2\pi k_B T_{c0} \approx 0.07 \Delta_0(\Gamma = 0)$.

For comparison with the clean case considered earlier we plot the scattering probabilities for spin up at the interface in fig. 4.4. This should be compared with the corresponding fig. 2.4. There are many similarities between the two, but also differences. One of the major differences between the two is the appearance of the subgap impurity band in the present case. At the position of the impurity band the probability of Andreev reflection is reduced, while the normal transmission probability is enhanced. When the transparency is reduced all scattering probabilities decrease, except for normal reflection (as expected), but as can be noted the probability for Andreev reflection decreases faster than the transmission probabilities. This is due to the fact that Andreev

reflection goes as $\mathcal{O}(\mathcal{D}^2)$ while normal transmission goes as $\mathcal{O}(\mathcal{D})$. From this we can expect single particle tunneling to dominate for small transparencies. The other thing to note is the effective Zeeman field created by the aligned impurities manifesting itself as a constant energy-shift of all the scattering probabilities. The scattering probabilities for spin down have the same features, but are mirrored in the Fermi surface $\varepsilon = 0$, since for the present parameters the impurity band for spin down lies at positive energies.

Since the transport properties in the end are given by the scattering probabilities we can expect that features seen in the scattering probabilities will also be seen in the transport. Looking at the fig. 4.5, where we plot the transport properties, we see that this is exactly what happens. The reduction in the probability for Andreev reflection can clearly be seen in the charge conductance, see fig. 4.5(a), for the high transparency case, with a decrease in the conductance at the impurity band as a result. When the transparency decreases we eventually reach a point when the conductance at the impurity band is higher than elsewhere in the subgap region, due to the faster decrease in the probability for Andreev reflection compared to single-particle transfer. Because of the aligned impurity spins the impurity bands are spin-polarized, which can clearly be seen in fig. 4.5(b), with a spin conductance there as a result. The polarization of the conductance at the impurity band approaches 100% when we reach the extreme tunneling regime with $\mathcal{D} \ll 1$. From the differential noise, see fig. 4.5(d), we can directly note that the subgap noise does no longer go to zero everywhere for the completely reflecting and transparent cases, but is enhanced at the position for the impurity band. This can easily be understood from the fact that the impurity band opens more transport channels, so there is no longer a single one for those cases, and if there is more than one channel open there will be fluctuations between them. Finally in fig. 4.5(e) we can see that when we approach the tunneling limit the differential Fano factor gets an even more peculiar behavior than before. Above the gap edge the differential Fano factor is unity and below it is twice that *except* for at the impurity band where it is unity again. This means that above the gap as well as at the impurity band the dominating process is single-particle transfer.

The conclusion from all of this is that a superconductor with ferromagnetically aligned impurities can be used as a source of single quasi-particles with almost exclusively a single spin-orientation, a sought after capability for spintronics use[24]. The fact that the impurity band can be well separated from the continuum can also be utilized since this means it will be easier to switch the spin production on/off with just a small voltage adjustment.

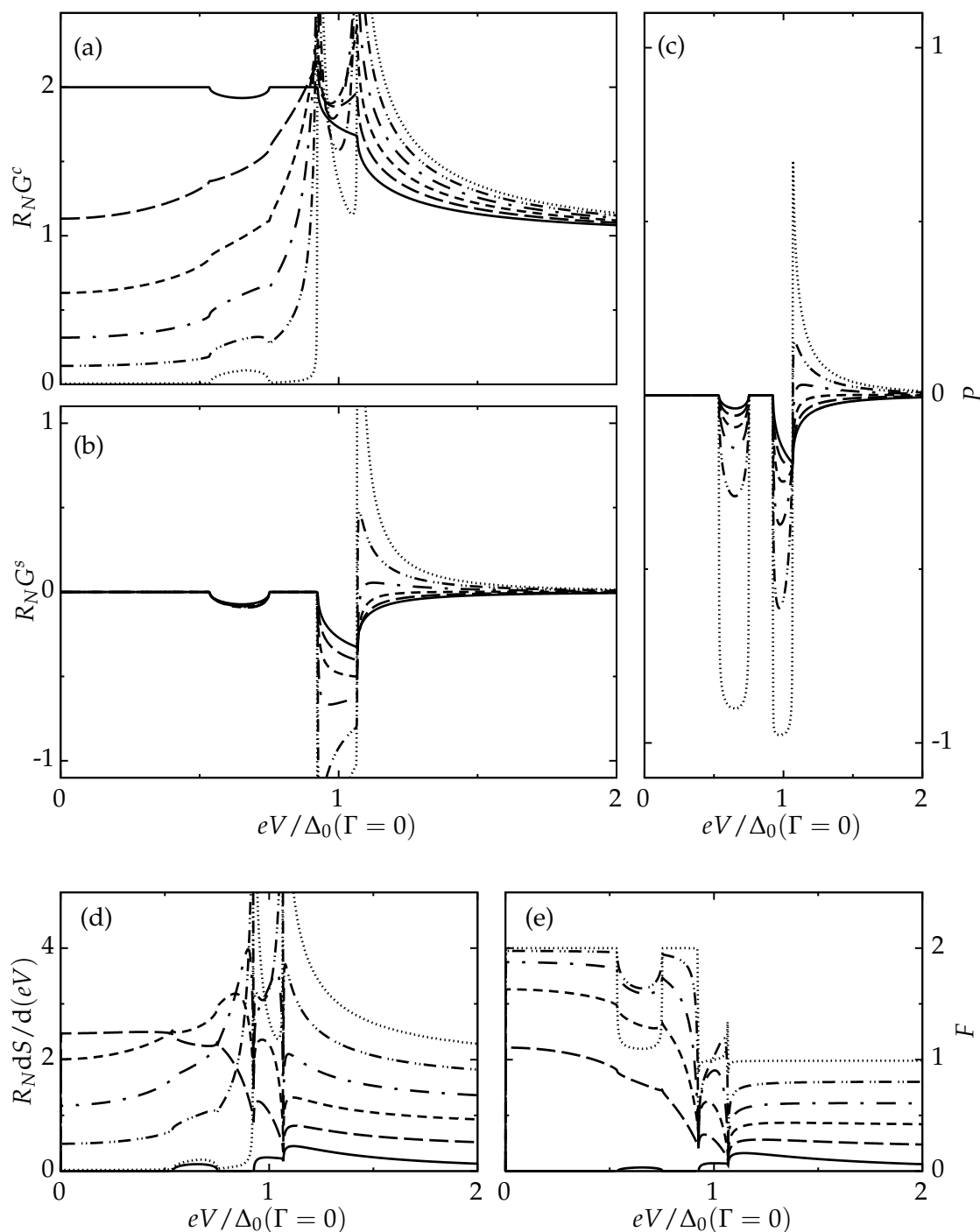


Figure 4.5: Zero temperature transport properties for a system with ferromagnetically aligned impurities with $\alpha > 0$. The system properties are $\Gamma/2\pi k_B T_{c0} = 0.005$, $u_S = 4$. The plots show: (a) the charge conductance (b) the spin conductance (c) the polarization (d) the differential noise and (e) the differential Fano factor. The transparencies are $\mathcal{D} = 0.01, 0.2, 0.4, 0.6, 0.8, 1.0$ from the top to bottom curve at $eV \gg \Delta_0$. The charge conductance is an even function in the voltage, while the rest are odd.

5

Conclusions & Outlook

This thesis has been concerned with transport properties of superconductors connected to other materials.

Papers I and II was a joint theoretical and experimental work, and concerned junctions made of superconductors using InAs nanowires as weak links. This thesis describe the theoretical model used to model the experiments, the experimental aspects of the topic has been written about elsewhere[95]. The theoretical model allowed us to bridge the crossover from ballistic to diffusive transport. A reasonable good fit was found between the theory and experiments, but there were also features that the theory was unable to capture. For example, the reduction in the supercurrent is not completely understood, but could perhaps be due to some depairing mechanism, such as magnetic scattering.

In Papers III and IV, a model of a superconductor with a concentration of magnetic impurities was discussed. Two extreme cases of the impurities were considered; that the impurity spins were completely random and that the impurity spins were aligned. In both cases the scattering off the magnetic impurities induce subgap states, that for certain choices of the model parameters, can be far separated from the gap edges. When the impurity spins are random the subgap states are spin-degenerate, but they spin polarize as the impurity spins align.

Aligning the impurity spins has other consequences. The aligned spins will create a background magnetic field, which acts as a Zeeman field. This is an effect often overlooked, but which can have drastic effects. In Paper III, thermodynamic properties of the superconductor were computed, and it could be shown that, as the concentration of impurities grows, the background Zeeman field will eventually drive the system into a regime where the superconducting phase transition no longer is 2nd order, but rather

1st. In this regime the transition between the superconducting and normal state will not be smooth, but abrupt, with a sudden appearance of an order parameter with a finite magnitude as the temperature is lowered to the superconducting transition temperature.

Finally, in Paper IV, the signature of the impurity bands in transport was considered. By studying both the conductance and the differential noise and computing the so-called differential Fano factor, the relative role of single- and two-particle processes could be dechiffred. From this we could show that in the tunneling limit the dominating process in the impurity band is single particle transfer. We could also show that, in the aligned impurity case, the current in the impurity band is highly polarized, with a spin polarization approaching 100% in the tunneling case. Since the impurity bands can be well separated from the continuum states, these spin-polarized currents can be switched on/off or from spin up to down by simply tuning the applied bias. This makes these type of systems suitable for spintronics applications, where the ability to produce spins with a predetermined orientation is a prerequisite for their operation.

5.1 Outlook

The two different parts of this thesis offer rich possibilities of future directions.

For the nanowire part it would be interesting to see what current fluctuations could reveal, a calculation that would then tie directly to the second part. The nanowires used in the experiments are made of InAs, which is known to have a strong spin-orbit interaction. If also this was included in the model, perhaps the correspondence with the experiments would increase. With the ongoing push to use semiconducting nanowires in proximity to superconductors to induce topologically protected states, a possibility would be to extend our model to capture this kind of physics.

A first possible extension to the second part of the thesis is to investigate the finite frequency noise. Finite frequency noise has previously been shown to be able to reveal information about internal dynamics of systems[116], and also as a help to characterize the system[117]. Since the system depends on many parameters, which can not always be resolved from simple conductance and shot noise measurements, the finite frequency noise can help with this.

Since the existence of impurity bands is a bulk properties the spin currents they generate should be long-range, which would make it interesting to compute how these currents evolve spatially, in e.g. an NSN setup. In principle an incoming, unpolarized, current in one of the normal metals, should in the impurity band in the superconductor be converted to a completely polarized current, making the current in the other normal metal of a single desired spin direction.

Another thing to consider impurity spins create an electron-hole asymmetry. This asymmetry drops out of equilibrium properties, but it will matter if we consider the linear response of the superconductor to an external temperature gradient. Then the

asymmetry would give rise to an enhanced thermo-electric effect. This effect has already been studied in bulk by Kalenkov *et al.* in Ref. [118], but a possible extension to their work is to consider an NS-junction. They also only consider the case of random impurity spins, so another possibility is to align the impurity spins.

Finally, one could consider extending this work by also studying, for example, superconducting point contact junctions, with one, or both, of the superconductors with a concentration of magnetic impurities. Since both the equilibrium, phase-dependent, and the non-equilibrium, voltage-biased, currents depend on the subgap structure of the superconductors, we expect them to be heavily modified by the subgap states induced by the magnetic impurities.

Appendices

Technical Details

A.1 Convolution Product

The noncommutative Convolution product between two functions $a(t, t')$ and $b(t, t')$ is in the time domain defined as

$$a \circ b(t, t') = \int dt'' a(t, t'') b(t'', t'). \quad (\text{A.1})$$

Fourier transforming to the energy domain the product reads

$$a \circ b(\varepsilon, \varepsilon') = \int \frac{d\varepsilon''}{2\pi} a(\varepsilon, \varepsilon'') b(\varepsilon'', \varepsilon'). \quad (\text{A.2})$$

The product can in the mixed representation be written as

$$a \circ b(\varepsilon, t) = e^{\frac{i}{2}(\partial_\varepsilon^a \partial_t^b - \partial_t^a \partial_\varepsilon^b)} a(\varepsilon, t) b(\varepsilon, t). \quad (\text{A.3})$$

A.2 Properties of the Riccati Equations

The Retarded component of the first Riccati equation, as given by eq. 2.6, can be written as

$$i\hbar \mathbf{v}_F \cdot \nabla + E \circ \gamma - \gamma \circ \tilde{E} - \gamma \circ \tilde{\Delta} \circ \gamma + \Delta = 0,$$

with $E \equiv \varepsilon - \Sigma$ and $\tilde{E} \equiv -\varepsilon - \tilde{\Sigma}$ and initial condition $\gamma(0) = \gamma_i$.

It has been shown [119] that associated with any solution to a Riccati differential equation are three functions g , h and f obeying the equations

$$\begin{aligned} i\hbar\mathbf{v}_F \cdot \nabla g + (E - \gamma \circ \tilde{\Delta}) \circ g &= 0 & g(0) &= 1 \\ i\hbar\mathbf{v}_F \cdot \nabla h + (-\tilde{E} - \tilde{\Delta} \circ \gamma) \circ h &= 0 & h(0) &= 1 \\ i\hbar\mathbf{v}_F \cdot \nabla f + h \circ \tilde{\Delta} \circ f &= 0 & f(0) &= 0. \end{aligned}$$

Now if we know the solution γ_0 for a particular initial condition $\gamma_0(0) = \gamma_{i0}$, with the associated functions g_0 , h_0 and f_0 , any other solution with a different initial condition $\gamma_i = \gamma_{i0} + \delta$ can be obtained along the entire trajectory through

$$\gamma(x) = \gamma_0(x) + g_0(x) \circ (1 + \delta \circ f_0(x))^{-1} \circ h_0(x).$$

This is very useful, for example when you have a periodicity condition in your system.

A.3 Numerics

In systems with high a concentration of scatterers we can no longer solve the problem analytically, since the self-energies now will be spatially dependent.

An efficient way of dealing with this problem is to utilize that we *can* solve the problem for constant self-energies. So to approximate the solution we divide our problem area into a number of subsections, where we in each subsection let the self-energies be constant. Given a starting value for the coherence functions at the start of their respective trajectories, and starting values for the self-energies in each of the subsections, we can propagate the coherence functions along the trajectories. These coherence functions are then used to update the self-energies. This scheme is then repeated until we achieve self-consistency, or a maximum number of iterations.

The algorithm is described below.

- 1: Choose starting values for the coherence functions and the self-energies. In a normal region we can use $\tilde{\Sigma}_{imp} = 0$ for the self-energies.
- 2: Calculate the outgoing γ :s at the right and left border of the subsections. γ^+ and $\tilde{\gamma}^-$ are calculated from left to right, and γ^- and $\tilde{\gamma}^+$ the other way, from right to left. The \pm superscript on the coherence functions denote if the projection of the Fermi velocity on the x -axis is positive (negative). Given a section i the equation for the γ :s look like:

- I. $\gamma_i^+(x) = -\frac{\Delta}{\epsilon+i\Omega} + \frac{2i\Omega C \exp(-2\Omega x)}{1-\tilde{\Delta} C \exp(-2\Omega x)}$, with C obtained from $\gamma_i^+(x_{i-1}) = \gamma_{i-1}^+(x_{i-1})$
- II. $\tilde{\gamma}_i^-(x) = \frac{\tilde{\Delta}}{\epsilon+i\Omega} + \frac{2i\Omega C \exp(-2\Omega x)}{1+\Delta C \exp(-2\Omega x)}$, with C obtained from $\tilde{\gamma}_i^-(x_{i-1}) = \tilde{\gamma}_{i-1}^-(x_{i-1})$
- III. $\gamma_i^-(x) = -\frac{\Delta}{\epsilon+i\Omega} + \frac{2i\Omega C \exp(2\Omega x)}{1-\tilde{\Delta} C \exp(2\Omega x)}$, with C obtained from $\gamma_i^-(x_{i+1}) = \gamma_{i+1}^-(x_{i+1})$

IV. $\tilde{\gamma}_i^+(x) = \frac{\tilde{\Delta}}{\epsilon+i\Omega} + \frac{2i\Omega C \exp(2\Omega x)}{1+\Delta C \exp(2\Omega x)}$, with C obtained from $\tilde{\gamma}_i^+(x_{i+1}) = \tilde{\gamma}_{i+1}^+(x_{i+1})$

- 3: New self-energies are calculated from these outgoing γ :s. The self-energy in the i :th subsection is approximated to be its value in the middle of the subsection, so at position $(x_i + x_{i-1})/2$.
- 4: Steps 2 and 3 are repeated until we have reached a desired accuracy or a maximum number of iterations.

B

Gibbs free energy

The derivation of the free energy difference is quite an involved task, but below we give a brief outline of the process. To see more detailed explanations on how to do it, we refer the reader to the references that are given below.

The free energy is a functional of the quasiclassical Green's function, and the self-energies

$$\delta\Omega[\hat{g}, \hat{\sigma}, \hat{\Delta}, T] = \Omega_S[\hat{g}, \hat{\sigma}, T] - \Omega_N[\hat{g}, \hat{\sigma}, T], \quad (\text{B.1})$$

which means that the superconducting state is more energetically favorable when $\delta\Omega < 0$ (since we want to minimize the free energy).

Following Refs. [56, 58, 120, 121] we write

$$\Omega_S[\hat{g}, \sigma, T] = \Omega_N[\hat{g}, \sigma, T = 0] - \frac{1}{2} N_F \int \frac{d\Omega_{\mathbf{p}_F}}{4\pi} k_B T \sum_{|\varepsilon_n| < \varepsilon_c} \text{Tr} \left\{ \hat{\sigma}(\mathbf{p}_F, \varepsilon_n) \hat{g}(\mathbf{p}_F, \varepsilon_n) + \int_{-\varepsilon_c}^{\varepsilon_c} d\zeta_{\mathbf{k}} \ln \left[-\hat{G}^{-1}(\mathbf{k}, \varepsilon_n) + \hat{\sigma}(\mathbf{p}_F, \varepsilon_n) \right] \right\} + \delta\Phi(\hat{g}), \quad (\text{B.2})$$

where $\hat{G}^{-1}(\mathbf{k}, \varepsilon_n) = i\varepsilon_n \hat{\tau}_3 - \zeta_{\mathbf{k}}$, with $\zeta_{\mathbf{k}}$ being the single-particle spectrum in the normal state. The last term is given by $\delta\Phi[\hat{g}] = \Phi_S[\hat{g}] - \Phi_N[\hat{g}]$, with $\Phi[\hat{g}]$ being a functional generating the perturbation expansion of the skeleton self-energy diagrams. Using the impurity self-energy of our models, and assuming a quadratic energy spectrum in the normal state, we obtain the free energy difference as a sum of five different terms

$$\delta\Omega = \delta\Omega_1 + \delta\Omega_2 + \delta\Omega_3 + \delta\Omega_4 + \delta\Omega_5, \quad (\text{B.3})$$

where the different terms are given by

$$\begin{aligned}
\delta\Omega_1 &= -2\pi k_B N_F T \sum_{\varepsilon_n > 0} \left(\sqrt{\Delta_{\uparrow} \tilde{\Delta}_{\uparrow} - \frac{1}{4}(\varepsilon_{\uparrow} + \tilde{\varepsilon}_{\uparrow})^2} + \sqrt{\Delta_{\downarrow} \tilde{\Delta}_{\downarrow} - \frac{1}{4}(\varepsilon_{\downarrow} + \tilde{\varepsilon}_{\downarrow})^2} - \right. \\
&\quad \left. \sqrt{-\frac{1}{4}(\varepsilon_{\uparrow}^N + \tilde{\varepsilon}_{\uparrow}^N)^2} - \sqrt{-\frac{1}{4}(\varepsilon_{\downarrow}^N + \tilde{\varepsilon}_{\downarrow}^N)^2} \right) \\
\delta\Omega_2 &= \frac{1}{2} \pi k_B N_F T \sum_{\varepsilon_n > 0} \left\{ \frac{(\sigma_{11,\uparrow} + \sigma_{22,\uparrow})(\varepsilon_{\uparrow} + \tilde{\varepsilon}_{\uparrow}) + \sigma_{12,\uparrow} \tilde{\Delta}_{\uparrow} + \sigma_{21,\uparrow} \Delta_{\uparrow}}{\sqrt{\Delta_{\uparrow} \tilde{\Delta}_{\uparrow} - \frac{1}{4}(\varepsilon_{\uparrow} + \tilde{\varepsilon}_{\uparrow})^2}} + \right. \\
&\quad \frac{(\sigma_{11,\downarrow} + \sigma_{22,\downarrow})(\varepsilon_{\downarrow} + \tilde{\varepsilon}_{\downarrow}) + \sigma_{12,\downarrow} \tilde{\Delta}_{\downarrow} + \sigma_{21,\downarrow} \Delta_{\downarrow}}{\sqrt{\Delta_{\downarrow} \tilde{\Delta}_{\downarrow} - \frac{1}{4}(\varepsilon_{\downarrow} + \tilde{\varepsilon}_{\downarrow})^2}} - \\
&\quad \left. \frac{(\sigma_{11,\uparrow}^N + \sigma_{22,\uparrow}^N)(\varepsilon_{\uparrow}^N + \tilde{\varepsilon}_{\uparrow}^N)}{\sqrt{-\frac{1}{4}(\varepsilon_{\uparrow} + \tilde{\varepsilon}_{\uparrow})^2}} - \frac{(\sigma_{11,\downarrow}^N + \sigma_{22,\downarrow}^N)(\varepsilon_{\downarrow}^N + \tilde{\varepsilon}_{\downarrow}^N)}{\sqrt{-\frac{1}{4}(\varepsilon_{\downarrow}^N + \tilde{\varepsilon}_{\downarrow}^N)^2}} \right\} \\
\delta\Omega_3 &= \frac{1}{2} \pi k_B N_F \Delta_0 T \sum_{\varepsilon_n > 0} \left[\frac{\Delta_{\uparrow} + \tilde{\Delta}_{\uparrow}}{\sqrt{\Delta_{\uparrow} \tilde{\Delta}_{\uparrow} - \frac{1}{4}(\varepsilon_{\uparrow} + \tilde{\varepsilon}_{\uparrow})^2}} + \frac{\Delta_{\downarrow} + \tilde{\Delta}_{\downarrow}}{\sqrt{\Delta_{\downarrow} \tilde{\Delta}_{\downarrow} - \frac{1}{4}(\varepsilon_{\downarrow} + \tilde{\varepsilon}_{\downarrow})^2}} \right] \\
\delta\Omega_4 &= -2\pi k_B N_F \Gamma \beta u_S T \sum_{\varepsilon_n > 0} \left[\frac{\varepsilon_{\uparrow} + \tilde{\varepsilon}_{\uparrow}}{\sqrt{\Delta_{\uparrow} \tilde{\Delta}_{\uparrow} - \frac{1}{4}(\varepsilon_{\uparrow} + \tilde{\varepsilon}_{\uparrow})^2}} - \frac{\varepsilon_{\downarrow} + \tilde{\varepsilon}_{\downarrow}}{\sqrt{\Delta_{\downarrow} \tilde{\Delta}_{\downarrow} - \frac{1}{4}(\varepsilon_{\downarrow} + \tilde{\varepsilon}_{\downarrow})^2}} \right] \\
\delta\Omega_4 &= -2\pi k_B N_F \Gamma T \sum_{\varepsilon_n > 0} \left\{ \ln \left[1 + u_0^2 - \alpha^2 u_S^2 + 2\alpha u_S \frac{\varepsilon_{\uparrow} + \tilde{\varepsilon}_{\uparrow}}{\sqrt{\Delta_{\uparrow} \tilde{\Delta}_{\uparrow} - \frac{1}{4}(\varepsilon_{\uparrow} + \tilde{\varepsilon}_{\uparrow})^2}} \right] + \right. \\
&\quad \ln \left[1 + u_0^2 - \alpha^2 u_S^2 - 2\alpha u_S \frac{\varepsilon_{\downarrow} + \tilde{\varepsilon}_{\downarrow}}{\sqrt{\Delta_{\downarrow} \tilde{\Delta}_{\downarrow} - \frac{1}{4}(\varepsilon_{\downarrow} + \tilde{\varepsilon}_{\downarrow})^2}} \right] - \\
&\quad \left. \ln [(1 + u_0^2 - \alpha^2 u_S^2)^2 + 4\alpha^2 u_S^2] \right\}.
\end{aligned} \tag{B.4}$$

Here the quantities with the superscript “N” stand for the normal state (i.e. taking the limit $\Delta_0 \rightarrow 0$) value of that particular quantity.

Some of the terms in this expression are not zero in the normal state, which mean that they contribute to the normal state free energy. We want to find the free energy difference between the superconducting state and the normal state, which is why we have to subtract their normal state value.

Bibliography

- [1] G. E. Moore. Cramming More Components onto Integrated Circuits. *Electronics*, 38(8):114–117, April 1965.
- [2] G. E. Moore. Progress in digital integrated electronics. In *Electron Devices Meeting, 1975 International*, volume 21, pages 11–13. IEEE, 1975.
- [3] S. A. Wolf, D. D. Awschalom, R. A. Buhrman, J. M. Daughton, S. von Molnár, M. L. Roukes, A. Y. Chtchelkanova, and D. M. Treger. Spintronics: A spin-based electronics vision for the future. *Science*, 294(5546):1488–1495, 2001.
- [4] Y. Cui and C. M. Lieber. Functional nanoscale electronic devices assembled using silicon nanowire building blocks. *Science*, 291(5505):851–853, 2001.
- [5] L. Hofstetter, S. Csonka, J. Nygard, and C. Schonenberger. Cooper pair splitter realized in a two-quantum-dot Y-junction. *Nature*, 461(7266):960–963, oct 2009.
- [6] Y. Wu, Y. Cui, L. Huynh, C. J. Barrelet, D. C. Bell, and C. M. Lieber. Controlled growth and structures of molecular-scale silicon nanowires. *Nano Letters*, 4(3):433–436, 2004.
- [7] L. Samuelson. Self-forming nanoscale devices. *Materials Today*, 6(10):22 – 31, 2003.
- [8] C. Thelander, P. Agarwal, S. Brongersma, J. Eymery, L.F. Feiner, A. Forchel, M. Scheffler, W. Riess, B.J. Ohlsson, and U. G. Nanowire-based one-dimensional electronics. *Materials Today*, 9(10):28 – 35, 2006.
- [9] I. van Weperen, S. R. Plissard, E. P. A. M. Bakkers, S. M. Frolov, and L. P. Kouwenhoven. Quantized conductance in an insb nanowire. *Nano Letters*, 13(2):387–391, 2013. PMID: 23259576.
- [10] M. T. Björk, C. Thelander, A. E. Hansen, L. E. Jensen, M. W. Larsson, L. R. Wallenberg, and L. Samuelson. Few-electron quantum dots in nanowires. *Nano Letters*, 4(9):1621–1625, 2004.

- [11] A. Das, Y. Ronen, Y. Most, Y. Oreg, M. Heiblum, and H. Shtrikman. Zero-bias peaks and splitting in an Al-InAs nanowire topological superconductor as a signature of Majorana fermions. *Nat Phys*, 8(12):887–895, dec 2012.
- [12] M. T. Deng, C. L. Yu, G. Y. Huang, M. Larsson, P. Caroff, and H. Q. Xu. Anomalous zero-bias conductance peak in a nb-insb nanowire-nb hybrid device. *Nano Letters*, 12(12):6414–6419, 2012. PMID: 23181691.
- [13] C. Nayak, S. H. Simon, A. Stern, M. Freedman, and S. Das Sarma. Non-abelian anyons and topological quantum computation. *Rev. Mod. Phys.*, 80:1083–1159, Sep 2008.
- [14] H. Kamerlingh Onnes. *Comm. Phys. Lab. Univ. Leiden*, 120b, 122b, 124c, 1911.
- [15] W. Meißner and R. Ochsenfeld. Ein neuer effekt bei eintritt der supraleitfähigkeit. *Naturwissenschaften*, 21(44):787–788, 1933.
- [16] J. Bardeen, L. N. Cooper, and J. R. Schrieffer. Microscopic theory of superconductivity. *Phys. Rev.*, 106:162–164, Apr 1957.
- [17] L. N. Cooper. Bound electron pairs in a degenerate fermi gas. *Phys. Rev.*, 104:1189–1190, Nov 1956.
- [18] B. D. Josephson. Possible new effects in superconductive tunnelling. *Physics Letters*, 1(7):251 – 253, 1962.
- [19] A. F. Andreev. Thermal conductivity of the intermediate state of superconductors. *Zh. Eksp. Teor. Fiz.*, 46:1823, 1964. [Sov. Phys.–JETP **19**, 1228 (1964)].
- [20] P. G. De Gennes and E. Guyon. Superconductivity in “normal” metals. *Physics Letters*, 3(4):168 – 169, 1963.
- [21] P. G. De Gennes. Boundary effects in superconductors. *Rev. Mod. Phys.*, 36:225–237, Jan 1964.
- [22] A. A. Abrikosov and L. P. Gor’kov. Contribution to the theory of superconducting alloys with paramagnetic impurities. *Zh. Eksp. Teor. Fiz.*, 39:1781, 1960. [Sov. Phys.–JETP **12**, 1243 (1961)].
- [23] F. S. Bergeret, A. F. Volkov, and K. B. Efetov. Odd triplet superconductivity and related phenomena in superconductor-ferromagnet structures. *Rev. Mod. Phys.*, 77:1321–1373, Nov 2005.
- [24] M. Eschrig. Spin-polarized supercurrents for spintronics. *Physics Today*, 64(1):43, 2011.

- [25] J. Linder and J. W. A. Robinson. Superconducting spintronics. *Nature Physics*, 11(4):307–315, apr 2015.
- [26] M. Eschrig. Spin-polarized supercurrents for spintronics: a review of current progress. *Reports on Progress in Physics*, 78(10):104501, 2015.
- [27] Y. Luh. Bound state in superconductors with paramagnetic impurities. *Acta Physica Sinica*, 21(1):75, 1965.
- [28] H. Shiba. Classical spins in superconductors. *Progress of Theoretical Physics*, 40:435–451, 1968.
- [29] A. I. Rusinov. Superconductivity near a Paramagnetic Impurity. *Soviet Journal of Experimental and Theoretical Physics Letters*, 9:85, January 1969.
- [30] M. Ruby, F. Pientka, Y. Peng, F. von Oppen, B. W. Heinrich, and K. J. Franke. Tunneling processes into localized subgap states in superconductors. *Phys. Rev. Lett.*, 115:087001, Aug 2015.
- [31] G. C. Ménard, S. Guissart, C. Brun, S. Pons, Stolyarov V. S., F. Debontridder, M. V. Leclerc, E. Janod, L. Cario, D. Roditchev, P. Simon, and T. Cren. Coherent long-range magnetic bound states in a superconductor. *Nat. Phys.*, 11(12):1013–1016, oct 2015.
- [32] S. Nadj-Perge, I. K. Drozdov, B. A. Bernevig, and Ali Yazdani. Proposal for realizing Majorana fermions in chains of magnetic atoms on a superconductor. *Phys. Rev. B*, 88:020407, Jul 2013.
- [33] F. Pientka, L. I. Glazman, and F. von Oppen. Topological superconducting phase in helical Shiba chains. *Phys. Rev. B*, 88:155420, Oct 2013.
- [34] J. Klinovaja, P. Stano, A. Yazdani, and D. Loss. Topological superconductivity and majorana fermions in rkky systems. *Phys. Rev. Lett.*, 111:186805, Nov 2013.
- [35] S. Nadj-Perge, I. K. Drozdov, J. Li, H. Chen, S. Jeon, J. Seo, A. H. MacDonald, B. A. Bernevig, and A. Yazdani. Observation of Majorana fermions in ferromagnetic atomic chains on a superconductor. *Science*, 346(6209):602–607, 2014.
- [36] Y. Peng, F. Pientka, L. I. Glazman, and F. von Oppen. Strong Localization of Majorana End States in Chains of Magnetic Adatoms. *Phys. Rev. Lett.*, 114:106801, Mar 2015.
- [37] J. B. Johnson. Thermal agitation of electricity in conductors. *Phys. Rev.*, 32:97–109, Jul 1928.
- [38] H. Nyquist. Thermal agitation of electric charge in conductors. *Phys. Rev.*, 32:110–113, Jul 1928.

- [39] H. B. Callen and T. A. Welton. Irreversibility and generalized noise. *Phys. Rev.*, 83:34–40, Jul 1951.
- [40] R. Kubo. The fluctuation-dissipation theorem. *Reports on Progress in Physics*, 29(1):255, 1966.
- [41] W. Schottky. Über spontane Stromschwankungen in verschiedenen Elektrizitätsleitern. *Annalen der Physik*, 362:541–567, 1918.
- [42] R. De-Picciotto, M. Reznikov, M. Heiblum, V. Umansky, G. Bunin, and D. Mahalu. Direct observation of a fractional charge. *Nature*, 389(6647):162–164, sep 1997.
- [43] L. Saminadayar, D. C. Glattli, Y. Jin, and B. Etienne. Observation of the $e/3$ fractionally charged Laughlin quasiparticle. *Phys. Rev. Lett.*, 79:2526–2529, Sep 1997.
- [44] M. Büttiker. Scattering theory of current and intensity noise correlations in conductors and wave guides. *Phys. Rev. B*, 46:12485–12507, Nov 1992.
- [45] Ya. M. Blanter and M. Büttiker. Shot noise in mesoscopic conductors. *Phys. Rep.*, 336(1-2):1–166, 2000.
- [46] V. A. Khlus. Current and voltage fluctuations in microjunctions between normal metals and superconductors. *Zh. Eksp. Teor. Fiz.*, 66(December 1987):1243–1249, 1987.
- [47] M. J. M. de Jong and C. W. J. Beenakker. Doubled shot noise in disordered normal-metal–superconductor junctions. *Phys. Rev. B*, 49:16070–16073, Jun 1994.
- [48] B. A. Muzykantskii and D. E. Khmelnitskii. Quantum shot noise in a normal-metal–superconductor point contact. *Phys. Rev. B*, 50:3982–3987, Aug 1994.
- [49] M. P. Anantram and S. Datta. Current fluctuations in mesoscopic systems with Andreev scattering. *Phys. Rev. B*, 53:16390–16402, Jun 1996.
- [50] T. Martin. Wave packet approach to noise in N-S junctions. *Physics Letters A*, 220:137–142, February 1996.
- [51] D. Averin and H. T. Imam. Supercurrent noise in quantum point contacts. *Phys. Rev. Lett.*, 76:3814–3817, May 1996.
- [52] J. C. Cuevas, A. Martín-Rodero, and A. Levy Yeyati. Shot noise and coherent multiple charge transfer in superconducting quantum point contacts. *Phys. Rev. Lett.*, 82:4086–4089, May 1999.
- [53] Y. Naveh and D. V. Averin. Nonequilibrium current noise in mesoscopic disordered superconductor–normal-metal–superconductor junctions. *Phys. Rev. Lett.*, 82:4090–4093, May 1999.

- [54] P. Dieleman, H. G. Bukkems, T. M. Klapwijk, M. Schicke, and K. H. Gundlach. Observation of andreev reflection enhanced shot noise. *Phys. Rev. Lett.*, 79:3486–3489, Nov 1997.
- [55] R. Cron, M. F. Goffman, D. Esteve, and C. Urbina. Multiple-charge-quanta shot noise in superconducting atomic contacts. *Phys. Rev. Lett.*, 86:4104–4107, Apr 2001.
- [56] G. Eilenberger. Transformation of gorkov’s equation for type ii superconductors into transport-like equations. *Z. Phys.*, 214:195, 1968.
- [57] A. I. Larkin and Y. N. Ovchinnikov. Quasiclassical method in the theory of superconductivity. *Zh. Éksp. Teor. Fiz.*, 55:2262, 1968 [*Sov. Phys. JETP*, 28:1200, 1969].
- [58] J. W. Serene and D. Rainer. The quasiclassical approach to superfluid ^3He . *Phys. Rep.*, 101:221–311, Dec 1983.
- [59] A. L. Shelankov. On the derivation of quasiclassical equations for superconductors. *Journal of Low Temperature Physics*, 60(1):29–44, 1985.
- [60] L. V. Keldysh. Diagram technique for nonequilibrium processes. *Zh. Éksp. Teor. Fiz.*, 47:1515, 1964 [*Sov. Phys. JETP*, 20:1018, 1965].
- [61] J. Rammer. QUANTUM FIELD THEORY OF NON-EQUILIBRIUM STATES. pages 1–550, 2012.
- [62] N. Schopohl. Transformation of the Eilenberger Equations of Superconductivity to a Scalar Riccati Equation. *cond-mat/9804064 (unpublished)*, 1998.
- [63] M. Eschrig. Distribution functions in nonequilibrium theory of superconductivity and andreev spectroscopy in unconventional superconductors. *Phys. Rev. B*, 61:9061–9076, Apr 2000.
- [64] M. Eschrig. Scattering problem in nonequilibrium quasiclassical theory of metals and superconductors: General boundary conditions and applications. *Phys. Rev. B*, 80:134511, 2009.
- [65] A. Shelankov and M. Ozana. Quasiclassical theory of superconductivity: A multiple-interface geometry. *Physical Review B*, 61(10):7077–7100, mar 2000.
- [66] A. V. Zaitsev. Quasiclassical equations of the theory of superconductivity for contiguous metals and the properties of constricted microcontacts. *Sov. Phys. JETP*, 59:1015–1024, May 1984.
- [67] G. Kieselmann. Self-consistent calculations of the pair potential and the tunneling density of states in proximity contacts. *Phys. Rev. B*, 35:6762–6770, May 1987.

- [68] A. Millis, D. Rainer, and J. A. Sauls. Quasiclassical theory of superconductivity near magnetically active interfaces. *Phys. Rev. B*, 38:4504–4515, Sep 1988.
- [69] M. Fogelström. Josephson currents through spin-active interfaces. *Phys. Rev. B*, 62:11812–11819, Nov 2000.
- [70] E. Zhao, T. Löfwander, and J. A. Sauls. Nonequilibrium superconductivity near spin-active interfaces. *Phys. Rev. B*, 70:134510, Oct 2004.
- [71] T. Löfwander, M. Fogelström, and J. A. Sauls. Shot noise in normal metal–*d*-wave superconducting junctions. *Phys. Rev. B*, 68:054504, Aug 2003.
- [72] D. Xu, S. K. Yip, and J. A. Sauls. Nonlinear meissner effect in unconventional superconductors. *Phys. Rev. B*, 51:16233–16253, Jun 1995.
- [73] K. D. Usadel. Generalized diffusion equation for superconducting alloys. *Phys. Rev. Lett.*, 25:507–509, Aug 1970.
- [74] J. A. X. Alexander, T. P. Orlando, D. Rainer, and P. M. Tedrow. Theory of fermi-liquid effects in high-field tunneling. *Phys. Rev. B*, 31:5811–5825, May 1985.
- [75] J. C. Hammer, J. C. Cuevas, F. S. Bergeret, and W. Belzig. Density of states and supercurrent in diffusive s-n-s junctions: Roles of nonideal interfaces and spin-flip scattering. *Phys. Rev. B*, 76:064514, Aug 2007.
- [76] H. le Sueur, P. Joyez, H. Pothier, C. Urbina, and D. Esteve. Phase controlled superconducting proximity effect probed by tunneling spectroscopy. *Phys. Rev. Lett.*, 100:197002, May 2008.
- [77] P. Dubos, H. Courtois, B. Pannetier, F. K. Wilhelm, A. D. Zaikin, and G. Schön. Josephson critical current in a long mesoscopic s-n-s junction. *Phys. Rev. B*, 63:064502, Jan 2001.
- [78] J. C. Cuevas and F. S. Bergeret. Magnetic interference patterns and vortices in diffusive s-n-s junctions. *Phys. Rev. Lett.*, 99:217002, Nov 2007.
- [79] L. Angers, F. Chiodi, G. Montambaux, M. Ferrier, S. Guéron, H. Bouchiat, and J. C. Cuevas. Proximity dc squids in the long-junction limit. *Phys. Rev. B*, 77:165408, Apr 2008.
- [80] V. Ambegaokar and A. Baratoff. Tunneling between superconductors. *Phys. Rev. Lett.*, 10:486–489, Jun 1963. Errata: [81].
- [81] V. Ambegaokar and A. Baratoff. Errata: Tunneling between superconductors. *Phys. Rev. Lett.*, 11:104–104, Jul 1963.

- [82] A. Barone and G. Paternò. *Physics and applications of the Josephson effect*. Wiley, 1982.
- [83] G. E. Blonder, M. Tinkham, and T. M. Klapwijk. Transition from metallic to tunneling regimes in superconducting microconstrictions: Excess current, charge imbalance, and supercurrent conversion. *Phys. Rev. B*, 25:4515–4532, Apr 1982.
- [84] J. Tersoff and D. R. Hamann. Theory of the scanning tunneling microscope. *Phys. Rev. B*, 31:805–813, Jan 1985.
- [85] J. Li, W.-D. Schneider, and R. Berndt. Local density of states from spectroscopic scanning-tunneling-microscope images: Ag(111). *Phys. Rev. B*, 56:7656–7659, Sep 1997.
- [86] V. S. Shumeiko, E. N. Bratus, and G. Wendin. Scattering theory of superconductive tunneling in quantum junctions. *Low Temperature Physics*, 23(3), 1997.
- [87] J. C. Cuevas and M. Fogelström. Quasiclassical description of transport through superconducting contacts. *Phys. Rev. B*, 64:104502, Aug 2001.
- [88] F. Hübner, M. J. Wolf, D. Beckmann, and H. v. Löhneysen. Long-range spin-polarized quasiparticle transport in mesoscopic al superconductors with a zee-man splitting. *Phys. Rev. Lett.*, 109:207001, Nov 2012.
- [89] C. H. L. Quay, D. Chevallier, C. Bena, and M. Aprili. Spin imbalance and spin-charge separation in a mesoscopic superconductor. *Nat Phys*, 9(2):84–88, feb 2013.
- [90] R. Meservey and P.M. Tedrow. Spin-polarized electron tunneling. *Physics Reports*, 238(4):173–243, mar 1994.
- [91] R. Meservey, P. M. Tedrow, and Peter Fulde. Magnetic field splitting of the quasi-particle states in superconducting aluminum films. *Phys. Rev. Lett.*, 25:1270–1272, Nov 1970.
- [92] F. Giazotto and F. Taddei. Superconductors as spin sources for spintronics. *Phys. Rev. B*, 77:132501, Apr 2008.
- [93] T. Krishtop, M. Houzet, and J. S. Meyer. Nonequilibrium spin transport in zeeman-split superconductors. *Phys. Rev. B*, 91:121407, Mar 2015.
- [94] R. J. Schoelkopf, P. J. Burke, A. A. Kozhevnikov, D. E. Prober, and M. J. Rooks. Frequency Dependence of Shot Noise in a Diffusive Mesoscopic Conductor. *Phys. Rev. Lett.*, 78:3370–3373, Apr 1997.
- [95] S. Abay Gebrehiwot. *Charge transport in InAs nanowire devices*. Chalmers University of Technology, Göteborg, 2013. Diss. (sammanfattning) Göteborg : Chalmers tekniska högskola, 2013.

- [96] S. Datta. *Electronic Transport in Mesoscopic Systems*. Cambridge University Press, 1995. Cambridge Books Online.
- [97] G. B. Arnold. Superconducting tunneling without the tunneling hamiltonian. ii. subgap harmonic structure. *Journal of Low Temperature Physics*, 68(1):1–27, 1987.
- [98] E. N. Bratus', V. S. Shumeiko, and G. Wendin. Theory of subharmonic gap structure in superconducting mesoscopic tunnel contacts. *Phys. Rev. Lett.*, 74:2110–2113, Mar 1995.
- [99] D. Averin and A. Bardas. ac josephson effect in a single quantum channel. *Phys. Rev. Lett.*, 75:1831–1834, Aug 1995.
- [100] J. C. Cuevas, A. Martín-Rodero, and A. Levy Yeyati. Hamiltonian approach to the transport properties of superconducting quantum point contacts. *Phys. Rev. B*, 54:7366–7379, Sep 1996.
- [101] W. Belzig, C. Bruder, and Gerd Schön. Local density of states in a dirty normal metal connected to a superconductor. *Phys. Rev. B*, 54:9443–9448, Oct 1996.
- [102] A. A. Golubov, M. Y. Kupriyanov, and E. Il'ichev. The current-phase relation in josephson junctions. *Rev. Mod. Phys.*, 76:411–469, Apr 2004.
- [103] A. Zehnder, Ph. Lerch, S. P. Zhao, Th. Nussbaumer, E. C. Kirk, and H. R. Ott. Proximity effects in nb/al – alo_x – Al/Nb superconducting tunneling junctions. *Phys. Rev. B*, 59:8875–8886, Apr 1999.
- [104] E. Scheer, W. Belzig, Y. Naveh, M. H. Devoret, D. Esteve, and C. Urbina. Proximity effect and multiple andreev reflections in gold atomic contacts. *Phys. Rev. Lett.*, 86:284–287, Jan 2001.
- [105] W. Belzig. *Magnetic and Spectral Properties of Superconducting Proximity-systems*. Shaker Verlag GmbH, Germany, 1999.
- [106] P. Samuelsson, Å. Ingerman, G. Johansson, E. V. Bezuglyi, V. S. Shumeiko, G. Wendin, R. Kürsten, A. Richter, T. Matsuyama, and U. Merkt. Coherent current transport in wide ballistic josephson junctions. *Phys. Rev. B*, 70:212505, Dec 2004.
- [107] M. Y. Kupriyanov, A. Brinkman, A.A. Golubov, M. Siegel, and H. Rogalla. Double-barrier josephson structures as the novel elements for superconducting large-scale integrated circuits. *Physica C: Superconductivity*, 326-327:16 – 45, 1999.
- [108] N. F. Mott. *Metal-Insulator Transitions*. Taylor and Francis, London, 1990.
- [109] A. V. Balatsky, M. I. Salkola, and A. Rosengren. Impurity-induced virtual bound states in *d*-wave superconductors. *Phys. Rev. B*, 51:15547–15551, Jun 1995.

- [110] Y. Okabe and A. D. S. Nagi. Role of potential scattering in the Shiba-Rusinov theory of the magnetic impurities in superconductors. *Phys. Rev. B*, 28:1320–1322, Aug 1983.
- [111] R. Grein, T. Löfwander, and M. Eschrig. Inverse proximity effect and influence of disorder on triplet supercurrents in strongly spin-polarized ferromagnets. *Phys. Rev. B*, 88:054502, 2013.
- [112] A. M. Clogston. Upper Limit for the Critical Field in Hard Superconductors. *Phys. Rev. Lett.*, 9:266–267, Sep 1962.
- [113] B. S. Chandrasekhar. A Note on the Maximum Critical Field of High-Field Superconductors. *Appl. Phys. Lett.*, 1(1):7–8, 1962.
- [114] L. P. Gor'kov and A. I. Rusinov. Ferromagnetism in Superconducting Alloys. *Zh. Eksp. Teor. Fiz.*, 46:1363, 1964. [Sov. Phys.–JETP **19**, 922 (1964)].
- [115] Y. A. Izyumov and Y. N. Skryabin. Problem of the Coexistence of Superconductivity and Ferromagnetism. *Phys. Status Solidi B*, 61(1):9–64, 1974.
- [116] M. Braun, J. König, and J. Martinek. Frequency-dependent current noise through quantum-dot spin valves. *Phys. Rev. B*, 74:075328, Aug 2006.
- [117] A. Cottet, B. Douçot, and W. Belzig. Finite Frequency Noise of a Superconductor-Ferromagnet Quantum Point Contact. *Physical Review Letters*, 101(25):257001, dec 2008.
- [118] M. S. Kalenkov, A. D. Zaikin, and L. S. Kuzmin. Theory of a Large Thermoelectric Effect in Superconductors Doped with Magnetic Impurities. *Physical Review Letters*, 109(14):147004, oct 2012.
- [119] W. T. Reid. *Riccati differential equations*. Mathematics in Science and Engineering. Elsevier Science, 1972.
- [120] J. Keller, K. Scharnberg, and H. Monien. Free energy of anisotropic superconductors. *Physica C*, 152(4):302–314, 1988.
- [121] J. A. Sauls. Fermi-liquid theory of unconventional superconductors. In K. S. Kevin S. Bedell, Z. Wang, D. E. Meltzer, A. V. Balatsky, and E. Abrahams, editors, *Strongly Correlated Electronic Materials: The Los Alamos Symposium 1993*. Addison-Wesely, Reading, MA, 1994.